STICKY LIPOSOMES: A NEW BINDING GEOMETRY WITH IMPLICATIONS IN THE TARGETED THERAPY OF HER2-NEGATIVE BREAST CANCER

By

MICHELLE SEMPKOWSKI

A dissertation submitted to the Graduate School-New Brunswick

Rutgers, The State University of New Jersey

In partial fulfillment of the requirements

For the degree of

Doctor of Philosophy

Graduate Program in Biomedical Engineering

Written under the direction of

Stavroula Sofou

And approved by

_____

_____

_____

_____

New Brunswick, New Jersey

October 2017

ABSTRACT OF THE DISSERTATION

Sticky Liposomes: A New Binding Geometry with

Implications in the Targeted Therapy of HER2-negative Breast Cancer

By MICHELLE SEMPKOWSKI

Dissertation Director:

Stavroula Sofou

HER2-targeted nanoparticles encapsulating chemotherapeutics have shown promise for reducing the severity of side effects associated with traditional chemotherapeutics. However, the ability for conventionally functionalized HER2-targeted nanoparticles to effectively target stops to hold on cancer cells expressing less than 200,000 HER2 receptors per cell (<1+ HER2 by immunohistochemistry). For cases of cancer with HER2 expression below this threshold, there is a lack of targeted treatment options because tumors are still considered untargetable.

In this dissertation, we describe pH-responsive lipid nanocarriers (liposomes) that present HER2-targeting lipopeptides on lipid domains with high local multivalency ('sticky patches'). Sticky patches are formed by inducing preferential partitioning of lipopeptides into lipid raft-like domains that are triggered to form on the liposome membrane at acidic pH values ($6.5 < pH < 7.0$) matching the tumor interstitial pH. We investigate the preclinical feasibility of HER2-targeting sticky liposomal doxorubicin by first characterizing and understanding their binding geometries with cell receptor(s), then testing the reactivity and efficacy against a variety of breast cancer cells with variable

expression of targeting receptors, and multicellular spheroids expressing a wide range of HER2. Overall, our results demonstrate the potential of sticky liposomes as an effective targeted therapy for breast cancers expressing low HER2 copies and, in particular, for Triple Negative Breast Cancers.

ACKNOWLEDGEMENTS

I would first like to thank my dissertation advisor, Dr. Stavroula Sofou, for her constant support and guidance in the completion of this work. Ever since I joined her lab six years ago as an REU student, she has always demanded the best of me as a scientist and a person. Her mentorship has not only been crucial in my success as a Ph.D. student, but it has also prepared me for whatever may lie ahead. I would also like thank my dissertation committee members, Dr. Prabhas Moghe, Dr. Charles Roth, and Dr. Yannis Kevrekidis, for their continued support and positive criticism of this work. I can still remember the first verification meeting I had with my committee, and how much I sweat as I struggled to derive equations on the board.

It is also imperative that I mention those colleagues in Sofou Lab who have been instrumental in my success at the benchtop. Most importantly, I would like to thank former lab members, Dr. Amey Bandekar, Dr. Charles Zhu and Ms. Ana Gomez, for teaching me everything I needed to know in my first couple years as a Ph.D. student. I would also like to thank current lab members, Ms. Sally Stras, Mr. Trevan Locke and Mr. Aprameya Prasad, as well as former lab member, Mr. Thomas Linz, for always being available and willing to provide me support both inside and outside of the lab. I would like to especially thank Ms. Alaina Howe (current Sofou lab member) for asking me every single day during the month of May 2017 whether I worked on my thesis the night before. The looming guilt of potentially disappointing her (or having her yell at me) the next day is the only reason this document exists.

I would also like to thank my family. My parents, Gene and Carrie Sempkowski, raised me to work hard and always strive to be the best. They also made sure I had clean

clothes and food to eat no matter what time I came home from the lab, which was quite the perk. My older brother, Dan Sempkowski, was always an excellent role model for how someone could excel in both academics and athletics. Unfortunately for him though, the completion of this dissertation is a gentle reminder that I was the child graced with both the beauty and the brains. Finally, I would like to thank my fiancé, Seth Crow, for endlessly loving and supporting me on this journey, in times of failure and times of success. It must take a saint to deal with a stressed-out Ph.D. student every single day of every year for the past five years, but I promise to spend the rest of our lives together making it up to you.

Finally, I would like to thank the funding sources that supported the completion of this work, including the following: American Cancer Society Research Scholar Grant 12-044-01 (Stavroula Sofou), NSF CBET 1510015 (Stavroula Sofou), New Jersey Commission on Cancer Research Pre-Doctoral Fellowship (Michelle Sempkowski), and Graduate Assistance in Areas of National Need (Michelle Sempkowski).

TABLE OF CONTENTS

LIST OF FIGURES

LIST OF TABLES

CHAPTER 1: INTRODUCTION

1.1: Breast cancer

Approximately 1 in 8 women in the United States will develop breast cancer sometime in her life [1]. In 2017 alone, it is estimated that over 250,000 new cases of invasive breast cancer will be diagnosed and 40,000 women will die from the disease [2]. Although the mortality rates associated with breast cancer have significantly decreased mainly due to early detection through mammography screening, there is a still a need for more robust therapies to improve the quality of life and extend life expectancy of patients with advanced/metastatic disease.

1.2: HER2

Human epidermal growth factor receptor 2 (HER2/ERBB2) is a member of the human epidermal growth factor receptor (HER/EGFR/ERBB) family of tyrosine kinase receptors [3] [4]. Since HER2 is a ligand-orphan receptor, it remains in an open conformation ready for dimerization with HER1, HER3 or HER4. Consequently, HER2 gene amplification and receptor overexpression is correlated with cell growth and differentiation through a signal transduction cascade mediated by the activation of P12K/Akt and the Ras/Raf/MEK/MAPK pathways [5].

HER2 is commonly used for molecularly targeted therapies because it is highly expressed in approximately 30% of human breast cancers, and moderately expressed in a number of other cancers such as gastric, bladder, lung and endometrial [6]. In the clinic, HER2 levels are evaluated using Pathway (Ventana Medical Systems) or HercepTest (Dako), which are quasi-quantitative immunohistochemical (IHC) assays that grade

biopsied samples from 0 to 3+ [7]. Quantitative *in vitro* studies on varying cell lines have translated IHC scores of 0, 1+, 2+, and 3+ to HER2 quantities of 2×10^4, 1×10^5, 5×10^5 and $> 10^6$ per cell, respectively [8]. For a score of 0 to 1+, samples are considered "HER2-negative". If the score is 2+, samples are deemed "borderline." If the score is 3+, then samples are considered "HER2-positive".

1.3: HER2-targeted therapy in breast cancer

Hyperactivation of the downstream signaling pathways associated with HER2 are known to promote cancer progression, leading to high recurrence rates and increased mortality [4]. The development of HER2-targeted therapies has significantly improved the prognosis and outcome for patients with HER2-positive breast cancer by selectively delivering the therapy to HER2-positive breast cancer cells while minimizing off target effects and toxicities [9].

The most widely used targeted therapy for HER2-positive breast cancer patients is the humanized monoclonal antibody, trastuzumab [10]. Trastuzumab is directed against the extracellular domain of the HER2 receptor, which inhibits ligand-independent HER2 signaling and induces antibody-dependent cell mediated cytotoxicity (ADCC) [11]. It was first approved by the FDA as a monotherapy or in combination with paclitaxel or docetaxel for patients with metastatic HER2-positive breast cancer [12]. In 2007, clinical trials demonstrated that adjuvant trastuzumab resulted in a significant reduction in metastasis, rate of recurrence and patient mortality when compared to treatment without trastuzumab [13]. Since then, adjuvant trastuzumab has become the standard of care for patients with HER2-positive breast cancer in its early stages. HER2 overexpression is

also associated with sensitivity to anthracyclines (e.g. doxorubicin), suggesting that women whose tumors overexpress HER2 would benefit more from an anthracycline-containing adjuvant regimen [14] [15] [16]. However, concurrent treatment with anthracyclines and trastuzumab in a large randomized trial demonstrated unacceptably high rates of cardiotoxicity [17]. Because anthracyclines can trigger apoptosis in cardiomyocytes through the production of ROS, and trastuzumab can block the normal operation of HER2 signaling on cardiomyocytes, it is thought that the two work synergistically to prevent cardiac tissue repair. It is these issues with cardiac dysfunction that have prevented the concurrent use of anthracyclines and trastuzumab [18].

One alternative treatment for HER2-postive breast cancer undergoing FDA approval is the antibody-drug conjugate MM-302, developed by Merrimack Pharmaceuticals. MM-302 is a liposomal doxorubicin formulation targeted to the HER2 receptor using surface bound Polyethylene Glycol (PEG) coupled to HER2-targeting single-chain variable fragments (scFvs). This particle is designed to allow for the selective delivery of doxorubicin into HER2-overexpressing cancer cells, while minimizing the exposure to healthy tissue such as the heart [19]. In a Phase I study, MM-302 (alone or in combination with trastuzumab) established an acceptable safety profile and a median progression free survival (PFS) benefit of 5.7 months in pretreated patients (median of 4 prior treatments) [20]. MM-302 (alone or in combination with trastuzumab) proceeded to Phase II HERMIONE trails where the study was finally halted in December 2016 after it failed to improve PFS when compared to adjuvant trastuzumab-chemotherapy [21]. However, a useful retroactive finding of this clinical study emerged where the Enhance Retention and Permeability (EPR) effect was quantified in patients

using ^{64}Cu-labled MM302 [22]. The group demonstrated that the EPR effect is highly variable among patients and that patient EPR state at the time of therapy correlated with therapeutic response. Because tumor uptake of nanoparticles is driven by the EPR effect, pre-screening nanoparticle deposition in tumors can help identify those patients who are best suited for nanoparticle-based therapy.

Typical HER2-targeting liposomes, such as MM-302, are designed with uniformly functionalized HER-targeting ligands attached to the distal ends of PEG chains homogenously distributed across the surface. We refer to these nanocarriers as 'uniformly functionalized liposomes'. Specific targeting of uniformly functionalized liposomes ceases on breast cancer cells exhibiting < 200,000 HER2 copies/cell [23]. In addition, however, HER2 expression on cells comprising a HER2-overexpressing tumor may range from 0-100% [24]. This significantly compromises the therapeutic efficacy of uniformly functionalized liposomes against HER2-positive breast cancers. Concurrently, breast cancers that minimally express HER2 (or have a HER2 status of either 1+, 100,000 HER2 copies/cell, or below) have no therapeutic option that targets the HER2 receptor. The same issue arises for triple negative breast cancer (TNBC), in that there is no available therapeutic option for specifically targeting breast cancer cells that minimally express HER2, progesterone, or/and estrogen receptors. For these patients, the backbone of treatment is systemic chemotherapy [25]. Therefore, the major gap is a lack of a targeted chemotherapeutic approach that specifically targets low or too low HER2 expressing breast cancer cells and has the flexibility of ultimately targeting all low-receptor expressing breast cancers.

1.4: Dissertation summary

The aim of this dissertation is to investigate the potential of a new targeting geometry on liposomal chemotherapy to enable adequate binding to a single receptor. We call these liposomes "sticky liposomes" and they are loaded with doxorubicin for the targeted therapy of breast cancer with low or too low HER2-expression that is characterized as 'HER2-negative' for the conventional targeting geometries. Based on the above mentioned targeted liposomal doxorubicin clinical studies, we hypothesize that sticky liposomal doxorubicin can be a safe and effective targeted therapy for patients whose breast tumors and metastases minimally express the HER2 receptor. We tested our hypothesis with the following specific aims:

1.) Determine how the geometry of ligand presentation, extent of local multivalency and cluster size on HER2-targeting sticky liposomes affect apparent functionality,

2.) Develop HER2-targeting sticky liposomes loaded with doxorubicin and test their reactivity and efficacy *in vitro* against breast cancer cell monolayers expressing a variety of low degrees of HER2 (<100,000 HER2 copies/cell),

3) Evaluate the pre-clinical potential of HER2-targeting sticky liposomal doxorubicin therapy by treating multicellular spheroids comprised of Triple Negative Breast Cancer (TNBC) cells with liposomes under physiologically relevant exposure conditions.

In this study, lipid membrane patches - that form the foundation for the new binding geometry - were designed to be pH-responsive. Briefly, as reported before,[26, 27] liposome membranes contain two lipid types: one with a nontitratable headgroup and one with a titratable domain-forming headgroup; the tail lengths are different. The extent of ionization on the headgroups of the domain-forming lipids is controlled by the pH

which is used to shift the balance between electrostatic repulsions and H-bonding attractions. In particular, at neutral pH, the headgroups of the domain forming lipids are negatively-charged, opposing close proximity between lipids, resulting in uniform lipid membranes. As the pH is decreased, mimicking that of the tumor interstitium (pH 6.5-6.0 [28]), gradual headgroup protonation minimizes the electrostatic repulsion, and lipid rafts (patches) are formed driven mostly by H-bonding. To create sticky patches, we added a third lipid type, a peptide-labeled lipid with acyl-chain lengths identical to the acyl-tail lengths of the titratable domain forming lipid. This addition tunes the surface functionality as follows: at neutral pH, the lipid membranes are well mixed and the liposomes are not reactive since the peptide-labeled lipids are uniformly distributed over the liposome surface with low surface density. Upon patch formation at acidic pH, ligand-labeled lipids preferentially partition into the patches at very high local densities. This results in formation of sticky patches. Sticky liposomes are PEGylated to enable adequate blood circulation times (comparable to the blood AUCs of FDA-approved Doxil): a PEGylated lipid with acyl-tails identical to those on the non-titratable lipid is contained on the membrane.

In particular, in Chapter 2, we characterized the binding geometries of HER2-targeting sticky liposomes by varying the geometry of ligand presentation (clustered vs. uniform), the extent of local multivalency and the cluster/patch size. We observed that on both high and low HER2-expressing cell lines, the clustering of HER2-targeting ligands into a ‘sticky patch’ on the surface of the liposome resulted in increased binding reactivity when compared to a uniform presentation of HER2-targeting ligands on the liposome surface. We also found that varying the size of the sticky patch being presented

to a HER2 receptor varied the equilibrium dissociation constants and dissociation rate constants of the nanoparticles against low HER2-expressing cells. For larger patch sizes, we detected smaller K_D and k_{off} values that eventually converged to a maximum value for configurations extended over more than 30% of the total surface area of the liposome.

In Chapter 3, we further developed HER2-targeting sticky liposomes by loading the nanoparticles with doxorubicin and testing their binding reactivity and killing efficacy against a number of different breast cancer cell lines with variable HER2 expression (from 54,000 to 1,3000,000 HER2 copies per cell) and normal healthy cells expressing minimal, but not insignificant amounts of HER2 [29]. We found that at acidic pH values, sticky liposomes exhibited specific binding and effective killing after delivering lethal doses of chemotherapeutic to traditionally untargetable 'HER2-negative' MCF7 and Triple Negative Breast Cancer (TNBC) MDA-MB-231 cells. Sticky liposomes were not cytotoxic to normal breast epithelial cells and human cardiomyocytes. Additionally, we found that sticky liposomes utilized both clathrin- and caveolar-mediated endocytosis, and upon entering the cell, exhibited fast perinuclear localization which ultimately improves the trafficking of doxorubicin to its main molecular target (i.e. the nucleus). It was hypothesized that sticky liposomes utilize only one HER2-receptor underneath the projected area of the nanoparticle to bind to the cell, and this theory was corroborated by equilibrium dissociation constant (K_D) and dissociation rate constant (k_{off}) values which were independent of HER2-expression.

In Chapter 4, we tested the pre-clinical feasibility for HER2-targeting sticky liposomal doxorubicin to be used as a therapy for TNBC by testing liposomal efficacy against multicellular spheroids - treated as solid tumor surrogates - comprised of TNBC

cell lines under physiologically relevant exposure conditions. Here we utilized cell sublines extracted from the metastases in the auxiliary lymph node and lungs of a breast cancer mouse model which reliably forms metastases in distant organs following orthotopic human xenograft implantation. Multicellular spheroids were formed from these metastatic TNBC cell sublines then placed in a perfusion chamber system which exposed the spheroid to exponentially decaying concentrations of the therapy over time with $t_{1/2}$(clearance) similar to that *in vivo* (approximately 90 minutes following bolus i.v. administration in mice). The volume of these HER2-negative metastatic TNBC cell subline spheroids was significantly smaller after treatment with HER2-targeting sticky liposomal doxorubicin when compared to all other liposome constructs.

CHAPTER 2: STICKY LIPOSOME BINDING GEOMETRIES AFFECT APPARENT FUNCTIONALITY

Note: data in this chapter was adapted from the following manuscript which is in preparation:

Sempkowski, M., Sofou, S. "Ligand Presentation, Local Multivalency, and Cluster Size on Targeted Vesicles Determines Apparent Functionality".

2.1: Introduction

For nanoparticles in cancer chemotherapy, it is often desirable to accomplish long circulation times with rapid cellular uptake and intracellular delivery of the therapeutic payload (e.g. chemotherapeutics or radionuclides) to maximize therapeutic efficacy while minimizing the likelihood of drug resistance in cells [30]. This process is facilitated by the development of targeted delivery systems, such as liposomes, which are decorated with both polymeric hydrophilic protecting molecules and targeting-ligands, either in the form of antibodies, fusogenic proteins, hormones, or peptides [9]. Once attached to the surface of the nanoparticle, targeting ligands must be exposed and available to bind with receptors on the targeted cancer cell. For effective intracellular delivery, it is crucial that the ligand-receptor binding event leads to internalization of the nanoparticle and subsequent transport to the molecular target.

The presentation and density of ligands on the nanoparticle surface have a strong effect on ligand-receptor binding and the subsequent biological effects [31]. For conventionally targeted liposomes, the density of ligands on the surface is typically manipulated by adjusting the ratio of ligand-modified lipid to unmodified lipid, or

adjusting the chemistry and yield during the ligand-labeling process. However, these approaches are generally limited because they do not allow for control over the spatial distribution of ligands. Very few studies on ligand presentation, such as clustering of ligands on the nanoparticle surface, have been reported, yet still these groups use chemical (non-environmentally-responsive) approaches to explore the benefits of increased avidity [32] [33] [34, 35] [36]. Clustered ligand presentation has also only been explored in the context of increasing avidity to cells with high receptor expression. The influence of ligand clustering on targeting traditionally "untargetable" low receptor expressing cells is one major area of research which has gone unstudied.

In the present work, we describe a lipid-based nanoparticle system which utilizes environmental-responsiveness to control the presentation and local surface density of ligands at the carrier surface, and we test the reactivity and potential mechanism of action against both high and low HER2-expressing cells. These HER2-targeting liposomes (sticky liposomes) contain HER2-targeting short peptides (KCCYSL) [37] conjugated directly on the headgroups of lipids via a short linker (G-S-G). We have already demonstrated through acyl-tail matching that these functionalized lipids will preferentially partition into phase-separated raft-like lipid domains (patches) on the liposomes surface, resulting in high local multivalency (Figure 2.1) [38] [39]. To ensure binding selectivity, (sticky) patches are driven to form only under mildly acidic conditions, such as that of the tumor interstitium pH (pH 6.0-7.0) [28] [40]. As previously reported, decreasing (pH-tunable) electrostatic repulsion and increasing attractive (pH-independent) hydrogen bonding among the domain-forming lipids will result in lipid-phase separation and lipid-domain formation [38] [39]. This system provided a platform

for testing how cell binding would be impacted by both the effect of ligand density and ligand spatial distribution (in the form of variable cluster sizes) at the liposome surface.

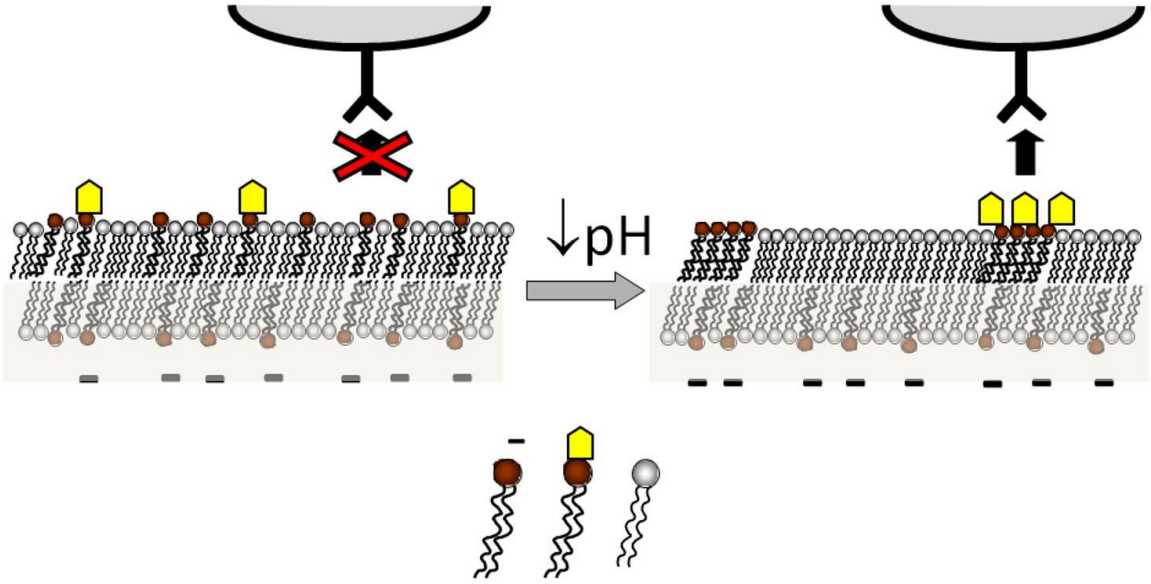

Figure 2.1: pH-dependent mechanism of sticky patch formation using ligand-labeled lipids (red lipids with yellow targeting ligands) with acyl tail lengths matching that of the titratable domain-forming lipids (plain red lipids) and mismatching that of the non-titratable lipids (plain gray lipids).

2.2: Materials and Methods

Liposome Preparation

The following lipids were used for liposome preparation: 1,2-dihenarachidoyl-sn-glycero-3-phosphocholine (21:0-PC), 1,2-diarachidoyl-sn-glycero-3-phosphocholine (20:0-PC),1,2-distearoyl-sn-glycero-3-phosphocholine (18:0-PC), 1,2-dipalmitoyl-sn-glycero-3-phosphocholine (16:0-PC), 1,2-dipalmitoyl-sn-glycero-3-phospho-L-serine (16:0-PS), 1,2-distearoyl-sn-glycero-3-phospho-L-serine (18:0-PS), 1,2-distearoyl-sn-glycero-3-phosphoethanolamine-N-[Methoxy(Polyethylene glycol)-2000] (Ammonium Salt; 18:0PE-PEG), 1,2-distearoyl-sn-glycero-3-

phosphoethanolamine-N-[PDP (Polyethylene Glycol) 2000] (Ammonium Salt; PDP-PEG), 1,2-dipalmitoyl-sn-glycero-3-phosphoethanolamineN-(succinyl) sodium salt-(Gly-Ser-Gly)-Lys-Cys-Cys-Tyr-Ser-Leu (16:0-PE-(linker)-peptide; 16:0-PE-lipopeptide), 1,2-dipalmitoyl-sn-glycero-3-phosphoethanolamine-N- (LissamineRhodamine B Sulfonyl) (Ammonium Salt; 16:0-PE-Rhodamine), 1,2-dipalmitoyl-sn-glycero-3-phosphoethanolamine-N-(7-nitro-2-1,3-benzoxadiazol-4-yl) (Ammonium Salt; 16:0-PE-NBD) and cholesterol (chol).

Liposomes were formed using the thin film hydration method. In brief, lipids suspended in chloroform or a chloroform-methanol mixture were added in a round bottom flask. All compositions contained 0-5.0 mole % cholesterol and were labeled with either 1 or 5 mole % 16:0-PE-Rhodamine. All targeted vesicles contained between 0.05-2.0 mole % of the peptide-conjugated lipid. The lipids were dried under vacuum and rotation at 55°C, followed by additional drying under N_2 gas, to result in a thin lipid film. Lipids were then hydrated in either phosphate buffered saline (PBS) with 1 mM Ethylenediaminetetraacetic acid (EDTA) at pH 7.4 for empty liposomes or 250 mM ammonium sulfate at pH 7.4 for doxorubicin-loaded liposomes and annealed at 55 °C for 2 hours. The resulting liposome suspension was extruded 21 times through two stacked polycarbonate filters (100 nm pore diameter), then eluted through a a Sepharose 4B column eluted with PBS (1 mM EDTA, pH 7.4) to separate out micelles.

Trastuzumab, the HER2-targeting monoclonal antibody, was conjugated to liposomes using standard 3-(2- pyridyldithio)propionate (PDP)-based and succinimidyl 4-(pmaleimidophenyl)butyrate (SMPB)-based click chemistry [41]. Antibodies not conjugated to liposomes were separated from antibody-labeled liposomes by passing the

lipid suspension through a Sepharose 4B column eluted with PBS (1 mM EDTA, pH 7.4). BCA assay was used to quantify the concentration of antibodies in the purified antibody-labeled liposome suspension. The average number of antibodies per liposome was then calculated on the basis of the total lipid, the headgroup surface area per lipid (48 $Å^2$ for lipids in the gel phase), and the measured mean size of liposomes.

Lipopeptide synthesis and characterization

Standard Fmoc solid-phase peptide synthesis procedures were used to prepare the peptide Gly-Ser-Gly-Lys-Cys-Cys-Tyr-Ser-Leu on a 0.10 nmole scale. In brief, 20% (v/v) piperidine/DMF was used for 30 minutes to remove the Fmoc group. Fmoc amino acids (0.5 mmoles) were then activated with HBTU (0.45 mmoles) and 5% (v/v) DIEA/DMF and allowed to react for 30 min at 60 °C using microwave irradiation. The carboxylic acid of the 1,2-dipalmitoyl-sn-glycero-3-phosphoethanolamine-N-(succinyl) lipid was coupled to the free amine at the N-terminus of the peptide (while still on the resin). Peptide coupling reactions were carried out using PyBOP, HOBt, and NMM for 1.0, 1.0, and 1.5 equivalents, respectively. The peptide and lipid were utilized at 5 and 7 times excess equivalents, respectively. Coupling was conducted in DMF overnight at room temperature with continuous agitation. The resin was filtered out with a fritted solid-phase extraction tube then washed with DCM (3 × 5 ml), DMF (3 × 5 ml), and DCM (3 × 5 ml). The cleavage cocktail TFA/thioanisole/H2O/phenol/EDT 82.5%/5%/5%/5%/2.5% (v/v/v/v/v) was used to cleave the lipopeptide from the resin and remove all amino acid protecting groups. The cleaved mixture was filtered and

concentrated using a rotary evaporator. The lipopeptide was precipitated by slowly adding cold diethyl ether.

The final lipopeptide product was characterized using a liquid chromatograph–mass spectrometer. About 1 mg of the lipopeptide was added in 1 ml of 0.1% aqueous TFA with methanol and 6 μL was injected into an LCMS with 75%/25% (v/v) methanol in 0.1% aqueous formic acid used as the eluent. Because the purity of the product was > 90%, no additional purification steps were taken.

Cell Lines

BT-474, MCF7 and MDA-MB-231 breast cancer cell lines were maintained in HybriCare, EMEM and DMEM cell culture media, respectively, supplemented with 10% FBS, 100 units/mL penicillin and 100 μg/mL streptomycin. EMEM media was additionally supplemented with 0.01 mg/mL bovine insulin. All cells were propagated in a humidified incubator at 37 °C and 5% CO2.

Cell Association of Liposomes as a Function of Extracellular pH

Cells were incubated in suspension with 16:0-PE-Rhodamine labeled liposomes (1:10 liposomes/HER2 receptors, 10×10^6 cells per mL) over a range of pH values for six hours in a humidified incubator at 37 °C and 5% CO_2. At the end of incubation, cells were washed thrice with sterile PBS (pH 7.4) via centrifugation, resuspended and measured for the fluorescence intensity of rhodamine (excitation/emission = 550 nm/590 nm). Depending on the rhodamine-lipid concentration, cells were lysed to relieve the self-quenching of 16:0-PE-Rhodamine before measurement.

Calcein Retention by Liposomes in the Presence of Cells

In parallel to cell association studies, cells were incubated in suspension with liposomes encapsulating 55 mM self-quenching calcein (1:10 liposomes/HER2 receptors, 10×10^6 cells per mL) over a range of pH values for six hours. At the end of incubation, cells were pellet via centrifugation and the supernatant only was collected and measured for calcein quenching efficiency (Q), defined as $Q = I_t/I_i$, where I_i and I_t represent the fluorescence intensity of calcein (excitation/emission = 495 nm/515 nm) measured before and after the addition of the detergent Triton-X 100 (5% w/v), respectively. Calcein release was quantified by calculating the relative decrease in calcein's self-quenching efficiency defined as $\%released = (Q_t\text{-}1)/(Q_{max}\text{-}1) \times 100$, where Q_t is the quenching efficiency at the time of the experiment, Q_{max} is the quenching efficiency of liposomes right before incubation with cells, and 1 corresponds to the lack of quenching.

Characterization of Liposomes' Effective Equilibrium Dissociation Constants (K_D) and Dissociation Rate Constants (k_{off})

Equilibrium dissociation constants for all functionalized liposome constructs were measuring on suspended cells at a fixed concentration, on ice, using saturation experiments of increasing concentrations of targeted fluorescent liposomes in the absence and presence of a 30-fold excess of targeted non-fluorescently-labeled liposomes at two different cell concentrations. K_D values were evaluated via the law of mass action ($liposome_{free} + antigen_{free} \overset{K_D = \frac{k_{off}}{k_{on}}}{\Longleftrightarrow} complex$) by first assuming that the measured cell-bound liposomes formed liposome–antigen complexes (C) (and that the complex

consisted of at least one antigen (Ag) associated with each bound liposome), and second, that at equilibrium the number of available (free) antigens was equal to the total number of antigens (Ag_{total}) corrected by the numbers of complexes ($Ag_{free} = Ag_{total} - C$).

Effective dissociation rate constants (k_{off}) of targeted liposomes were measured in the absence of cell internalization and under variable conditions for HER2 diffusion. For free HER2 receptor diffusing conditions, cells were first incubated for 30 minutes at 37 °C in the presence of 20 μg/mL chlorpromazine and 5 mg/mL genistein to shut down clathrin- and caveolar-mediated endocytosis, respectively. For little to no HER2 receptor diffusion, cells were pre-incubated for 30 minutes at 4 °C. HER2 receptor diffusion was permanently stopped by fixing cells in 4% paraformaldehyde then washing thrice in sterile PBS. After the pre-incubation steps, cells were incubated with 16:0-PE-Rhodamine labeled liposomes (10×10^6 cells per mL) for 2 hours at either 37 °C + inhibitors, 4 °C , or 37 °C + fixation at a 5:1 ratio of liposomes/HER2 receptors to result in significant amounts of bound liposomes to cells . The cells were then introduced to liposome-free cell culture medium at t=0 (at either 37 °C + inhibitors, 4 °C , or 37 °C + fixation) and the decreasing association of liposomes to cells was measured on aliquots of suspended cells over time. In parallel, dissociated rate constants of nonspecifically bound (physisorbed) liposomes were measured by performing the incubation under identical conditions with nonfunctionalized liposomes. Fluorescence intensities corresponding to specific cell-association by targeted liposomes was first corrected by subtraction of the corresponding fluorescence intensities of non-targeted liposome dissociation, then fitted with a single-exponential decay over time.

2.3: Results

The central design idea was to use a non-titratable lipid (shown with gray headgroups on Figure 2.1) with long saturated acyl-tails (21:0), and different ratios of two types of titratable patch-forming lipids (shown with red headgroups on Figure 2.1) with different acyl-tail lengths (16:0 and 18:0). Since phase-separation and patch formation is mostly driven by headgroup-headgroup interactions, systematic variation of the acyl-tail composition of the patch-forming lipids was expected to alter the extent to lipid packing order within patches and to, therefore, adjust to effective preferential partition of the peptide-conjugated lipid (on 16:0-PE) within the patches. The different partition function would result in different local peptide densities within the patches and different binding reactivities.

Cell Association of Liposomes as a Function of Extracellular pH: Effect of Lipid Headgroup and of Local Patch Valency

Figure 2.2 A and B show the effect of headgroup's specific apparent pKa (~6.0 for phosphatidyl serine [42] and ~5.5 for phosphatidic acid [43] on tuning the pH at which selective binding to the HER2 receptors occurs. In all cases, lowering of pH resulted in increased cell binding reactivity. For these studies the HER2-overexpressing cells BT474 were used. Each of Figures 2.2 A and B demonstrates that the measured binding reactivity was affected by the extent of partition of lipopeptide (with 16:0 acyl tails length) in lipid patches - formed with lowering pH - that were designed to contain variable combinations of 16:0 and 18:0 acyl-tail lengths. Clearly, increased levels of 16:0-PA lipid within the patch provided a better match in lipid packing with the

lipopeptide resulting in greater reactivities at less acidic pH, i.e. at functionalized patches of smaller sizes.

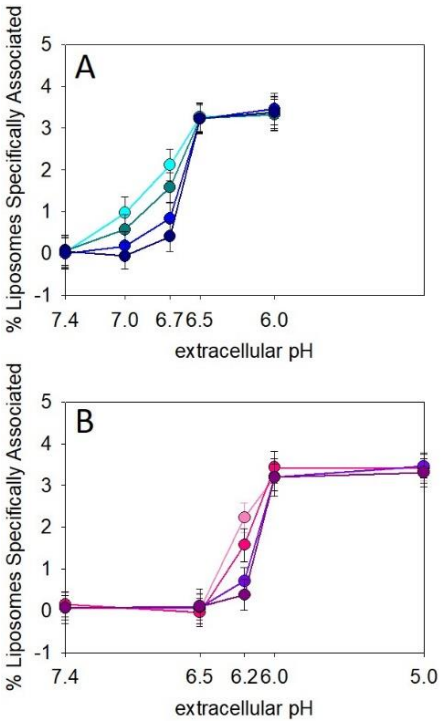

21:0-PC	**16:0-PS**	**18:0-PS**	16:0-PE-peptide conjugated lipid	18:0PE-PEG	cholesterol	pH-responsive
7	3	0	0.1	1.3	0.5	✓
7	2	1	0.1	1.3	0.5	✓
7	1	2	0.1	1.3	0.5	✓
7	0	3	0.1	1.3	0.5	✓
21:0-PC	**16:0-PA**	**18:0-PA**	16:0-PE-peptide conjugated lipid	18:0PE-PEG	cholesterol	pH-responsive
7	3	0	0.1	1.3	0.5	✓
7	2	1	0.1	1.3	0.5	✓
7	1	2	0.1	1.3	0.5	✓
7	0	3	0.1	1.3	0.5	✓

Figure 2.2: Effect of lipopeptide's sticky-patch partition on the binding reactivity of liposomes specifically associated with ***high HER2-expressing BT474 cells*** using (A) phosphatidyl serine and (B) phosphatidic acid titratable patch forming lipids. Specific association is calculated by subtracting the effect of the corresponding non-targeted liposomes. Lines are guides to the eye. Errors correspond to standard deviations of repeated measurements (one sample per vesicle preparation, three independent vesicle preparations). Liposome-to-receptor ratio incubation conditions were kept constant at 1-to-10 across all constructs and cell lines. Table values indicate molar ratios of lipids for each liposome composition.

Cell Association of Liposomes as a Function of Extracellular pH: Effect of Functionalized Lipid Concentration

Figure 2.3 shows the effect of lipopeptide concentration on the increasing cell binding reactivity with lowering pH (i.e. with increasing the extent of patch formation) using HER2-overexpressing cells. Comparison between Figures 2.3. A and B aims to demonstrate the effect of preferential partition of the lipopeptide (on 16:0-PE lipid)

relative to lipid patches composed of protonated 16:0-PS (in A) and 18:0-PS (in B). It is clear for the case of patches composed of lipids with identical acyl-tail lengths as the functionalized lipid, all different compositions of lipopeptide used resulted in similar binding activities, probably due to the already extensive partition within the lipid phase-separated patch. For the case where the partition was less optimal, variation in binding reactivity should be a demonstration of lower partition within the patch. FRET studies (data not shown) supported the different extents of partition within the phase-separated domains. Specific binding of targeted non-pH-responsive liposomes with 1.0 mole % 16:0-PE-peptide conjugated lipid demonstrated specific binding values around 2.0% independent of extracellular pH.

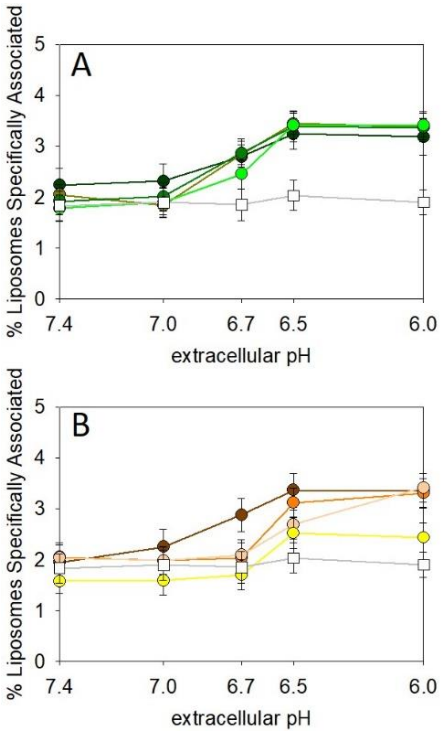

21:0-PC	16:0-PC	16:0-PS	**16:0-PE-peptide conjugated lipid**	18:0PE-PEG	cholesterol	pH-responsive
7	0	3	0.1	0.01	0.5	✓
7	0	3	0.02	0.01	0.5	✓
7	0	3	0.01	0.01	0.5	✓
7	0	3	0.005	0.01	0.5	✓
0	10	0	0.1	0.01	0.5	×

21:0-PC	16:0-PC	18:0-PS	**16:0-PE-peptide conjugated lipid**	18:0PE-PEG	cholesterol	pH-responsive
7	0	3	0.1	0.01	0.5	✓
7	0	3	0.02	0.01	0.5	✓
7	0	3	0.01	0.01	0.5	✓
7	0	3	0.005	0.01	0.5	✓
0	10	0	0.1	0.01	0.5	×

Figure 2.3: Effect of lipopeptide concentration on the binding reactivity of liposomes specifically associated with ***high HER2-expressing BT474*** cells using (A) phosphatidyl serine and (B) phosphatidic acid titratable patch forming lipids. Specific association is calculated by subtracting the effect of the corresponding non-targeted liposomes. Lines are guides to the eye. Errors correspond to standard deviations of repeated measurements (one sample per vesicle preparation, three independent vesicle preparations). Liposome-to-receptor ratio incubation conditions were kept constant at 1-to-10 across all constructs and cell lines. Table values indicate molar ratios of lipids for each liposome composition.

To observe the effect of HER2-targeting lipo-peptide density on sticky liposome binding to low HER2-expressing cells, MCF7 cells (54,000 HER2 copies per cell) were incubated with minimally PEGylated (0.1 mole %) liposomes (Figure 2.4). A table summarizing the lipid compositions is shown below. As shown in HER2-positive cells, increasing cell binding reactivity was observed with lowering pH and with increasing the concentration of functionalized lipids. Uniformly functionalized liposomes (either with the same

peptides or with HER2-targeting antibodies) exhibited only low and non-pH-dependent cell association.

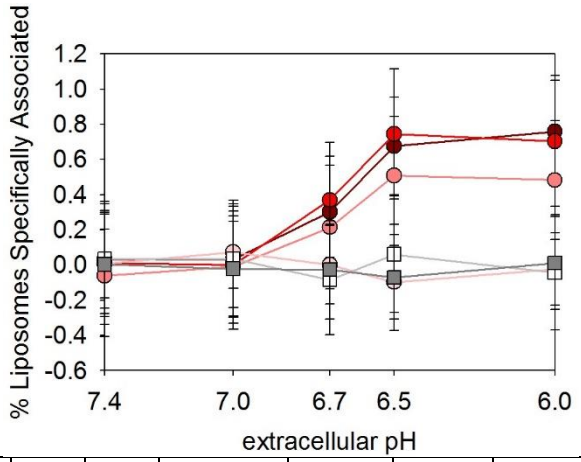

21:0-PC	16:0-PC	18:0-PC	16:0-PS	**16:0-PE-peptide conjugated lipid**	HER2-targeting Ab*	18:0PE-PEG	cholesterol	pH-responsive
7	0	0	3	0.2	0	0.01	0.5	✓
7	0	0	3	0.15	0	0.01	0.5	✓
7	0	0	3	0.1	0	0.01	0.5	✓
7	0	0	3	0.02	0	0.01	0.5	✓
0	10	0	0	0.1	0	0.01	0.5	×
0	0	7	0	0	19	0.5	3	×

Figure 2.4: Effect of lipopeptide concentration on the binding reactivity of liposomes specifically associated with ***low HER2-expressing MCF7*** cells using phosphatidyl serine titratable patch forming lipids. Specific association is calculated by subtracting the effect of the corresponding non-targeted liposomes. Lines are guides to the eye. Errors correspond to standard deviations of repeated measurements (one sample per liposome preparation, three independent liposome preparations). Liposome-to-receptor ratio incubation conditions were kept constant at 1-to-10 across all constructs and cell lines. Table values indicate molar ratios of lipids for each liposome composition. *values represent that average number of trastuzumab HER2-targeting antibodies conjugated per vesicle.

Cell Association of Liposomes as a Function of Extracellular pH: Effect of Cholesterol

Our group has previously demonstrated that cholesterol acts against phase separation and formation of domains comprised of lipids with long saturated acyl-tails [38]. Unlike liquid-ordered lipid domains whose formation is facilitated by the presence

of cholesterol, gel-phase-like domains exhibit opposite dependence. We have attributed this observation to the type of molecular lipid packing within the hydrophobic regions of the domains. In the case of gel-phase-like bilayers, cholesterol may possibly be perceived as an impurity that disrupts the tight packing between lipids which - for the lipid compositions studied herein - is primarily driven by hydrogen bonding originating in the headgroups resulting in smaller areas-per-headgroup. To understand the effect of cholesterol content on cell association to low HER2-expressing cells, MCF7 cells (54,000 HER2 copies per cell) were incubated with minimally PEGylated (0.1 mole %) and 16:0PE-peptide-functionalized (2.0 mole %) pH-responsive 16:0-PS (sticky) liposomes, and specific cell association was measured as a function of extracellular pH and percentage of cholesterol added to the membrane (Figure 2.5). The liposome compositions are shown below in a table. Figure 2.5 shows that lowering the amount of cholesterol increased that extent of binding at acidic pH values studied. Specific binding of liposomes with uniform presentation of the same concentration of lipopeptide was negligible on low HER2-expressing MCF7 cells.

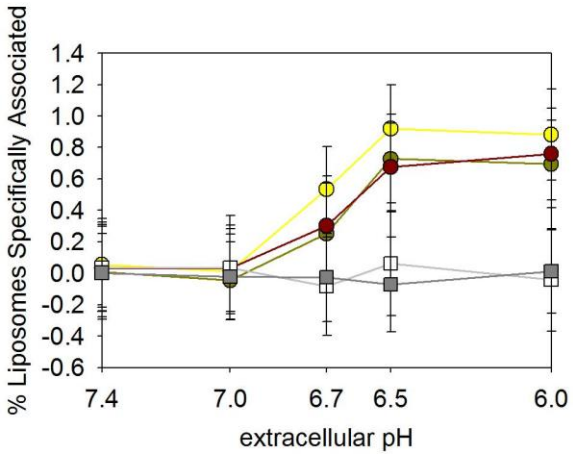

21:0-PC	16:0-PC	18:0-PC	16:0-PS	16:0-PE-peptide conjugated lipid	HER2-targeting Ab*	18:0PE-PEG	**cholesterol**	pH-responsive
7	0	0	3	0.2	0	0.01	0	✓
7	0	0	3	0.2	0	0.01	0.25	✓
7	0	0	3	0.2	0	0.01	0.5	✓
0	10	0	0	0.1	0	0.01	0.5	×**
0	0	7	0	0	19	0.5	3	×**

Figure 2.5: Effect of cholesterol on the binding activity of liposomes specifically associated with ***low HER2-expressing MCF7*** cells using phosphatidyl serine titratable patch-forming lipids. Specific association is calculated by subtracting the effect of the corresponding non-targeted liposomes. Lines are guides to the eye. Errors correspond to standard deviations of repeated measurements (one sample per liposome preparation, three independent liposome preparations). Liposome-to-receptor ratio incubation conditions were kept constant at 1-to-10 across all constructs and cell lines. Table values indicate molar ratios of lipids for each liposome composition. *values represent that average number of trastuzumab HER2-targeting antibodies conjugated per vesicle. ** compositions resulted in uniform presentation of ligands on the surface of liposomes.

Content Retention by Liposomes in the Presence of Cells

An inherent property of the lipid phase separation on these vesicles (as described in this thesis) is the formation of lipid-packing defects along the boundaries of the different lipid phases: 21:0 vs. 16:0 vs. 18:0 carbon lengths. The effects of titratable lipid composition on liposome content retention (the self-quenching fluorophore calcein, in the presence of BT-474 cells) as a function of pH, titratable lipid content and phospholipid tail lengths was studied. The various liposome compositions are shown on the table

below. Again, as shown in Figure 2.2, the pH at 50% of released contents depended on the effective pKa's of the titratable lipids used. In both Figures 2.6 A and B, the greater the difference between the acyl-tail lengths (21:0 and 16:0 vs. 21:0 and 18:0) the more extensive the content release with lowering pH.

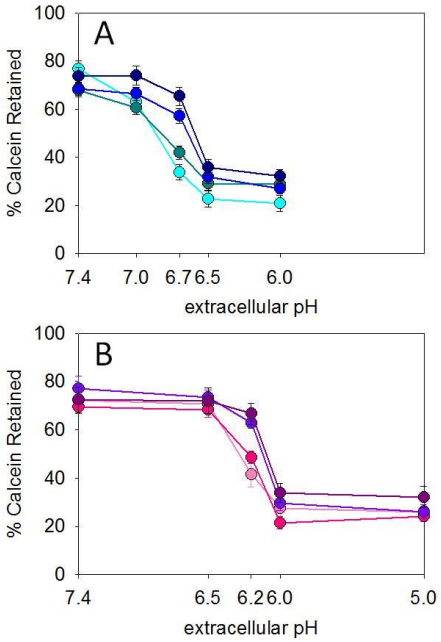

21:0-PC	**16:0-PS**	**18:0-PS**	16:0-PE-peptide conjugated lipid	18:0PE-PEG	cholesterol	pH-responsive
7	3	0	0.1	1.3	0.5	✓
7	2	1	0.1	1.3	0.5	✓
7	1	2	0.1	1.3	0.5	✓
7	0	3	0.1	1.3	0.5	✓
21:0-PC	**16:0-PA**	**18:0-PA**	16:0-PE-peptide conjugated lipid	18:0PE-PEG	cholesterol	pH-responsive
7	3	0	0.1	1.3	0.5	✓
7	2	1	0.1	1.3	0.5	✓
7	1	2	0.1	1.3	0.5	✓
7	0	3	0.1	1.3	0.5	✓

Figure 2.6: Content retention in the presence of BT-474 cells by PEGylated liposomes rich in (A) phosphatidyl serine and (B) phosphatidic acid titratable patch forming lipids. Lines are guides to the eye. Errors correspond to standard deviations of repeated measurements (one sample per vesicle preparation, three independent vesicle preparations). Table values indicate molar ratios of lipids for each liposome composition.

The amount of functionalized lipid did not affect content retention by sticky liposomes as shown on Figure 2.7 at different pH values. Calcein retention of non-pH responsive liposomes was stable and did not fluctuate with varying extracellular pH.

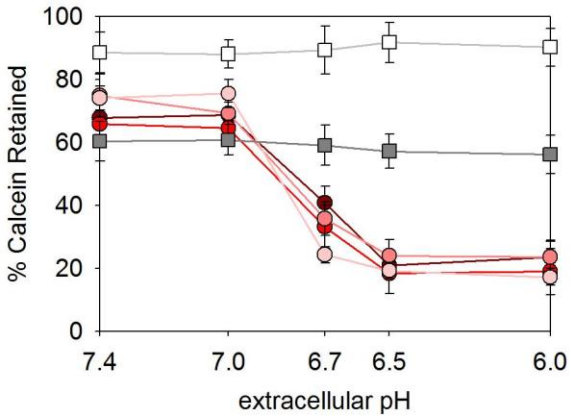

21:0-PC	16:0-PC	18:0-PC	16:0-PS	**16:0-PE-peptide conjugated lipid**	HER2-targeting Ab*	18:0PE-PEG	cholesterol	pH-responsive
7	0	0	3	0.2	0	0.01	0.5	✓
7	0	0	3	0.15	0	0.01	0.5	✓
7	0	0	3	0.1	0	0.01	0.5	✓
7	0	0	3	0.02	0	0.01	0.5	✓
0	10	0	0	0.1	0	0.01	0.5	×
0	0	7	0	0	19	0.5	3	×

Figure 2.7: Effect of lipopeptide content on calcein retention in the presence of MCF7 cells by PEGylated liposomes rich in phosphatidyl serine titratable patch-forming lipids and varying amounts of 16:0-PE peptide-conjugated lipid. Lines are guides to the eye. Errors correspond to standard deviations of repeated measurements (one sample per liposome preparation, three independent liposome preparations). Table values indicate molar ratios of lipids for each liposome composition. *values represent that average number of trastuzumab HER2-targeting antibodies conjugated per vesicle.

The effect of the amount of cholesterol on retention of liposome contents (calcein) is shown in Figure 2.8, and the specific vesicle compositions are shown in the table below. Increasing amounts of cholesterol resulted in greater content retention at higher pH values when lipid phase-separation was limited. This is in agreement with a role of cholesterol in decreasing the extents of defects in lipid packing within the phase-separated interphases and/or in compromising tight lipid packing within the phase-separated domains. Non-pH responsive liposomes with minimal PEGylation (0.1 mole %) and lipo-peptide-functionalization (2.0 mole %) or moderate PEGylation (5 mole %)

and trastuzumab-functionalization via PEG-tethers were also measured as a function of pH. Calcein retention of non-pH-responsive liposomes was stable and did not fluctuate with varying extracellular pH.

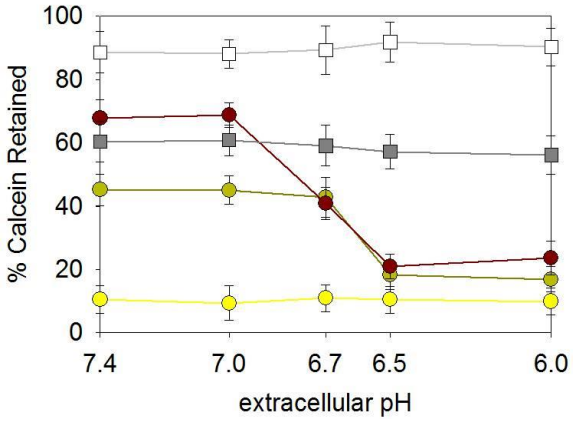

21:0-PC	16:0-PC	18:0-PC	16:0-PS	16:0-PE-peptide conjugated lipid	HER2-targeting Ab*	18:0PE-PEG	**cholesterol**	pH-responsive
7	0	0	3	0.2	0	0.01	0	✓
7	0	0	3	0.2	0	0.01	0.25	✓
7	0	0	3	0.2	0	0.01	0.5	✓
0	10	0	0	0.1	0	0.01	0.5	×
0	0	7	0	0	19	0.5	3	×

Figure 2.8: Effect of cholesterol on calcein retention in the presence of MCF7 cells by PEGylated liposomes rich in phosphatidyl serine titratable patch forming lipids. Lines are guides to the eye. Errors correspond to standard deviations of repeated measurements (one sample per liposome preparation, three independent liposome preparations). Table values indicate molar ratios of lipids for each liposome composition. *values represent that average number of trastuzumab HER2-targeting antibodies conjugated per vesicle.

Characterization of Liposomes' Effective Equilibrium Dissociation Constants (K_D) and Dissociation Rate Constants (k_{off})

On low HER2-expressing MDA-MB-231 cells, equilibrium dissociation constants (K_D) of pH-responsive sticky liposomes (presenting variable sized sticky patches) and non-pH-responsive liposomes (presenting an '100%' patch) at an extracellular pH of 6.5

were evaluated for different amounts of titratable lipid in the membrane and lipopeptide grafting densities (Table 2.1). For the same total concentration of lipopeptide, K_D values were significantly higher for smaller patch size liposomes (e.g. 5% patch) when compared to larger patch size liposomes (e.g. 30% and 50% patch) (*p*-value < 0.01). pH-responsive liposomes with larger patch sizes (50% patch) had comparable K_D values to '100%' patch liposomes with 5 mole % lipo-peptide.

Table 2.1: Equilibrium Dissociation Constants (K_D) at pH 6.5 at different experimental conditions for pH-responsive sticky liposomes (variable patch sizes) and non-pH-responsive ('infinite patch') liposomes on HER2-negative MDA-MB-231 breast cancer cells (83,000 HER2 receptor per cell). *assuming complete partitioning of lipo-peptide into the patch.

maximum projected [lipo-peptide] within patch (mole %)*	**% patch area of total vesicle surface area**	**Total [lipo-peptide] (mole %)**	**K_D (μM total lipid)**
20	5	1	29.8 ± 2.7
10	10	1	24.1 ± 2.1
3.3	30	1	17.3 ± 0.6
2.0	50	1	20.0 ± 1.7
3.0	100	3	25.5 ± 1.4
5.0	100	5	19.1 ± 2.5

On Table 2.2, comparison between the fifth the sixth columns (fixed cells at 37^{o}C vs. 4^{o}C) demonstrated that the effect of temperature on dissociation kinetics was undetectable. Comparison between the last four constructs with '100%' patch showed that at least approximately equal or greater than 3 mole % local peptide densities were necessary to result in binding to isolated HER2 receptors with this new binding geometry.

For all detectable constructs, significantly longer dissociation half-lives were witnessed when cells were incubated at 37 ºC in the presence of inhibitors when compared to cells incubated at either 4 ºC or 37 ºC after cell fixation (p-value < 0.01).

Table 2.2: Dissociation Rate Constants (k_{off}) at pH 6.5 at different experimental conditions for pH-responsive sticky liposomes (variable patch sizes) and '100% patch' liposomes on HER2-negative MDA-MB-231 breast cancer cells (83,000 HER2 receptor per cell). '100% patch' liposomes with 3 and 5 % lipopeptide have comparable dissociation half-lives under all incubation conditions (p-value > 0.05).

maximum projected [lipo-peptide] within patch (mole %)*	% patch area of total vesicle surface area	Total [lipo-peptide] (mole %)	*37ºC + endocytosis inhibitors (freely diffusing receptors)*		*4ºC (little/no receptor diffusion)*		*37ºC + fixed cells (no receptor diffusion)*	
			k_{off} (min^{-1})	$t_{1/2}$ (min)	k_{off} (min^{-1})	$t_{1/2}$ (min)	k_{off} (min^{-1})	$t_{1/2}$ (min)
20	5	1	0.0130 ± 0.0002	54 ± 1	0.0181 ± 0.0004	38 ± 1	0.0177 ± 0.0007	39 ± 2
10	10	1	0.0056 ± 0.0004	125 ± 8	0.0098 ± 0.0012	71 ± 9	0.0092 ± 0.0012	76 ± 10
3.3	30	1	0.0044 ± 0.0004	160 ± 13	0.0081 ± 0.0004	86 ± 4	0.0081 ± 0.0003	86 ± 3
2.0	50	1	0.0046 ± 0.0006	152 ± 19	0.0077 ± 0.0003	90 ± 3	0.0079 ± 0.0004	88 ± 5
1.0	100	1	undetectable	undetectable	undetectable	undetectable	undetectable	undetectable
2.0	100	2	undetectable	undetectable	undetectable	undetectable	undetectable	undetectable
3.0	100	3	0.0060 ± 0.0004	117 ± 7	0.0099 ± 0.0004	70 ± 3	0.00102± 0.0005	68 ± 3
5.0	100	5	0.0049 ± 0.0004	142 ± 13	0.0077 ± 0.0005	91 ± 6	0.0084 ± 0.0004	83 ± 4

Comparison between the fourth and sixth columns showed consistently increased half-lives of dissociation when free diffusion of HER2 receptors was allowed on the surface of cells. On Figure 2.9, the ratios of the dissociation kinetics in the presence over the absence of receptor diffusion at 37^{o}C converged with increasing patch sizes to values approximately not much greater than those exhibited by liposomes containing patches that occupied 30% of the vesicle's surface area. This behavior suggests the recruitment of additional receptors upon association with an initially isolated HER2 receptor.

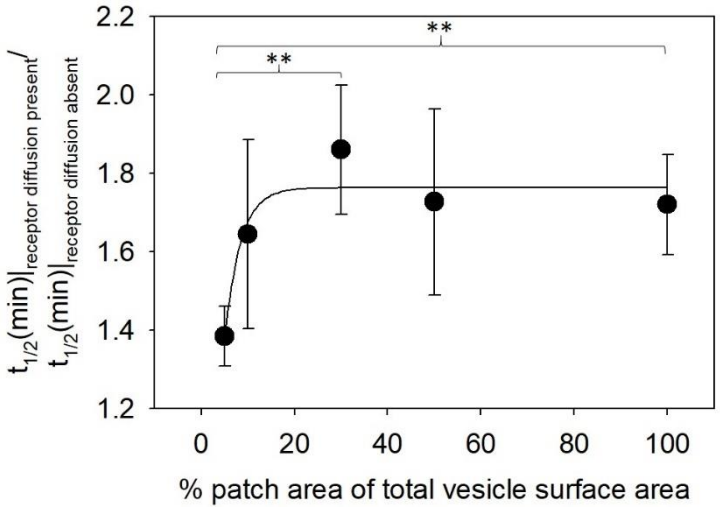

Figure 2.9: Ratio of dissociation half-lives in the presence over the absence of HER2 diffusion for liposomes presenting variable sized sticky patches. Lines are guides to the eye. Errors correspond to standard deviations of repeated measurements (one sample per liposome preparation, two independent liposome preparations).

2.4: Discussion

Targeted liposomes potentiate rapid cellular binding and internalization, and subsequent intracellular delivery of cancer therapies. Traditionally targeted liposomes are decorated with uniformly spaced antibodies or peptides, and at ligand densities which are often modified at the fabrication step through changing lipid composition, or later in the

development phase through chemical means. Consequently, ligand presentation and density on the surface of the nanoparticle has not been explored by means of environmental-responsiveness, and in terms of spatial distribution of the ligands. These phenomena have also been restricted to exploration on high receptor-expressing cells, and the effect on low receptor-expressing cells remains unanswered.

In this study, we characterized the binding geometries on HER2-targeting sticky liposomes by varying ligand presentation, local multivalency and cluster size. On high HER2-expressing BT474 cells, HER2-targeting sticky liposomes with minimal PEGylation in their non-phase separated form (pH 7.4) demonstrated measurable specific binding. This binding increased significantly at acidic pH values mimicking that of the tumor interstitium (pH 6.0-7.0) when the liposome's membrane was phase separated and presenting dense clusters of HER2-targeting ligands (sticky patches) with a very high local multivalency. When the same constructs were tested on BT-474 cells, but this time with dense PEGylation, masking of the lipopeptides at neutral pH prevented specific binding. Only when the liposome phase separated and PEG was pulled out and away from the sticky patch did the liposomes demonstrate specific binding capabilities. On low HER2-expressing MCF7 cells, minimally PEGylated HER2-targeting sticky liposomes exhibited measurable specific binding only under acidic conditions when ligands were densely packed into a sticky patch. Increasing the local density of lipopeptides in the patch resulted in a trend towards enhanced specific binding.

We are currently in the process, with collaborators, of constructing a mathematical model to simulate our observations on binding and internalization in the presence of surface diffusion of the HER2 receptors. Regarding our current mechanism

hypothesis, for clarity we consider a compartmental description, shown in Figure 2.10, to best present our current understanding of the processes involved, in the spirit of G. Bell's original incisive analysis [44] of cell/receptor interactions: (1) from the bulk solution (A) sticky lipid nanoparticles are transported to "near surface" compartment (B); we use a mass transfer rate constant k_{AB} (for "bulk-near") just for illustrative purposes here. (2) receptors from the "far surface" cell membrane (compartment C) diffuse to the "near surface" compartment; we again use a mass transfer rate constant k_{CB} for this step. All the action occurs in compartment B: if the sticky patch acquires the right orientation in the neighborhood of a free receptor, a binding event may take place. Receptors are few and far between. We do not expect two of them to lie within the projection footprint of our near-surface nanoparticle – and without the sticky patches, we know that single ligand-receptor binding events are too short-lived to keep the nanoparticle (subject to the Brownian interactions with the solvent) bound to the cell long enough to get internalized. The dissociation studies in the presence and absence of HER2 diffusion, suggest that at least a second receptor becomes associated with the specifically bound sticky liposomes.

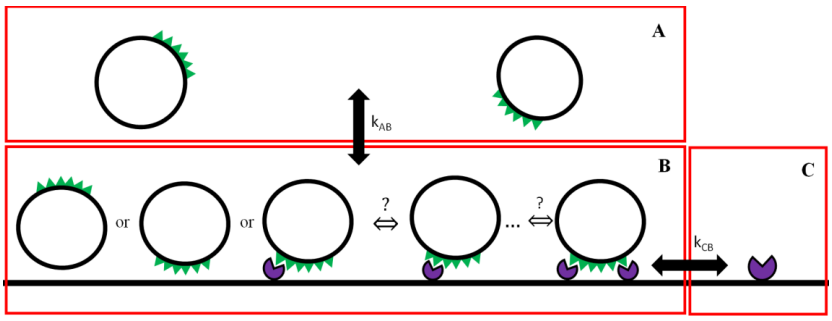

Figure 2.10: A caricature of our current mechanism hypothesis: nanoparticles are transported from the bulk (**A**) to near the cell surface (**B**); the (green) ligands in the sticky patch repeatedly bind/unbind to the (purple) nearby lone receptor; if the (repeated, we postulate) binding lasts long enough, a second, faraway (**C**) cell receptor may have time to wander nearby and participate.

In this work, we examined how the spatial distribution and density of HER2-targeting ligands on the surface of sticky liposomes affected cell binding to both high and low levels of HER2, in an effort to better understand how ligand patterning controls binding reactivity. Here we demonstrated that lipopeptide clustering resulted in high local multivalency leading to increase avidity on both high and low HER2-expressing cells. This high local multivalency can stretch over smaller or larger areas of the lipid nanoparticle as a function of smaller or larger sticky patch sizes, which strongly affects both binding and dissociation properties.

CHAPTER 3: HER2 EXPRESSION DICTATES REACTIVITY AND EFFICACY OF STICKY LIPOSOMAL DOXORUBICIN

Note: data in this chapter was adapted from the following publication:

Sempkowski, M., Zhu, C., Bruchertseifer, F., Morgenstern, A., Sofou, S. "Sticky Patches on Lipid Nanoparticles Enable the Selective Targeting and Killing of Untargetable Cancer Cells." *Langmuir*, 32 (2016) 8329–38.

3.1: Introduction

Targeted nanoparticles for the treatment of solid tumors is a major area of scientific research. [45]. However, the efficacy of current nanoparticles to effectively and selectively target cancer cells is restricted by the number of target receptors (molecular markers) on the surface of the cell [23]. In this sense, the word efficacy relates to the time in which the nanoparticle is bound to the surface of the cell being long enough to allow for internalization of the nanoparticle, resulting in the delivery of therapeutic payload in close proximity to its intracellular targets (e.g. the nucleus). However, in the case of uniformly (or conventionally) targeted nanoparticles, it is required that cancer cells express at least approximately 200,000 copies of the target receptor per cell with a 19 μm diameter (or ~220 receptors per μm^2 of cell surface area) for effective targeting to occur [23] [46]. This is equivalent to having at least two receptors underneath the project area of a nanoparticle bearing a 100 nm diameter and 3 nm PEGylated corona [47]. At this receptor density, multivalent interactions (i.e. avidity) can simultaneously occur between the many cell receptors on the cell surface and many targeting ligands on the nanoparticle. This type of multivalency is considered vital for successful targeting and killing of the cell.

A broadly studied molecular marker in targeted cancer therapy is the HER2 receptor because its overexpression is common in a number of different cancer types including breast, gastric, prostate and ovarian [6] and it is typically associated with poor prognosis [48]. In breast cancer particularly, targeted therapies for the HER2 receptor are only applicable to the 30% of patients who are considered to have HER2-overexpressing (HER-positive) tumors [49]. When evaluated by immunohistochemistry, HER2-positivity corresponds to a tumor grading of 3+, or in some instances, 2+, which maps to more than 1,000,000 and 500,000 HER2 receptors per cell, respectively [8]. For the 70% of breast cancer patients whose tumors are considered to be negative for HER2, no targeted therapeutic option utilizing the HER2 receptor exists. The phrase 'HER2-negative' refers to a tumor grading of less than 1+, or less than 200,000 copies of HER2 receptors per cell.

There are two additional challenges associated with HER2 expression and targeted nanoparticle therapy. First, because HER2 is present at normal organ sites [29], the use of targeted nanoparticles is limited to only HER2-overexpressing disease [50]. Second, for HER2-overexpressing tumors, there exists significant heterogeneity of HER2 receptor levels by cancer cells comprising the same tumor [51] [52], which may compromise the effectiveness of current targeted therapies. These challenges demand alternative solutions for targeting cancer cells with low (or variable) expression of the target receptor if the benefits of targeted therapies are to be fully utilized. In this work, we describe our efforts to design alternative binding geometries between functionalized nanoparticles and HER2 receptors on breast cancer cells to study their targeting reactivity against cells with a wide range of HER2 expression levels. Different binding geometries

between ligand-bearing nanoparticles and cell receptors are presented by exploiting an environmentally responsive clustered-ligand display on the surface of the nanoparticles. Clustering of ligands on a nanoparticle surface has been previously studied [32] [33] [34, 35] [36], but with the aim of exploring the potential benefits (increased avidity) of multiple ligand−receptor interactions; that is, between many ligands on the nanoparticle and many receptors on the cell. Remarkably, these reports have not evaluated the efficacy of ligand clustering in the context of cells with low receptor expression when there exists no more than one receptor under the projected footprint of the nanoparticle. It is also important to note that these previously studied approaches for ligand clustering use chemical (non-environmentally responsive) approaches, and this is contrary to our approach. Specifically, chemically organized patches of ligands are of molecular dimensions (~2-10 ligands), while our sticky patches are of the order of several tens of nm^2 and larger than the receptor itself. These chemically organized patches can only be compared to the limiting case of our sticky liposomes at infinitesimally small 'sticky patch' sizes. This is evidenced by a recent report which demonstrates that liposomes conjugated with chemically organized tetrameric HER2-targeting peptides (identical to what we use) and incubated with MDA-MB-231 cells (identical to what we use) did not show targeting selectivity and specific killing [53].

In the present study, we developed and characterized HER2-targeting lipid based nanoparticles (sticky liposomes) that contain HER2-targeting short peptides (KCCYSL) [37] conjugated directly on the headgroups of lipids via a short linker (G-S-G). We have already demonstrated through acyl-tail matching that these functionalized lipids preferentially partition (resulting in high local multivalency) into phase-separated raft-

like lipid domains (patches) on the surface of the liposome (Figure 3.1) [38] [39]. To ensure selectiveness in binding, (sticky) patches were prompted to form only under mildly acidic conditions, such as that of the tumor interstitial pH (pH 6.0-7.0) [28] [40]. As previously reported, decreasing (pH-tunable) electrostatic repulsion and increasing attractive (pH-independent) hydrogen bonding among the domain-forming lipids would result in lipid-phase separation and lipid-domain formation [38] [39].

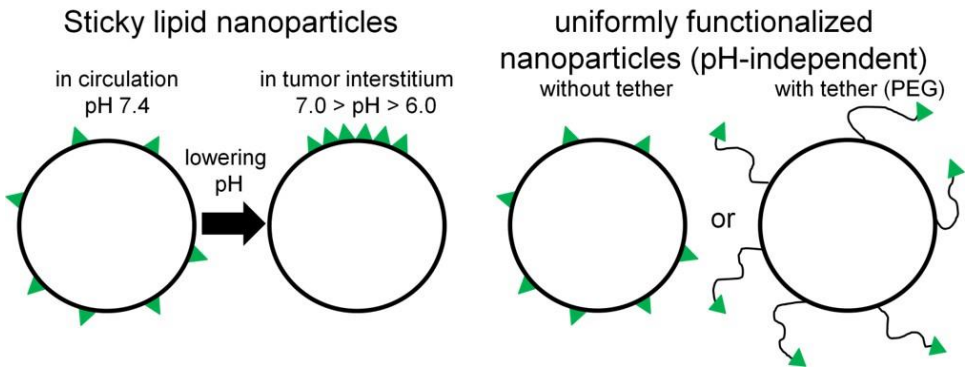

Figure 3.1: pH-responsive sticky liposomes (left) and conventionally functionalized liposomes with non-pH-responsive uniform distributions of targeting ligands (right). Sticky liposomes are engineered so that the ligands (shown in green) are homogenously distributed over the liposome's surface during circulation (pH 7.4), resulting in low reactivity. In the acidic tumor interstitium (pH 6.0-7.0), the ligand-labeled-lipids are designed to preferentially partition within a lipid phase-separated domain (sticky patch), resulting in high local multivalency and reactivity even with cells with few HER2 receptors. Uniformly functionalized particles with ligands homogenously distributed, either directly on the particles surface or associated via PEG tethers, exhibit binding reactivities that are measurable only on cells with high densities of target receptors and are undetectable on cells with low densities.

While tuning the extracellular pH, we evaluated the binding efficacy and internalization, intracellular distributions, and killing efficacy of sticky liposomes containing the clinically relevant chemotherapeutic agent, doxorubicin. We compared the performance of sticky liposomes against liposomes which were uniformly functionalized

with the same HER2-targeting peptide and liposomes uniformly functionalized with a HER2-targeting monoclonal antibody (trastuzumab) via a PEG linker (Figure 3.1). The latter construct was comparable to most of the currently pursued targeted lipid-nanoparticle constructs. All measurements were performed on breast cancer cells expressing a wide range of HER2 expression (triple negative breast cancer (TNBC) cell line MDA-MB-231, HER2-negative MCF7, and HER2-positive BT-474 cell lines), as well as normal breast cells (MCF 10A) and cardiomyocytes that express HER2 at minimal (but not insignificant) levels.

3.2: Materials and Methods

Liposome Preparation

The following lipids were used for liposome preparation: 1,2-dihenarachidoyl-sn-glycero-3-phosphocholine (21PC), 1,2-distearoyl-sn-glycero-3-phosphocholine (DSPC), 1,2-dipalmitoyl-sn-glycero-3-phosphocholine (DPPC), 1,2-dipalmitoyl-sn-glycero-3-phospho-L-serine (DPPS), 1,2-distearoyl-sn-glycero-3-phosphoethanolamine-N-[Methoxy(Polyethylene glycol)-2000] (Ammonium Salt; DSPE-PEG), 1,2-distearoyl-sn-glycero-3- phosphoethanolamine-N-[PDP (Polyethylene Glycol) 2000] (Ammonium Salt; PDP-PEG), 1,2-dipalmitoyl-sn-glycero-3-phosphoethanolamineN-(succinyl) sodium salt-(Gly-Ser-Gly)-Lys-Cys-Cys-Tyr-Ser-Leu (DPPE-(linker)-peptide; DPPE-lipopeptide), 1,2-dipalmitoyl-sn-glycero-3-phosphoethanolamine-N- (LissamineRhodamine B Sulfonyl) (Ammonium Salt; DPPE-Rhodamine), and cholesterol (chol).

Targeted liposomes contained the following components: sticky liposomes 21PC/DPPS/Chol/DPPE-lipopeptide/DSPE-PEG lipid in a 6.54:2.80:0.47:0.19:0.01 mole ratio, liposomes with uniform peptide functionalization DPPC/Chol/DPPE-lipopeptide/DSPE-PEG lipid in a 9.34:0.47:0.19:0.01 mole ratio, and liposomes with uniform antibody-tethered functionalization DSPC/Chol/DSPE-PEG/PDP-PEG lipid in a 6.67:2.86:0.29:0.19 mole ratio. Corresponding non-targeted liposome compositions did not contain functionalized lipids.

Liposomes were formed using the thin film hydration method. In brief, lipids suspended in chloroform or a chloroform-methanol mixture were added in a round bottom flask. The lipids were dried under vacuum and rotation at 55°C, followed by additional drying under N_2 gas, to result in a thin lipid film. Lipids were then hydrated in either phosphate buffered saline (PBS) with 1 mM Ethylenediaminetetraacetic acid (EDTA) at pH 7.4 for empty liposomes or 250 mM ammonium sulfate at pH 7.4 for doxorubicin-loaded liposomes and annealed at 55 °C for 2 hours. The resulting liposome suspension was extruded 21 times through two stacked polycarbonate filters (100 nm pore diameter), then eluted through a a Sepharose 4B column eluted with PBS (1 mM EDTA, pH 7.4) to separate out micelles and exchange the external buffer. Liposome size and polydispersity index were determined using a Zetasizer NanoZS90.

Liposomes were loaded with doxorubicin using the ammonium sulfate gradient method established by Haran et al [54]. In short, 1 mL of 1 mM doxorubicin dissolved in isotonic saline was added to 0.5 mL of liposomes (2.5 μmole total lipid) and incubated for 2 hours at 5°C above the highest T_g of the lipids. The lipid suspension was passed

through a Sepharose 4B column eluted with PBS (1 mM EDTA, pH 7.4, or pH 5.5 for antibody conjugation) to separate liposomes from un-entrapped doxorubicin.

Trastuzumab, the HER2-targeting monoclonal antibody, was conjugated to liposomes using standard 3-(2- pyridyldithio)propionate (PDP)-based and succinimidyl 4-(pmaleimidophenyl)butyrate (SMPB)-based click chemistry [41]. Antibodies not conjugated to liposomes were separated from antibody-labeled liposomes by passing the lipid suspension through a Sepharose 4B column eluted with PBS (1 mM EDTA, pH 7.4). BCA assay was used to quantify the concentration of antibodies in the purified antibody-labeled liposome suspension. The average number of antibodies per liposome was then calculated on the basis of the total lipid, the headgroup surface area per lipid (48 $Å^2$ for lipids in the gel phase), and the measured mean size of liposomes.

Cell Lines

BT-474, MDA-MB-231, and MCF7 breast cancer cell lines were maintained in HybriCare, DMEM and EMEM cell culture media, respectively, supplemented with 10% FBS, 100 units/mL penicillin, and 100 µg/mL streptomycin (plus 0.01 mg/mL bovine insulin for MCF7 cells). MCF10A cells were maintained in MEBM with MEGM SingleQuots (without gentamycin-amphotericin B mix) and 100 ng/mL cholera toxin. Human cardiomyocytes (Celprogen), derived from human cardiac tissue, were maintained in Human Cardiomyocyte Complete Media with Serum. All cells were propagated in a humidified incubator at 37 °C and 5% CO2. Trastuzumab radiolabeled with ^{111}In was used to evaluate the expression of cell HER2 expression using saturation experiments (of increasing concentrations of trastuzumab in the absence and presence of

a 50- fold excess of non-radiolabeled antibody) on fixed concentrations of cells on ice, as established by McDevitt et al [55].

Cell Association of Liposomes as a Function of Extracellular pH

Cells were incubated in suspension with DPPE-rhodamine-labeled liposomes (1:10 liposomes/HER2 receptors, 10×10^6 cells per mL) over a range of pH values for six hours in a humidified incubator at 37 °C and 5% CO_2. At the end of incubation, cells were washed thrice with sterile PBS (pH 7.4) via centrifugation, resuspended and measured for the fluorescence intensity of rhodamine (excitation/emission = 550 nm/590 nm). Depending on the rhodamine-lipid concentration, cells were lysed to relieve the self-quenching of DPPE-Rhodamine before measurement.

Drug Uptake by Cells, Drug Retention by Liposomes, and Liposome Cytotoxicity

Cell drug uptake was measured by plating 3000,00 cells per well on a six-well plate, followed by incubation with drug-loaded liposomes or free doxorubicin at either pH 7.4 or 6.5 for 6 hours (equivalent to the minimum circulation time of liposomes). For all constructs, doxorubicin was added at a concentration of 17.5 μg/mL using an average of 0.12 mM total lipid in a total final volume of 1 mL per well. At the end of incubation, cells were washed thrice with sterile PBS (pH 7.4), trypsinized, counted, and lysed to detect doxorubicin content (measured by fluorescence intensity, excitation/emission = 470 nm/592 nm).

Doxorubicin retention by liposomes was quantified by first collecting doxorubicin-loaded liposomes at the end of the incubation, then passing the liposome

suspension through a Sephadex G50 column equilibrated with PBS (pH 7.4) to separate out leaked doxorubicin. The percentage of doxorubicin retained in the liposomes was determined by measuring doxorubicin fluorescence intensity (excitation/emission = 470 nm/572 nm) before and after size exclusion chromatography.

In parallel to drug uptake and retention experiments, the cytotoxicity of doxorubicin loaded liposomes (or free doxorubicin) was determined using cells plated on 96-well plates at 10,000 cells per well and incubated with the same constructs at pH 7.4 and 6.5 as described above. At the end of 6 hours of incubations, cells were washed thrice with sterile PBS and further incubated with fresh medium for two population doubling times at 37 °C and 5% CO2 (38, 38, 48, 24, and 32 h for MDA-MB-231, MCF7, BT-474, cardiomyocytes, and MCF 10A, respectively). After the incubation, cell viability was measured using MTT assay.

Imaging of Intracellular Distributions of Liposomes

DPPE-rhodamine-labeled liposomes were incubated with breast cancer cell suspensions (10^6 cells/mL) at 37 °C and 5% CO_2 at a 10:1 ratio of liposomes/HER2 receptors. After different lengths of incubation, cell aliquots were removed, washed thrice with sterile PBS via centrifugation, and simultaneously fixed and stained with Hoescht 33342. Nuclei-stained and washed cells were then moved to an eight-well chambered coverglass and imaged as single cells in a monolayer using a Leica TCS SP2 confocal laser scanning microscope under an oil-immersion 100× objective. To determine the fraction of liposomes localized as a function of distance from the nucleus, an image-processing erosion algorithm was used to draw concentric circles (thickness = 3 pixels, or

0.9 μm) from the surface of the nucleus and outward until all cytoplasmic fluorescence had been accounted for.

Mechanism of Liposome Endocytosis

The internalization pathway of sticky liposomes was determined by means of endocytosis inhibition. Liposomes labeled with DPPE-Rhodamine were pre-incubated for 30 minutes in the presence of one of the following endocytosis inhibitors: 20 μg/mL chlorpromazine, hypertonic sucrose (cell culture medium supplemented with 0.45 M sucrose), 1 mg/mL Filipin III, 5 mg/mL genistein, 10 mM methyl-beta-cyclodextrin (MBCD), or for 3 hours in potassium-free buffer (50 mM HEPES, pH 7.4, 100 mM NaCl, 1 g/L glucose). At the end of incubation, functionalized liposomes were added and further incubated with cells for two hours. The cells were then pelleted via centrifugation, washed thrice with sterile PBS, then run through a flow cytometer.

Characterization of Liposomes' Effective Equilibrium Dissociation Constants (K_D), Dissociation Rate Constants (k_{off}), and Cell Internalization Rate Constants (k_{int}).

Equilibrium dissociation constants for all functionalized liposome constructs were measuring on suspended cells at a fixed concentration, on ice, using saturation experiments of increasing concentrations of targeted fluorescent liposomes in the absence and presence of a 50-fold excess of targeted non-fluorescently-labeled liposomes at two different cell concentrations. K_D values were evaluated via the law of mass action ($liposome_{free} + antigen_{free} \overset{K_D = \frac{k_{off}}{k_{on}}}{\Longleftrightarrow} complex$) by first assuming that the measured cell-bound liposomes formed liposome−antigen complexes (C) (and that the complex

consisted of at least one antigen (Ag) associated with each bound liposome), and second that at equilibrium the number of available (free) antigens was equal to the total number of antigens (Ag_{total}) corrected by a factor φ per complex, where φ was evaluated by the fit ($Ag_{free} = Ag_{total} - \varphi C$). The value of φ was used to characterize antigens that became spatially inaccessible after complex formation, for example, as a result of steric obstruction by already complexed liposomes.

Effective dissociation rate constants (k_{off}) of targeted liposomes were measured by first incubating cells on ice, with DPPE-Rhodamine-labeled liposomes (10×10^6 cells per mL) for 6 hours at a 1:10 ratio of liposomes/HER2 receptors to result in significant amounts of bound liposomes to cells. The cells were then introduced to liposome-free cell culture medium at t=0 and the decreasing association of liposomes to cells was measured on aliquots of suspended cells over time. In parallel, dissociated rate constants of nonspecifically bound liposomes were measured by performing the incubation under identical conditions with non-functionalized liposomes. Fluorescence intensities corresponding to specific cell-association by targeted liposomes was first corrected by subtraction of the corresponding fluorescence intensities of non-targeted liposome dissociation, then fitted with a single-exponential decay over time.

Cell internalization rate constants (k_{int}) were measured by first incubating cells on ice, with DPPE-Rhodamine-labeled liposomes (10×10^6 cells per mL) for 6 hours at a 1:10 ratio of liposomes/HER2 receptors to result in significant amounts of bound liposomes to cells. The cells were then incubated at 37 °C and at regular time points up to 30 minutes, cell associated (bound and internalized) liposomes were measured. Internalized liposomes were also measured after stripping off surface-bound liposomes.

Since the number of surface-bound liposomes demonstrated a significant decrease with time, k_{int} was determined from the linear slope of the plot of internalized liposomes vs the sum of surface-bound liposomes in time.

Statistical Analysis

Values are reported as the arithmetic mean of *n* independent measurements ± the standard deviation. For each measurement, the Student's *t* test was used to calculate the significant difference in behavior (e.g., in killing efficacy) between the various constructs. Calculated *p* values < 0.05 are considered to be significant.

3.3: Results

Liposome Preparation

On average, liposomes exhibited a diameter of 106 ± 4 nm with PDI = 0.075 ± 0.009 (*n* = 10). These measurements were independent of the absence or presence of functionalization. Liposomes bearing HER2-targeting lipopeptides contained 1882 lipopeptides per vesicle leaflet on average, under the assumption of lipid leaflet symmetry. For liposomes functionalized with HER2-targeting trastuzumab, 31 ± 3 antibodies were conjugated per liposomes on average. Under conditions of 50x receptor excess and in the absence of internalization, sticky vesicles exhibited specific immunoreactivities of 1.8 ± 0.2 and 2.6 ± 0.3% at pH 7.4 and 6.5, respectively ($p < 0.01$). Liposomes with a homogenous presentation of lipopeptides exhibited specific immunoreactivities of 2.0 ± 0.2 and 1.6 ± 0.2% at pH 7.4 and 6.5, respectively, and these values were pH independent ($p = 0.23$). Liposomes with a homogenous presentation of HER2-targeting trastuzumab also exhibited pH-independent specific immunoreactivities

of 18.2 ± 3.2 and 16.5 ± 2.7% at pH 7.4 and 6.5, respectively (p = 0.62). FITC-labeled trastuzumab exhibited pH-independent specific immunoreactivities of 86.3 ± 5.7 and 82.8 ± 6.7% at pH 7.4 and 6.5, respectively (p = 0.53). In the case where HER2 receptors on BT-474 cells were blocked with free peptide, there was a significant reduction in the specific immunoreactivity of sticky liposomes to 0.1 ± 0.4 and 0.2 ± 0.3% at pH 7.4 and 6.5, respectively. When sticky liposomes contained a scrambled version of the HER2-targeting peptide (CLKYCS), immunoreactivities on BT-474 cells also dropped to −0.1 ± 0.3 and 0.1 ± 0.3% at pH 7.4 and 6.5, respectively.

On average, the loading efficiency of doxorubicin into liposomes was 63.4 ± 9.1% (n = 18). This equated to 0.24 ± 0.02 mole of doxorubicin per mole of lipid. Doxorubicin was retained to significant extents by liposomes during the six hour incubations with cells for drug uptake and cytotoxicity studies (Table 3.1).

Doxorubicin retention by liposomes (%)	pH 7.4	pH 6.5
sticky liposomes	86.3 ± 5.6	75.4 ± 4.9
uniformly peptide-functionalized liposomes without tether	89.5 ± 3.0	88.6 ± 4.5
uniformly Ab-functionalized liposomes with tether	88.4 ± 5.3	88.9 ± 4.2

Table 3.1: Targeted Liposome retention of doxorubicin after six hours of incubation in the presence of BT-474 cells at extracellular pH 7.4 and pH 6.5. Errors correspond to standard deviations of repeated measurements (one sample per vesicle preparation, three independent vesicle preparations).

Characterization of Cell Lines HER2 Expression

As measured by ^{111}In-labeled trastuzumab, the HER2 expression per cell (HER2 copies/cell) was 1.3 ± 0.1 × 10^6 for BT- 474 (n = 5), 8.3 ± 0.8 × 10^4 for MDA-MB-231 (n

= 3), $5.4 \pm 0.9 \times 10^4$ for MCF7 (n = 3), $1.1 \pm 0.4 \times 10^4$ for cardiomyocytes (n = 2), and $4.8 \pm 3.9 \times 10^3$ for MCF 10A (n = 2).

Cell Association of Liposomes as a Function of Extracellular pH

Specific binding and internalization on breast cancer cells with low-HER2-expression using MDA-MB-231 and MCF7 cells was detectable only for sticky liposomes (red circles) under acidic pH conditions, with a sharp and significant increase (approximately 50%) ($p < 0.01$) between pH 7.4 and pH 6.0 (Figure 3.2A,B). For liposomes with uniform functionalization and no-phase separating capabilities, specific binding and internalization on MDA-MB-231 and MCF-7 cells was undetectable at all pH values tested. Specific binding and internalization of all functionalized liposome constructs was insignificant on cardiomyocytes and MCF 10A normal breast epithelial cells.

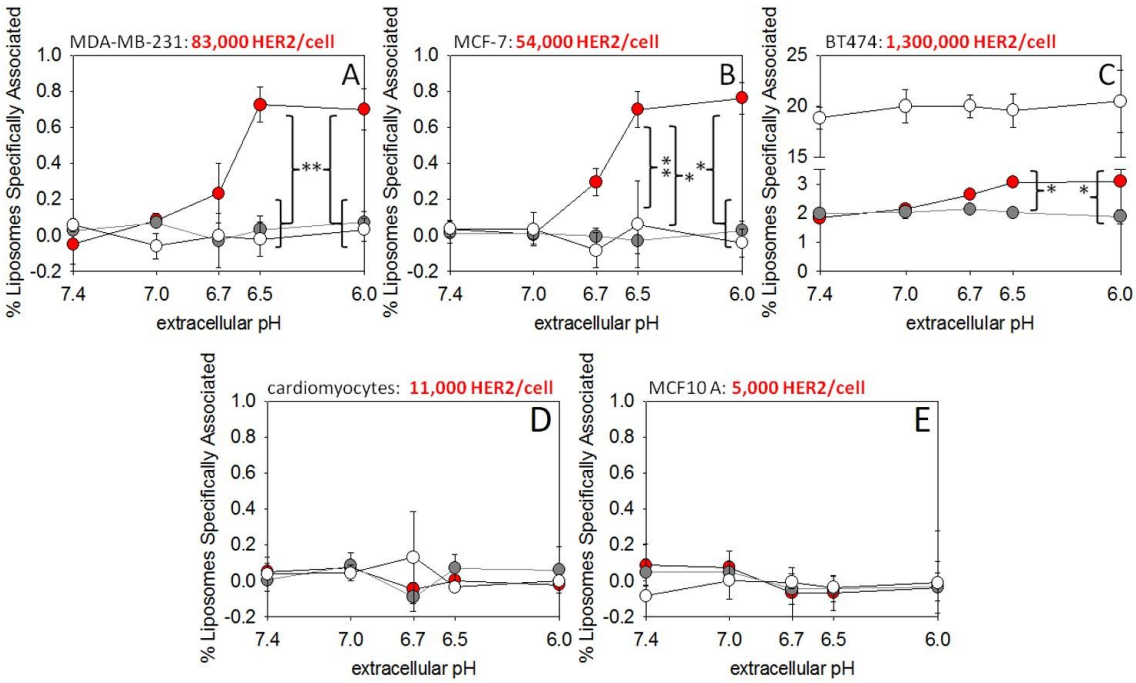

Figure 3.2: Specific binding and internalization of liposome as a function of extracellular pH on HER2-negative MDA-MB-231 cells (A), HER2-negative MCF-7 (B), HER2-positive BT-474 (C), human cardiomyocytes (D) and MCF 10A normal breast epithelial cells (E) for sticky liposomes (red symbols), liposomes with uniform peptide functionalization (gray symbols) and liposomes with uniform antibody functionalization (white symbols). Specific association is calculated by subtracting the effect from the corresponding non-targeted liposomes. Lines are guides to the eye. Errors correspond to standard deviations of repeated measurements (one sample per vesicle preparation, three independent vesicle preparations). Liposome-to-receptor ratio incubation conditions were kept constant at 1-to-10 across all constructs and cell lines.
* indicates *p*-values < 0.01, ** indicates *p*-values <0.05.

Drug Uptake by Cells and Liposome Cytotoxicity

Figure 3.3 illustrates that HER2-targeting sticky liposomes (red bars) loaded with doxorubicin delivered significantly more chemotherapeutic agent per cell at extracellular pH of 6.5 (used to mimic the average pH in the tumor interstitium) on low HER2-expressing cells when compared to uniformly functionalized liposomes (Figure 3.3A,B). This effect translated to significantly greater killing efficacy on MDA-MB-231 and MCF7 cells (32.3 ± 10.4 and 39.5 ± 5.6 % viability, respectively) (Figure 3.4A,B). At

extracellular pH of 7.4, the amount of doxorubicin accumulated in HER2-negative MDA-MB-231 and MCF7 cells by all HER2-targeting vesicles was less than 22.3 fg per cell and did not result in a decrease in cell viability (Figure 3.3A,B) (Figure 3.4A,B). Corresponding non-targeted liposomes loaded with doxorubicin (indicated by the dashed lines on all figures) delivered on average 17.7 ± 2.4 and 18.0 ± 1.8 fg/cell at pH 7.4 and 6.5, respectively, resulting in negligible cytotoxicities. On cardiomyocytes and normal breast epithelial cells MCF 10A, all doxorubicin-loaded constructs resulted in insignificant cytotoxicities (Figure 3.4D,E).

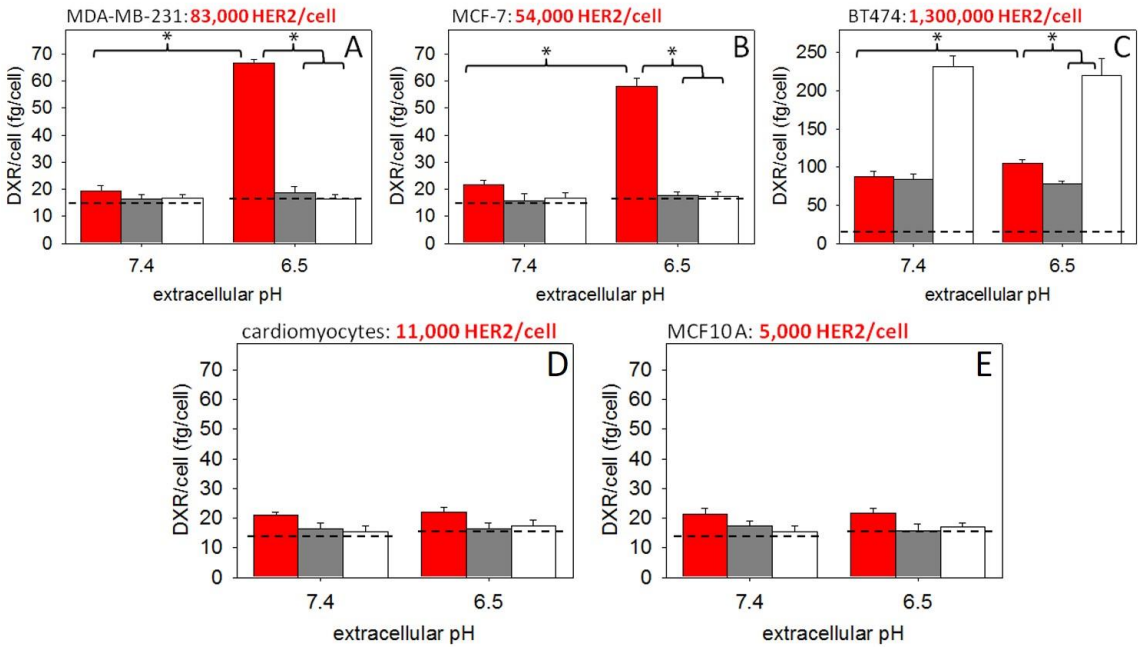

Figure 3.3: Uptake of doxorubicin by HER2-negative MDA-MB-231 cells (A), HER2-negative MCF-7 (B), HER2-positive BT-474 (C), human cardiomyocytes (D) and MCF 10A normal breast epithelial cells (E) for sticky liposomes (red bars), liposomes with uniform peptide functionalization (gray bars) and liposomes with uniform antibody functionalization (white bars). Errors correspond to standard deviations of repeated measurements (one sample per vesicle preparation, three independent vesicle preparations). * indicates $p < 0.01$. The dashed line represents the average amount of doxorubicin taken up by cells following incubation with non-targeted liposomes across all cell lines and vesicle constructs (17.7 ± 2.4 and 18.0 ± 1.8 fg/cell at pH 7.4 and 6.5, respectively). All vesicles were loaded on average with 0.18 mg of doxorubicin per mg of lipid, and cells were incubated on average with 0.10 mg of lipid per mL.

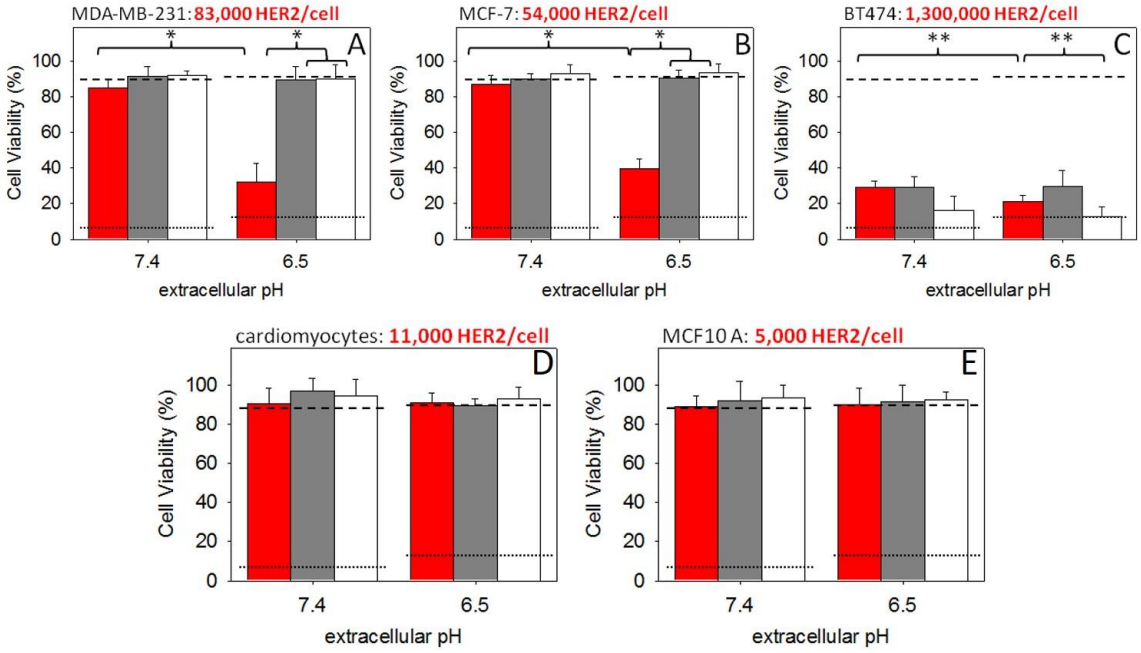

Figure 3.4: Cell viability after treatment with chemotherapeutics of HER2-negative MDA-MB-231 cells (A), HER2-negative MCF-7 (B), HER2-positive BT-474 (C), human cardiomyocytes (D) and MCF 10A normal breast epithelial cells (E) for sticky liposomes (red bars), liposomes with uniform peptide functionalization (gray bars) and liposomes with uniform antibody functionalization (white bars). Errors correspond to standard deviations of repeated measurements (one sample per vesicle preparation, three independent vesicle preparations). * indicates $p < 0.01$. ** indicates p-values <0.05. The dashed line indicates the average cell viability following incubation with non-targeted liposomes across all cell lines and vesicle constructs (90.4 ± 3.5 and 91.8 ± 2.5% at pH 7.4 and 6.5, respectively). The dotted line indicates the average cell viability following incubation with an identical concentration of free doxorubicin across all cell lines and vesicle constructs (7.13 ± 2.6 and 13.4 ± 3.5% at pH 7.4 and 6.5, respectively). All vesicles were loaded on average with 0.18 mg of doxorubicin per mg of lipid, and cells were incubated on average with 0.10 mg of lipid per mL.

Imaging of Intracellular Distributions of Liposomes

Internalization of liposomes by breast cancer cells with low HER2 expression was detected only for DPPE-Rhodamine labeled sticky liposomes at extracellular pH 6.5. On both MDA-MD-231 and MCF7 breast cancer cells (Figure 3.5), sticky liposomes showed fast perinuclear localization that became more distinct over longer exposure times.

Endocytosis of uniformly functionalized liposomes was undetectable on HER2-negative MDA-MB-231 and MCF7 breast cancer cells at both extracellular pH 7.4 and pH 6.5 (Figure A1). On HER2-positive BT-474 cells, the cytoplasmic distribution of all functionalized liposome constructs was similar with fast perinuclear localization of internalized liposomes (Figure A2).

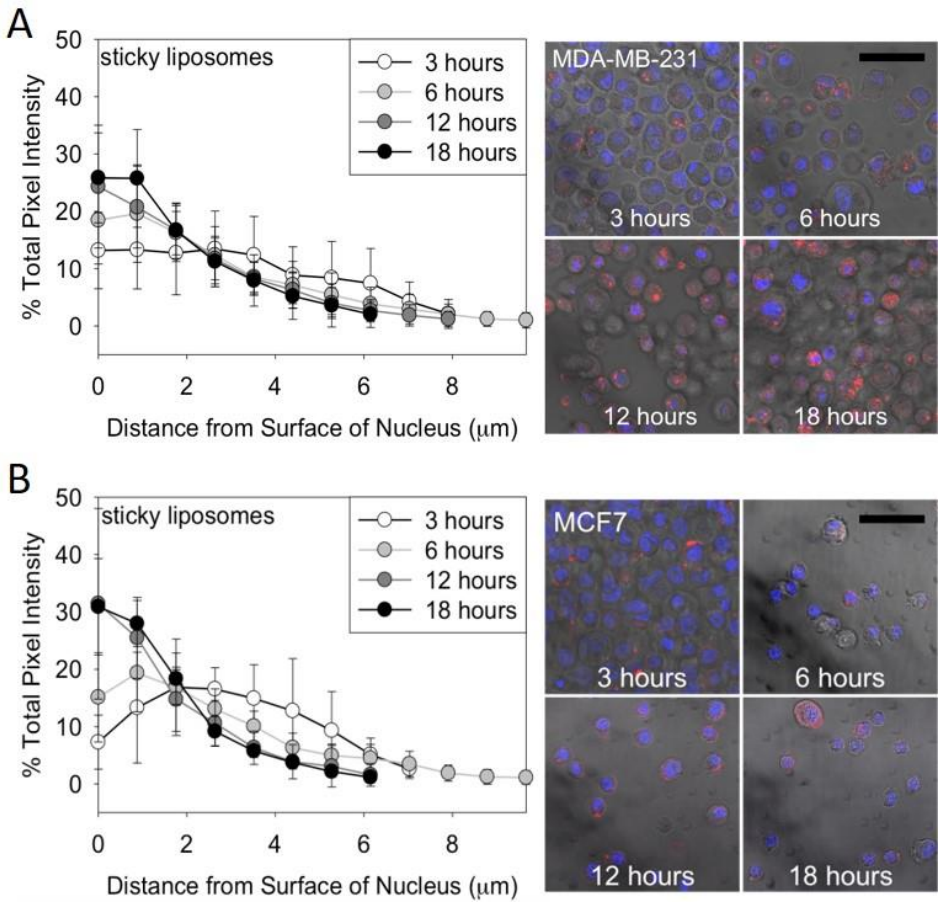

Figure 3.5: Cytoplasmic distributions and characteristic confocal fluorescence images of sticky liposome uptake over time at extracellular pH 6.5 in HER2-negative MDA-MB-231 (A) and HER2-negative MCF7 (B) breast cancer cells. Per time point, n=10 cells were analyzed and averaged. Scale bar: 50 μm.

Mechanism of Liposome Endocytosis

Pathways of endocytosis were determined using flow cytometry by qualitatively analyzing the fluorescent peak shifts between cell samples either kept at 37 °C, or pre-incubated with endocytosis inhibitors, prior to incubation with sticky liposomes. For sticky liposomes incubated with cells at extracellular pH of 6.5, there was a peak shift to the left for cells pre-incubated with either clathrin- or caveolar-mediated endocytosis inhibitors (Figure 3.6, Table A.1). This phenomenon was independent of HER2 expression, as demonstrated by MCF7 and BT-474 cells with approximately 5.4×10^4 and 1.3×10^6 receptors per cell, respectively.

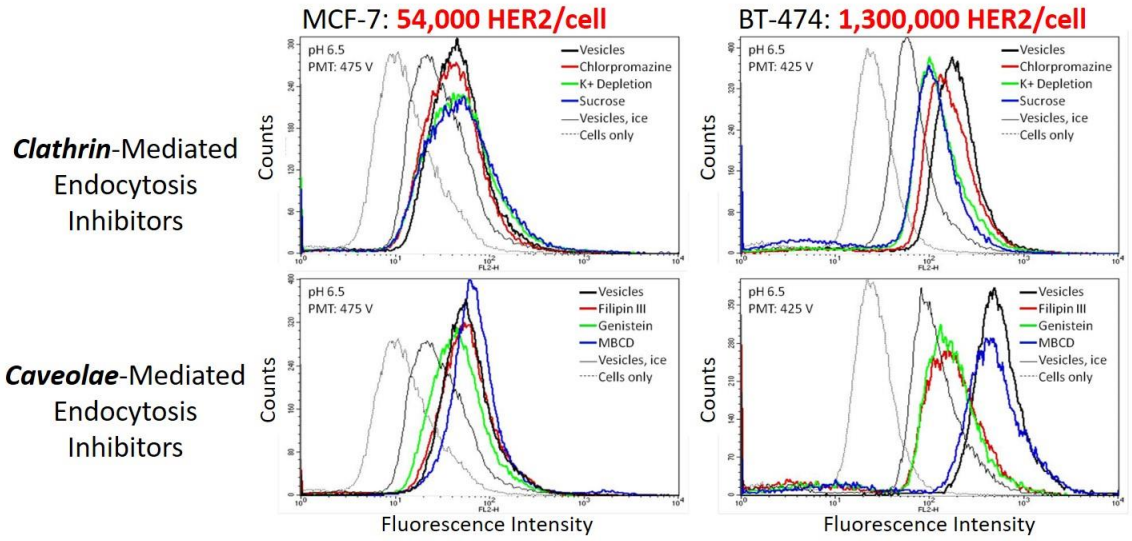

Figure 3.6: Endocytosis inhibition studies using flow cytometry to identify the internalization pathway used by sticky liposomes on HER2-negative MCF-7 and HER2-positive BT-474 breast cancer cells at an extracellular pH of 6.5.

Characterization of Liposomes' Effective Equilibrium Dissociation Constants (K_D), Dissociation Rate Constants (k_{off}), and Cell Internalization Rate Constants (k_{int}).

Equilibrium dissociation constants (K_D) of sticky liposomes at the extracellular pH of 6.5 were independent of HER2 expression (Table 3.2A). Consistently, dissociation rate constants (k_{off}) did not vary by more than a factor of 2 ($p > 0.01$) across all breast cancer cell lines of varying HER2 expression (Table 3.2A). Sticky liposomes at the extracellular pH of 7.4, and not in the phase-separated form, were not reactive towards breast cancer cell lines with low HER2 expression; i.e.; K_D and k_{off} values were undetectable (Table 3.2B). Only on high HER2-expressing BT-474 cells were uniformly functionalized liposomes detected and exhibited pH independent activity (Table 3.2).

Table 3.2: Equilibrium Dissociation Constants (K_D), Dissociation Rate Constants (k_{off}), and Internalization Rate Constants (k_{int}) at (A) pH 6.5 and (B) pH 7.4 for sticky liposomes and uniformly functionalized liposomes for HER2-negative MCF7, HER2-negative MDA-MB-231 and HER2-positive BT-474 breast cancer cells. *Measured values were comparable to the values measured for non-targeted liposomes (0.020 ± 0.004 min^{-1}).

A. ***pH 6.5***	Sticky vesicles (heterogeneously functionalized with HER2-targeting peptides)	Vesicles uniformly functionalized with HER2-targeting peptides	Vesicles uniformly functionalized with HER2-targeting Ab via PEG tethers
K_D, nM			
MCF7	69 ± 24	undetectable	undetectable
MDA-MB-231	49 ± 19	undetectable	undetectable
BT-474	115 ± 35	160 ± 52	5 ± 2
k_{off}, min^{-1} ($t_{1/2}$, min)			
MCF7	0.005 ± 0.002 (140 ± 54)	undetectable*	undetectable*
MDA-MB-231	0.009 ± 0.003 (82 ± 34)	undetectable*	undetectable*
BT-474	0.006 ± 0.002 (123 ± 40)	0.004 ± 0.001 (183 ± 35)	0.005 ± 0.001 (130 ± 25)
k_{int}, min^{-1} ($t_{1/2}$, min)			
MCF7	0.024 ± 0.002 (29 ± 2)	undetectable	undetectable
MDA-MB-231	0.025 ± 0.002 (27 ± 2)	undetectable	undetectable
BT-474	0.026 ± 0.002 (27 ± 2)	0.031 ± 0.002 (23 ± 1)	0.023 ± 0.004 (30 ± 4)

B. ***pH 7.4***	Sticky vesicles (heterogeneously functionalized with HER2-targeting peptides)	Vesicles uniformly functionalized with HER2-targeting peptides	Vesicles uniformly functionalized with HER2-targeting Ab via PEG tethers
K_D, nM			
MCF7	undetectable	undetectable	undetectable
MDA-MB-231	undetectable	undetectable	undetectable
BT-474	197 ± 11	215 ± 7	3 ± 0
k_{off}, min^{-1} ($t_{1/2}$, min)			
MCF7	undetectable*	undetectable*	undetectable*
MDA-MB-231	undetectable*	undetectable*	undetectable*
BT-474	0.004 ± 0.001 (172 ± 21)	0.004 ± 0.001 (163 ± 42)	0.005 ± 0.001 (142 ± 12)
k_{int}, min^{-1} ($t_{1/2}$, min)			
MCF7	undetectable	undetectable	undetectable
MDA-MB-231	undetectable	undetectable	undetectable
BT-474	0.027 ± 0.001 (25 ± 1)	0.020 ± 0.001(34 ± 2)	0.025 ± 0.004 (29 ± 4)

Independent of HER2 expression, effective internalization rate constants, $k_{int,}$ of sticky liposomes at an extracellular pH of 6.5 were similar ($p > 0.01$) to that of liposomes with uniform functionalization. Uniformly functionalized liposomes, however, were only measurable on HER2-overexpressing BT-474 cells. At the extracellular pH of 7.4, sticky liposomes (not in the phase-separated form) and uniformly functionalized liposomes exhibited comparable internalization rates, which were detectable only on HER2-overexpressing BT-474 cells (Table 3.2B).

3.4: Discussion

Targeted therapies are a promising strategy for cancer therapy because they aim to selectively target and kill cancer cells using specific molecular markers, ultimately improving therapeutic index and minimizing toxicities [9]. However, the use of targeted therapies is currently limited to patients with tumors expressing high degrees of the target receptor. In the realm of HER2, approximately 20% of breast cancers are considered to be triple-negative breast cancer (TNBC). For these patients, there exists no targeted therapeutic option [56] utilizing the HER2 receptor. Many efforts have focused on widening this therapeutic window to include more patients who are eligible for targeted therapies, but this is driven by the discovery of new molecular markers which are overexpressed by the cancer cells (e.g. ICAM-1 and EGFR) [57] [58] instead of exploring alternative mechanisms for targeting.

In this work, we studied the potential to utilize alternative binding geometries between receptors and ligand-labeled liposomes as an alternative mechanism for targeting. These binding geometries showed specific binding at low levels of receptor

expression (typically considered ‘untargetable’) where typical functionalized nanoparticles would fail. Specifically, we developed liposomes (which we refer to as sticky liposomes) that present a different geometry for binding with the HER2 receptor. These liposomes utilize a clustered presentation of HER2-targeting ligands that is only formed in an acidic environment. At pH values mimicking that of the tumor interstitium, sticky liposomes exhibited selective targeting and effective killing against both TNBC MDA-MB-231 and HER2-negative MCF7 breast cancer cells. At neutral (physiological) pH, these liposomes were unreactive and showed no cytotoxicity. We also demonstrated that sticky liposomes did not affect the viability of normal breast epithelial cells or human cardiomyocytes, which are often sites of toxicity *in vivo*. Studies inhibiting the mechanisms of internalization by BT-474 and MCF7 cells showed that sticky liposomes are internalized by both caveolar- and clathrin-mediated endocytosis. Once sticky liposomes were internalized by cells, they exhibited fast perinuclear localization. This ultimately improved the therapeutic efficacy and trafficking of delivered drug to the nucleus, which is the target site for doxorubicin.

Despite the fact that the interaction between sticky liposomes and HER2 receptors is not fully elucidated at this point, our hypothesis is supported by the following observations. First, the mean residence time of bound sticky liposomes on the cell surface was long enough ($t_{1/2}$ of dissociation spanned from 82 to 140 min) to allow for liposome internalization ($t_{1/2}$ of internalization spanned from 27 to 29 min), and this phenomenon was independent of HER2 expression. Second, the amounts of doxorubicin specifically delivered (defined as the amount of drug delivered by functionalized liposomes corrected by the amount of drug delivered by non-functionalized liposomes in a parallel

experiment) by sticky liposomes directly correlated with the number of HER2 receptors on cells considered HER2-negative (Table 3.3).

Table 3.3: Specific doxorubicin uptake per HER2 receptor following incubation with HER2-tageting sticky liposomes on HER2-negative breast cancer cells lines MDA-MB-231 and MCF7, and cardiomyocytes and MCF 10A normal breast epithelial cells.

Ratio of doxorubicin uptake per HER2 receptor (fg per HER2 receptor)	
MDA-MB-231	$57 \pm 6 \times 10^{-5}$
MCF7	$69 \pm 12 \times 10^{-5}$
cardiomyocytes	$34 \pm 34 \times 10^{-5}$
MCF 10A	$48 \pm 74 \times 10^{-5}$

We have two hypotheses for the detected specific interactions between sticky liposomes and cells with low HER2 expression which result in longer residences times at the cell surface. First, we hypothesize that the interaction should be dependent on the cooperativity between transport and binding. As the initial bond between one HER2-targeting ligand on a sticky liposome and the cell receptor dissociates, yet prior to the liposomes being driven away by Brownian water molecule collisions, there exists many other HER2-targeting ligands in close proximity to form a new bond. This phenomenon may repeat, and repeat, and repeat, until the liposome becomes internalized. This effectively lowers the constant for unbinding between the cell and the sticky liposome, which as was demonstrated by our experiments, was independent of HER2 expression. Second, we hypothesize that if the time in which the singly bound (and constantly rebinding) liposome lingers is long enough, then this would provide a time window for a further away, second receptor to freely diffuse by and bind to another ligand in the cluster of ligands comprising the sticky patch. While each of these receptors may dissociate and

rebind, the likelihood of both becoming unbound at the same time for long enough gets profoundly reduced. This may inadvertently provide additional time for a third and fourth (and so on) receptor to wander nearby, to significantly improve the probability of liposome internalization.

Since HER2 receptors on the surface of a cell with low HER2 expression are sparse, we infer that at any given time there does not exist more than one receptor under the projected area of the nearby liposome. This may provide an explanation for why liposomes with homogenously presented targeting ligands (subject to Brownian interactions with the surround solution) demonstrated comparable k_{off} values to that of non-targeted liposomes; that is, single ligand-receptor binding times were too short to allow for liposome internalization. This limitation does not seem to be the case for that of sticky liposomes.

Here we use the simplest model for mass-action to represent the association of liposomes with cells at equilibrium (K_D). However, we introduce a term φ (Figure 3.7) which characterizes the degree to which surface receptors become inaccessible for additional binding events after formation of a complex (liposome bound to the cell), that becomes increasingly relevant for HER2-overexpressing cancer cells. The rationale here is that there are different effective distances between the surface of the liposomes and the surface of the cell for which a liposome is bound, originating from the presence or absence of PEG chains used for ligand tethering. For liposomes functionalized with HER2-targeting antibodies via PEG tether, the distance from the surface of the cell to surface of the liposome is a combination of the (1) PEG chain length (which is 2000 MW and equivalent to 3.4 nm assuming a Gaussian coil) [47], and (2) overall length of the

antibody (approximately 10 nm) [59]. This relatively long distance between the liposome surface and cell surface may afford underlying non-bound receptors to freely diffuse away from the area of the complex and become available for binding with other liposomes. Analogous to this, the effective distance for liposomes functionalized with HER2-targeting peptides directly attached to lipid headgroups should be much shorter because it is only a function of the length of the peptide itself (3.4 nm = 9 amino acids x 0.38 nm per amino acid) [60]. This relatively short distance may, upon complexation of a liposome to the cell, impede the underlying (initially) non-bound receptors from diffusing away from the complex to become available for additional binding events. Using HER2-overexpressing BT-474 breast cancer cells as an example in this model, we find φ fitted values of 4 and 25 for liposomes functionalized with and without PEG tethering, respectively. For low HER2-expressing MDA-MB-231 and MCF7 breast cancer cells, the fitted value of φ dropped to 15, which is qualitatively sensible at lower HER2-expression levels. However, to fully understand the detailed interactions between sticky liposomes and HER2 receptors, real-time single-particle tracking studies will need to be investigated.

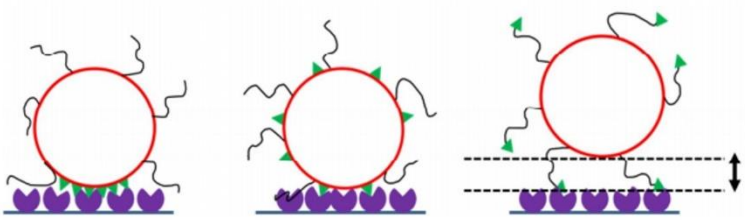

Figure 3.7: Schematic representation of receptor inaccessibility for additional binding after complexation of a liposome with the cell surface in support of the term φ. This term explains the variable effective distances between receptors on the cell (purple) and the surface of the liposome (red), and originates from the presence or absence of a PEG tether for ligand functionalization.

In this work, we examined how the presentation of HER2-targeting ligands on the surface of a liposome, either as a clustered or uniform display, affected the binding to cells with low levels of HER2, in an effort to provide a potential targeted therapeutic strategy for cancer with low HER2-expression. Only liposomes with a clustered display of targeting ligands demonstrated measurable effectiveness against breast cancer cells with low HER2-expression. This suggests a binding geometry exits for sticky liposomes to linger long enough on the cell surface to enable internalization and selectivity in the killing of low HER2-expressing cells.

CHAPTER 4: PRELIMINARY STUDIES ON THE PRE-CLINICAL FEASIBILITY OF TARGETED LIPOSOMAL DOXORUBICIN ON METASTATIC TNBC

Note: data in this chapter was adapted from the following manuscript which is in preparation:

Sempkowski, M., Howe, A., Sofou, S. "Targeted Liposomal Chemotherapy Selectively Slows the Progression of Triple Negative Metastatic Breast Cancer *In Vivo*".

4.1: Introduction

Triple-negative breast cancers (TNBCs) are defined by the absence of progesterone and estrogen receptors, as well as an absence of HER2 overexpression [61]. These cancers comprise approximately 15% of all breast cancers and are typically associated with poor prognosis and shorter overall survival times, especially for those patients with advanced-stage disease[62]. The standard of care for these patients is systemic chemotherapy, with the most common first line of treatment being a combination of anthracycline and taxanes [63].

The receptor-negative nature of TNBC means that TNBC patients are unresponsive to both hormonal therapies and anti-HER2 agents. For example, the HER2-targeting antibody trastuzumab shows no clinical efficacy on women with HER2-negative tumors [18]. It is the same case with conventionally targeted nanoparticle therapies such as MM-302, which is a HER2-targeting liposomal doxorubicin construct which reached Phase II trials for the treatment of HER2-positive breast cancer [20]. Specific targeting of constructs such as MM-302 ceases on breast cancer cells exhibiting

< 200,000 HER2 copies/cell [23]. These limitations demand alternative ways to target cancer cells with a low (or variable) expression of receptors if the advantages of targeted therapies are to be harnessed.

In the present study, we describe our efforts to exploit a previously designed and characterized HER2-targeting lipid vesicle and examine the pre-clinical feasibility for TNBC therapy. Our group has developed HER2-targeting liposomes (sticky liposomes) that are triggered to present a clustered display (sticky patch) of HER2-targeting peptides (KCCYSL) [37] on the surface of the liposome under acidic conditions matching that of the tumor interstitium (pH 7.0 > pH ≥ 6.0) [28, 40]. We have previously shown that these sticky liposomes demonstrate selective targeting and killing of otherwise "untargetable" breast cancer cells, expressing as few as 54,000 HER2 receptors per cell [64].

Here we tested peptide-functionalized pH-responsive (sticky) liposomes loaded with the anthracycline doxorubicin. We evaluated the efficacy of these liposome against both 2D cell monolayers and 3D multicellular spheroids as surrogates to the avascular regions of solid tumors [65]. Studies on 3D multicellular spheroids were performed under step-wise and exponentially-decaying therapy exposure profiles using a perfusion chamber system to examine the differences in therapeutic efficacy under both constant concentrations of therapy and exponentially decaying concentrations of therapy with a half-life of clearance similar to that *in vivo*. The studies were performed on the TNBC cell line, MDA-MB-231, as well as lung and lymph node metastatic TNBC cell sublines harvested from a metastatic mouse model inoculated with MDA-MB-231 cells in the mammary fat pad. We also examined potential toxicities to a human cardiomyocyte cell

line because doxorubicin in its free form is associated with cardiac dysfunction [65]. In all cases, we compared the efficacy of sticky liposomes against non-functionalized releasing liposomes, trastuzumab-functionalized non-releasing liposomes, and non-functionalized non-releasing liposomes, where non-releasing liposomes have membranes similar to that of Doxil [66]. We finally demonstrated that a published orthotopic TNBC xenograft model was a good candidate to evaluate the ability of sticky liposome chemotherapy to control metastatic growth and/or spreading.

4.2: Materials and Methods

Liposome Preparation

The following lipids were used for liposome preparation: 1,2-diarachidoyl-sn-glycero-3-phosphocholine (20PC), 1,2-distearoyl-sn-glycero-3-phosphocholine (DSPC), 1,2-dipalmitoyl-sn-glycero-3-phospho-L-serine (DPPS), 1,2-distearoyl-sn-glycero-3-phosphoethanolamine-N-[Methoxy(Polyethylene glycol)-2000] (Ammonium Salt; DSPE-PEG2000), 1,2-distearoyl-sn-glycero-3- phosphoethanolamine-N-[PDP (Polyethylene Glycol) 2000] (Ammonium Salt; DSPE-PEG-PDP), 1,2-dipalmitoyl-sn-glycero-3-phosphoethanolamineN-(succinyl) sodium salt-(Gly-Ser-Gly)-Lys-Cys-Cys-Tyr-Ser-Leu (DPPE-(linker)-peptide; DPPE-lipopeptide), 1,2-dipalmitoyl-sn-glycero-3-phosphoethanolamine-N- (LissamineRhodamine B Sulfonyl) (Ammonium Salt; DPPE-Rhodamine), and cholesterol (chol).

Targeted pH-responsive (sticky) liposomes designed to present dense (sticky) patches of HER2-targeting peptides on the liposomes surface were composed of 20PC/DPPS/Chol/DPPE-lipopeptide/DSPE-PEG in a 8.18:0.91:0.45:0.09:0.36 mole

ratio. Targeted non-releasing liposomes designed to uniformly present HER2-targeting antibodies at the distal end of PEG tethers were composed of DSPC/chol/DSPE-PEG-2000/DSPE-PEG-PDP lipid in a 6.67:2.86:0.29:0.19 mole ratio. The corresponding non-targeted liposome compositions did not contain functionalized lipids. When fluorescent labeling of the membrane was required, all vesicles were composed with 1 mole % DPPE-Rhodamine.

Liposomes were prepared using the thin film hydration method. Briefly, lipids dissolved in chloroform or a chloroform-methanol mixture were combined in a round bottom flask and dried under vacuum and rotation at 55°C, followed by further drying under N_2 gas, to yield a thin lipid film. Lipids were hydrated in either phosphate buffered saline (PBS) with 1 mM Ethylenediaminetetraacetic acid (EDTA) at pH 7.4 for empty liposomes, 250 mM ammonium sulfate at pH 7.4 for doxorubicin-loaded liposomes, or 140 mM citrate buffer with 5 mg/ml 1,4,7,10-tetraazacyclododecane-1,4,7,10-tetraacetic acid (DOTA) and 2.1 mg/mL ascorbic acid at pH 5.0 for Actiniun225-loaded liposomes, and incubated at 55°C for 2 hours. The lipid suspension was extruded 21 times through two stacked polycarbonate membranes with 100 nm pore diameter, then eluted through a Sepharose 4B column eluted with PBS (1 mM EDTA, pH 7.4) or metal-free HEPES buffer (20 mM HEPES, 250 mM sucrose, pH 7.4). Liposome size and polydispersity index were determined using a Zetasizer NanoZS90.

Loading of doxorubicin was accomplished using the ammonium sulfate gradient technique as previously described by Haran et al [54]. Briefly, 1 mL of 1 mM doxorubicin dissolved in saline was incubated with 0.5 mL of liposomes (2.5 μmole total lipid) and incubated for 2 hours at 5°C above the highest T_g of lipids comprising the

membrane. The lipid suspension was passed through a Sepharose 4B column eluted with PBS (1 mM EDTA, pH 7.4, or pH 5.5 for antibody conjugation) to separate liposomes from un-encapsulated doxorubicin.

HER2-targeting monoclonal antibodies, trastuzumab, were conjugated to non-pH-responsive liposomes using standard 3-(2- pyridyldithio)propionate (PDP)-based and succinimidyl 4-(pmaleimidophenyl)butyrate (SMPB)-based chemistry [41]. Nonconjugated antibodies were separated from antibody-labeled liposomes by passing the lipid suspension through a Sepharose 4B column eluted with PBS (1 mM EDTA, pH 7.4). The BCA assay was used to quantify the concentration of antibodies in the purified antibody-labeled liposome suspension. The average number of antibodies per liposome was then calculated on the basis of the total lipid, the headgroup surface area per lipid (48 $Å^2$ for lipids in the gel phase), and the measured mean size of liposomes.

Liposome Retention of Doxorubicin

Retention of doxorubicin by liposomes was determined by incubating doxorubicin-loaded nanoparticles in DMEM cell culture media supplemented with 10% FBS and equilibrated overnight to pH 7.4, pH 6.5, pH 6.0, or pH 5.5 using 1N HCl. After six hours of incubation, the liposome-media mixture was passed through a Sephadex G50 column to separate liposomes from leaked doxorubicin. The percentage of doxorubicin retained in the liposomes was determined by measuring its fluorescence intensity (excitation/emission = 470 nm/572 nm) before and after size exclusion chromatography.

Animals and Isolation of Metastatic TNBC Cell Sublines

Five-to-six-week-old NOD *scid* gamma (NSG) mice were surgically inoculated with 500,000 MDA-MB-231 cells in the second mammary fat pad on the right side using the mouse model for human breast cancer metastasis previously established by Iorns et al [67]. At 35-46 days post-inoculation, animals were euthanized according to the human endpoints established by IACUC. Right axillary lymph node and lung tissues were harvested from mice inside a tissue culture hood, cut into 2-3 mm pieces and ground between microscope slides. The resulting homogenized tissue was then placed on top of a 40 micron cell strainer and rinsed with DMEM media containing 10% fetal bovine serum, 100 units/mL penicillin, and 100 µL streptomycin to isolate metastatic cancer cells. The media rinse was collected inside one well of a 6-well tissue culture plate then incubated at 37°C and 5% CO_2. After 2-3 days, medium was changed out to separate any non-surviving mouse cells from viable metastatic cancer cells. The selected metastatic cell TNBC sublines harvested from right axillary lymph node (231-ALN1, 231-ALN2, 231-ALN3), lung (231-LUNG1, 231-LUNG2, 231-LUNG3), and primary tumor (231-PRI3) tissue were cryopreserved in liquid N_2 for future use.

Cell and Spheroid Culture

MDA-MB-231 cells (purchased from ATCC) and MDA-MB-231-derived metastatic cell sublines were maintained in DMEM cell culture media supplemented with 10% fetal bovine serum. 100 units/mL penicillin, and 100 µL streptomycin at 37°C and 5% CO_2. Human cardiomyocytes, harvested from human cardiac tissue, were purchased from Celprogen and cultured in Human Cardiomyocyte Primary Cell Culture Media. Spheroids were initiated by seeding 500 cells per well (suspended in 2.5% Matrigel™

and culture media) onto polyHEMA-coated 96-well round-bottom plates. The plates were centrifuged for 10 minutes at 1000 x gravity then incubated until reaching a diameter of 400 microns (typically 5-7 days).

Metastatic TNBC Cell Subline Characterization: Population Doubling Time and HER2 expression

Population doubling times (PDTs) for all metastatic cell TNBC sublines were quantified using two assays: counting and MTT assay. Cells were plated on 96-well plates at a density of 10,000 cells per well and incubated from 3-68 hours at 37°C and 5% CO_2. At different timepoints, cells were either trypsinized and counted using a hemocytometer or incubated for standard MTT assay. PDTs were calculated by fitting the data with an exponential growth formula.

HER2 receptors were counted using antibodies radiolabeled with Indium-111 (^{111}In). Briefly, DTPA functionalized with isothiocyanate was added to HER2-targeted trastuzumab antibodies at a 15:1 mole ratio in 1 M carbonate buffer (pH 9.0) and incubated overnight with shaking. Trastuzumab-DTPA was separated from nonconjugated DTPA by eluting the mixture through a 10-DG column equilibrated with 1 M acetate buffer (pH 4.5). ^{111}In dissolved in 0.2 M HCl was added to trastuzumab-DTPA and allowed to react at 37°C for 1 hour. Unreacted ^{111}In was separated from the radiolabeled antibodies by first adding 50 µL of 10 mM EDTA then passing the mixture through a 10-DG column eluted with PBS (1mM EDTA, pH 7.4). Radiochemical purity was evaluated using instant thin layer chromatography (iTLC) using a mobile phase of 10 mM EDTA.

Cytotoxicity Studies on Cell Monolayers

Cells were plated on 96-well plates at a density of 20,000 cells per well. Liposomes were loaded with doxorubicin, split into two aliquots, and equilibrated to either pH 7.4 or pH 6.5 overnight at 37 °C and 5% CO_2. After the incubation period, liposomes were passed through a Sephadex G50 column eluted with PBS (1 mM EDTA) at the corresponding pH to separate out leaked contents. Drug-loaded liposomes (or free doxorubicin) were then added to cells at pH 7.4 or pH 6.5 at varying concentrations of doxorubicin (0.1-200 µM). After 6 hours of incubation, cells were washed thrice with sterile PBS (1 mM EDTA, pH 7.4) and further incubated with fresh medium for two population doubling times at 37 °C and 5% CO_2. Cell viability was evaluated using MTT assay.

Blood Clearance Half-life in Animals

Half-life of liposome clearance from the blood in healthy athymic nude mice was determined by following levels of radioactivity in the blood post-injection of Actinium-225 (^{225}Ac) labeled liposomes. Liposomes were loaded with ^{225}Ac using methods previously described in the literature [68]. In brief, 1 mL of liposomes (2.5 mM total lipid) was added to 80 µL of a mixture comprising 30 µL of ^{225}Ac dissolved in 0.03 mM HCl and 50 µL of 0.37 mg/mL calcium ionophore A23187 in a 1:1 mixture of chelex water and ethanol. The lipid suspension was incubated for 1 hour at 71 °C. Unentrapped ^{225}Ac was chelated with 50 µL of 10 mM DTPA and the lipid suspension was passed through a Sephadex G50 column eluted with PBS (1 mM EDTA, pH 7.4) to separate out

liposomes from unentrapped ^{225}Ac. Actinium-loaded liposomes were administered via retro-orbital injection. At pre-determined timepoints, animals were bled using tail vein nick and a 5-10 µL sample of blood was collected. The level of radioactivity in each blood sample was determined using liquid scintillation counting after reaching secular equilibrium.

Perfusion System Design and Fabrication

A perfusion system was constructed by first connecting a PHD Ultra Syringe Pump to a continuously stirred-tank reactor (CSTR) using microbore PTFE tubing. The CSTR was connected via tubing to a perfusion chamber assembled using a CoverWell™ chamber (4 chamber device, 6.35 mm x 19 mm chamber dimensions, 2.5 mm chamber depth) pressed to a microscope slide. The outlet of each chamber was fitted with mesh from a 100 µm pore diameter cell strainer in order to prevent spheroid loss from the chamber under dynamic flow conditions. The perfusion chamber was connected via tubing to a second syringe pump, to draw fluid from the CSTR to the perfusion chamber.

Liposome and Doxorubicin Penetration into Spheroids

To evaluate the interstitial distribution of liposomes and doxorubicin, spheroids were incubated with fluorescently-labeled liposomes or liposomes encapsulating non-self quenching fluorescent doxorubicin under a step-wise exposure profile and an exponentially decaying exposure profile. To ensure an equal mass of delivered lipid or doxorubicin on each platform over the 6-hour incubation period, liposomes were incubated with spheroids at a concentration of 0.5 and 1.6 µM total lipid for step-wise

and exponentially-decaying exposure profiles, respectively. Following the uptake of liposomes for pre-determined lengths of time, spheroids were either immediately placed in OCT, frozen, and sliced at 20 µm thickness, or incubated in fresh media for additional clearance time points prior to freezing and cryosectioning (step-wise conditions only). Spheroid slices were imaged using fluorescence microscopy and the concentration of liposomes as a function of depth from the spheroid core was determined using a MATLAB erosion algorithm that analyzes pixel intensity in concentric circles from the edge of the spheroids to the core. Calibration curves were created by correlating pixel intensities to known dilutions of liposome concentrations in a 20 µm pathlength cuvette.

Spheroid Treatment

Spheroids were incubated for six hours at 37 °C and 5% CO_2 with cell culture media containing either free doxorubicin or doxorubicin-loaded liposomes under either static or continuously infusing flow (20 µL/min) conditions, to achieve a step-wise therapy exposure profile, or flow (20 µL/min) conditions using the perfusion chamber (with CSTR) system described, to achieve an exponentially decaying therapy concentration profile with $t_{1/2}$(clearance) mimicking that *in vivo*. To ensure an equal delivered dose on each platform over the 6-hour incubation period, liposomes were incubated with spheroids at a concentration of 6.2 µM doxorubicin under static conditions with a step-wise therapy exposure, 6.2 µM doxorubicin under flow conditions (20 µL/min) with a step-wise therapy exposure, or 20 µM doxorubicin under flow conditions (20 µL/min) with exponentially decaying therapy concentrations. At the end of the incubation, spheroids were washed and transferred to fresh medium and incubated

at 37 °C and 5% CO_2. Spheroid volume was tracked for 10 days and determined as $Volume = \frac{\pi*(a*b^2)}{6}$, where a and b are the major and minor axes, respectively, of the assumed ellipsoid. After 10 days, spheroids were transferred to flat-bottom 96-well plates to allow for outgrowth of viable cells. Once spheroids receiving no treatment reached confluency in the well (after approximately 8 days), cells were trypsinized and counted using a hemocytometer.

Statistical Analysis

Values are reported as the arithmetic mean of *n* independent measurements ± the standard deviation. For each measurement, the Student's *t* test was used to calculate the significant difference in behavior (e.g., in spheroid growth) between the various constructs. Calculated *p* values < 0.05 are considered to be significant.

4.3: Results

Liposomes Characterization

Liposomes exhibited an average size of 114 ± 12 nm in diameter (PDI = 0.087 ± 0.010, *n* = 3) independent of the presence of absence of functionalization. Liposomes preformed with HER2-targeting lipopeptides contained, on average, 943 lipopeptides per vesicle leaflet (assuming symmetry of lipid leaflets). On average (*n* = 3), 22 ± 7 antibodies were conjugated per liposome.

The efficiency of doxorubicin loading into liposomes was 61 ± 11 % (*n* = 12), resulting in 0.24 ± 0.04 mole of doxorubicin per mole of lipid. Both pH-responsive (releasing) and non-pH-responsive liposomes (non-releasing) with and without

functionalization exhibited stable retention of doxorubicin after 6 hours of incubation in 10% serum-supplemented media at pH 7.4 (Table 4.1). At more acidic pH values (pH 6.5-5.5), releasing liposomes demonstrated lower retention values while non-releasing liposomes stably retained their contents.

Table 4.1: Percent retention of doxorubicin as a function of cell culture medium pH after 6 hours of incubation. Errors correspond to standard deviations of repeated measurements (n=3 independent liposome preparations).

	sticky (releasing) liposomes	*non-functionalized releasing liposomes*	*trastuzumab-functionalized non-releasing liposomes*	*non-functionalized non-releasing liposomes*
pH 7.4	91.6 ± 3.3	89.1 ± 2.5	91.4 ± 1.4	92.4 ± 1.7
pH 6.5	83.7 ± 2.1	83.0 ± 3.1	92.3 ± 3.8	90.8 ± 1.9
pH 6.0	65.4 ± 6.5	68.1 ± 2.7	91.2 ± 1.7	90.9 ± 2.7
pH 5.5	43.2 ± 2.5	47.2 ± 5.9	87.3 ± 0.9	87.2 ± 1.0

Metastatic TNBC Cell Subline Characterization

Evidence of metastases in the right cervical lymph node (red), right axillary lymph node (green), lungs (cyan and magenta), liver (yellow), and kidneys (burgundy) from the primary tumor (blue) was revealed in the T1-weighted MRI scan shown in Figure 4.1A after - on average - 33 days upon tumor inoculation. Macro-metastases were consistently observed in right axillary lymph nodes (100% of mice) and lungs (89% of mice), and sporadically observed in other organs such as the liver (22%) (Figure 4.1B). Metastases in the right axillary lymph node (Figure 4.1C), lung (Figure 4.1D) and liver (Figure 4.1E) showed steady growth for up to 17 days after being first evidenced by MRI.

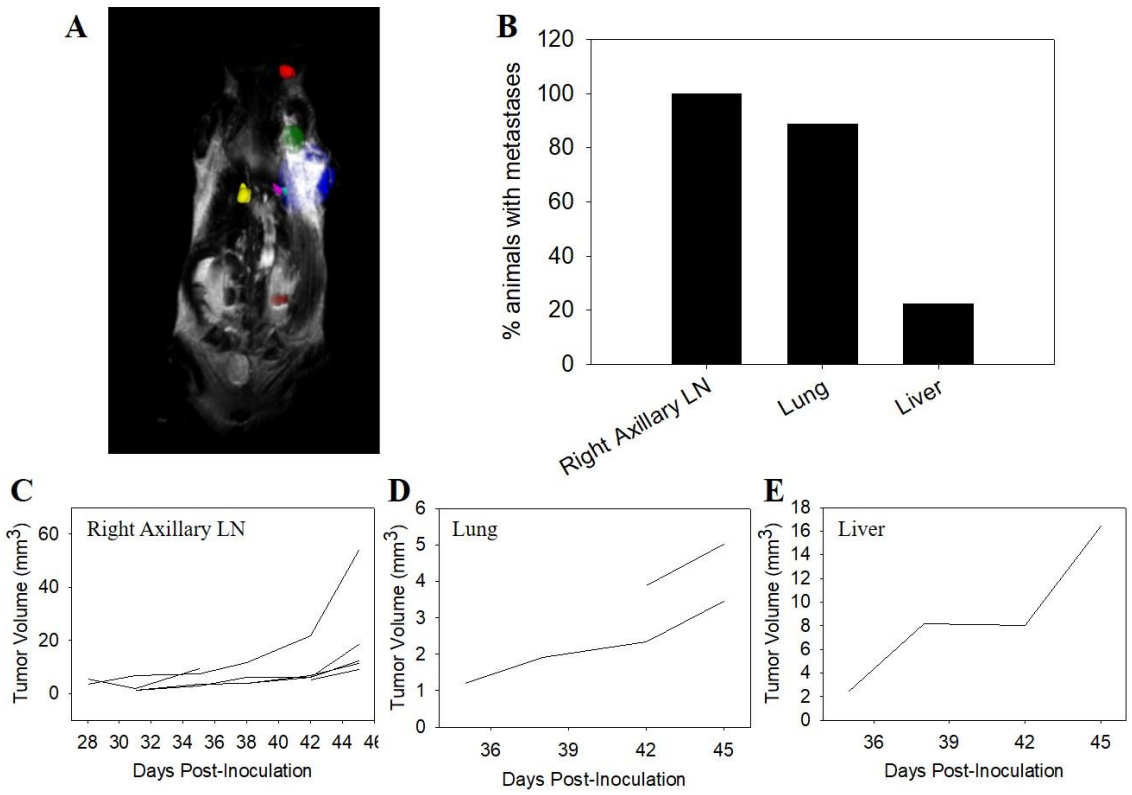

Figure 4.1: A. T1-weight MRI scan of NSG mouse inoculated with MDA-MB-231 cells in the right mammary fat pad (blue; orthotopic xenograft) and bearing metastases in the right cervical lymph node (red), right axillary lymph node (green), lungs (cyan and magenta), liver (yellow), and kidney (burgundy). **B.** Frequency of metastases in organs of mice observed at the experimental endpoint. **C.** Growth of metastases over time observed using MRI in right axillary lymph nodes. **D.** Growth of metastases over time observed using MRI in lungs. **E.** Growth of metastases over time observed using MRI in livers.

Analysis of PDTs revealed significantly faster doubling times for all metastatic TNBC cell sublines when compared to the parent MDA-MB-231 cell line purchased from ATCC (Table 4.2). Studies using ^{111}In-trastuzumab quantified the HER2 levels of each metastatic TNBC cell subline from 3.1 x 10^4 to 9.8 x 10^4 HER2 receptors per cell.

Table 4.2: Population doubling time (PDT) [hours] and HER2 receptor quantification for metastatic TNBC cell sublines and the parent MDA-MB-231 cell line purchased from ATCC in order of increasing HER2 expression. Errors correspond to standard deviations of repeated measurements (n=2-4 independent measurements).

cell line	*PDT (hours)*	*HER2 receptors per cell ($x10^4$)*
cardiomyocytes	24.5 ± 2.0	1.1 ± 0.4
231-ALN3	26.1 ± 0.6	3.1 ± 0.3
231-LUNG2	27.0 ± 1.0	4.0 ± 0.8
231-ALN1	26.3 ± 0.5	6.0 ± 0.2
231-ALN2	26.5 ± 0.2	6.6 ± 0.4
231-PRI3	26.1 ± 1.7	7.2 ± 0.2
231-LUNG1	25.1 ± 0.4	7.3 ± 1.0
MDA-MB-231	34.8 ± 1.3	8.3 ± 0.8
231-LUNG3	23.7 ± 0.1	9.8 ± 1.2

Cytotoxicity Studies on TNBC Cell Monolayers

Table 4.3 summarizes the lethal dose at which 50% of cells are killed (LD_{50}) after incubation with either free doxorubicin or doxorubicin-loaded liposomes. On cell monolayers, the LD_{50} values for non-releasing liposomes with and without antibody-functionalization were undetectable within the range of measured values (up to 200 µM doxorubicin). For releasing liposomes, LD_{50} values were only detectable at pH 6.5. LD_{50} values were significantly lower for sticky liposomes when compared to their non-functionalized form on all cell lines, with the exception of cardiomyocytes, 231-ALN3 and 231-LUNG2 which express 1.1 x 10^4, 3.1 x 10^4 and 4.0 x 10^4 HER2 receptors per cell, respectively. The lowest LD_{50} values were recorded for free doxorubicin conditions across all cell lines, with a decrease from pH 7.4 to pH 6.5.

Table 4.3: LD_{50} Values (μM doxorubicin) of free doxorubicin and doxorubicin-loaded liposomes as a function of extracellular pH. Errors correspond to standard deviations of repeated measurements (n=3 independent measurements). 'undetectable' indicates LD_{50} values which are undetectable, or do not reach less than 50% cell viability at any doxorubicin concentration up to 200 μM.

	HER2 receptors per cell ($x10^4$)	*Free doxorubicin*	*sticky liposomes*	*non-functionalized releasing liposomes*	*trastuzumab-functionalized non-releasing liposomes*	*non-functionalized non-releasing liposomes*
pH 7.4						
cardiomyocytes	1.1 ± 0.4	3.5 ± 0.3	undetectable	undetectable	undetectable	undetectable
231-ALN3	3.1 ± 0.3	3.0 ± 0.9	undetectable	undetectable	undetectable	undetectable
231-LUNG2	4.0 ± 0.8	3.0 ± 0.9	undetectable	undetectable	undetectable	undetectable
231-ALN1	6.0 ± 0.2	4.1 ± 0.6	undetectable	undetectable	undetectable	undetectable
231-ALN2	6.6 ± 0.4	5.3 ± 1.6	undetectable	undetectable	undetectable	undetectable
231-PRI3	7.2 ± 0.2	3.3 ± 1.7	undetectable	undetectable	undetectable	undetectable
231-LUNG1	7.3 ± 1.0	2.8 ± 1.4	undetectable	undetectable	undetectable	undetectable
MDA-MB-231	8.3 ± 0.8	4.3 ± 1.0	undetectable	undetectable	undetectable	undetectable
231-LUNG3	9.8 ± 1.2	3.7 ± 1.6	undetectable	undetectable	undetectable	undetectable
pH 6.5						
cardiomyocytes	1.1 ± 0.4	6.3 ± 0.7	177.1 ± 12.7	170.9 ± 19.1	undetectable	undetectable
231-ALN3	3.1 ± 0.3	7.0 ± 3.7	165.6 ± 7.4	195.6 ± 40.7	undetectable	undetectable
231-LUNG2	**4.0 ± 0.8**	5.1 ± 2.1	196.5 ± 19.7	221.6 ± 30.0	undetectable	undetectable
231-ALN1	6.0 ± 0.2	7.3 ± 2.6	80.2 ± 10.3	171.9 ± 11.7	undetectable	undetectable
231-ALN2	6.6 ± 0.4	8.4 ± 3.2	84.1 ± 10.7	220.3 ± 36.1	undetectable	undetectable
231-PRI3	7.2 ± 0.2	6.7 ± 4.2	69.0 ± 16.6	181.1 ± 10.9	undetectable	undetectable
231-LUNG1	7.3 ± 1.0	7.0 ± 3.7	65.6 ± 7.4	195.6 ± 40.7	undetectable	undetectable
MDA-MB-231	8.3 ± 0.8	8.7 ± 3.2	94.8 ± 15.4	187.9 ± 28.4	undetectable	undetectable
231-LUNG3	9.8 ± 1.2	6.9 ± 4.4	74.3 ± 17.3	179.3 ± 11.4	undetectable	undetectable

Blood Clearance Half-life in Animals

Liposome clearance from the blood of healthy athymic nude mice after injection with radiolabeled liposomes is presented in Table 4.4 and Figure A1. Levels of radioactivity in the blood were analyzed using single exponential decay models and half-lives of clearance were calculated as $t_{1/2}(clearance) = \frac{\ln(2)}{\lambda}$, where λ is the elimination

rate constant. Half-lives of clearance for all constructs loaded with ^{225}Ac were around 70 minutes and the difference among these results was not statistically significant.

Table 4.4: Blood circulation half-lives, $t_{1/2}$(clearance), of functionalized and non-functionalized, releasing and non-releasing radiolabeled liposomes. Errors correspond to standard deviations of repeated measurements (n=5 animals).

	sticky liposomes	*non-functionalized releasing liposomes*	*trastuzumab-functionalized non-releasing liposomes*	*non-functionalized non-releasing liposomes*
$t_{1/2}$(clearance), minutes	67 ± 10	71.4 ± 4	68 ± 11	73 ± 19

Perfusion System Design and Fabrication

A schematic of the perfusion chamber system is given in Figure 4.2. The perfusion chamber system was designed to pump a diluent, typically media, into a continuous stirred tank reactor (CSTR), typically containing the therapy of interest (e.g. liposomes, free doxorubicin). The fluid from the CSTR was then drawn into the inlet of the perfusion chamber containing multicellular spheroids using a withdrawing pump at the outlet of the chamber.

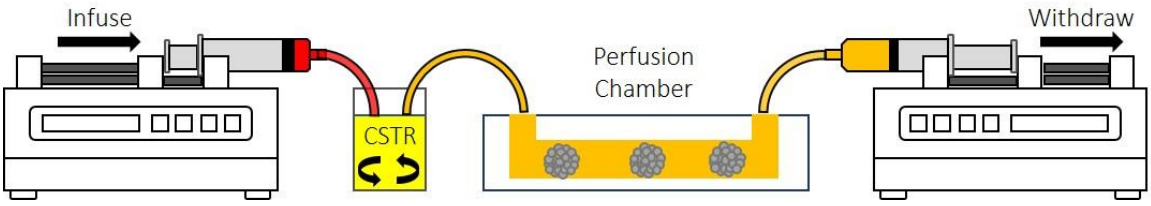

Figure 4.2: Schematic of perfusion chamber system.

To examine the infusion and clearance profile of contents within the perfusion chamber, the CSTR was filled with a non-self-quenching concentration of calcein (1 mM) then drawn through the system at 20 µL/minute. The pixel intensity of calcein

within the chamber was captured as a function of time using an inverted fluorescent microscope and plotted in Figure 4.3. In order to determine the half-life of clearance of calcein from the chamber, data points from 30 to 360 minutes were fitted with a single exponential decay model and $t_{1/2}$(clearance) was calculated as previously described for blood circulation half-life experiments. On average, the half-life of clearance of calcein within the chamber was 85 ± 5 minutes, which was comparable to the half-life of clearance of functionalized and non-functionalized, releasing and non-releasing radiolabeled liposomes in healthy athymic nude mice.

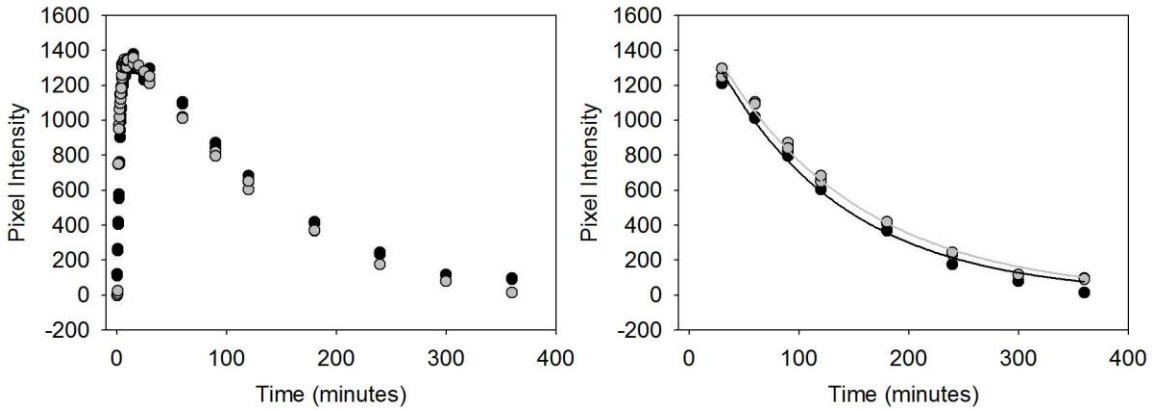

Figure 4.3: (A) Raw temporal pixel intensities of calcein (used as drug surrogate) within the perfusion chamber where spheroids, surrogates of tumor avascular regions, were placed, and the resulting (B) exponential decay fits (n=2).

Liposome and Doxorubicin Penetration into Spheroids

The purpose of this experimental design was to show that not only the AUC of the therapeutics' temporal profile but its actual temporal function may play a role in affecting (1) the spatiotemporal profiles of therapeutics diffusing within the spheroids' interstitium, altering, therefore, (2) the observed therapeutic effect. Time integration of spatiotemporal profiles given in Figures A.4, A.5, A.6 and A.7 demonstrated that doxorubicin exposure

towards the core was measurably higher under step-wise incubation profiles (round symbols), whereas liposome exposure was comparable between incubation platforms (Figure 4.4).

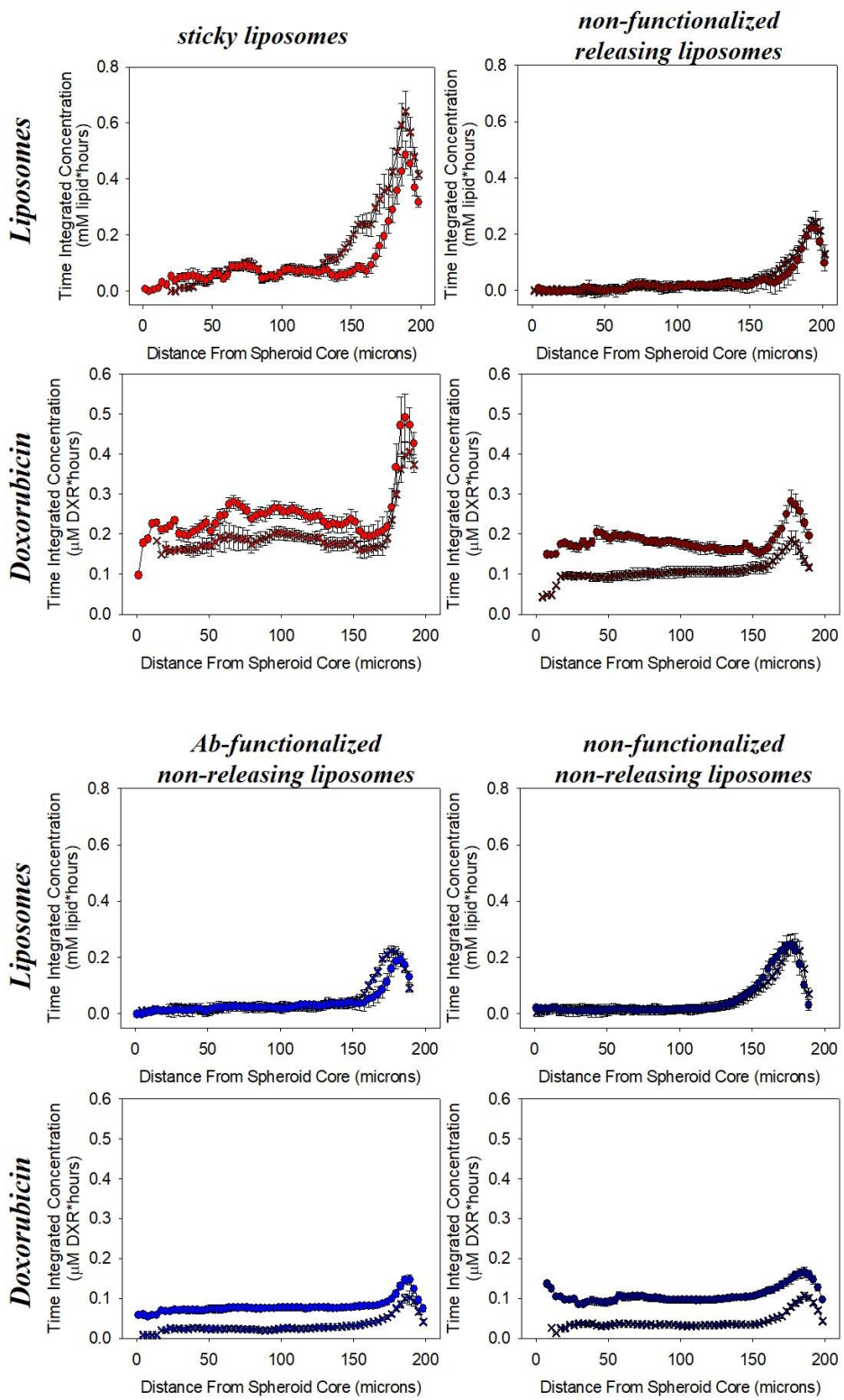

Figure 4.4: Time integrated spatiotemporal profiles for liposomes and doxorubicin (from liposomes loaded with non-self-quenching doxorubicin) after incubation with MDA-MB-231 spheroids using step-wise (rounds symbols) and exponentially decaying (X symbols) exposure profiles.

Spheroid Treatment

Independent of the therapeutics' temporal profiles, sticky liposomal doxorubicin (red symbols) resulted in significantly smaller volumes of MDA-MB-231 spheroids (8.3 x 10^4 HER2 receptors per cell) at day 10 post-therapy when compared all other liposomal constructs (p-values < 0.01) (Figure 4.5A,B And Figure A.8). Correspondingly, spheroids treated with sticky liposomal doxorubicin exhibited 8% and 12% comparable outgrowth under step-wise therapy exposure and exponentially decaying therapy exposure, respectively. The temporal function of therapeutics significantly affected the outgrowth levels resulted from exposure to non-functionalizing releasing liposomal doxorubicin (burgundy bars, Figure 4.6A,B and Figure A.9). The outgrowth values for sticky liposomal doxorubicin were significantly lower than all other liposomal constructs (p-values < 0.01) (Figure 4.6A,B and Figure A.9). On all testing platforms, free doxorubicin (white symbols) out-performed all liposomal doxorubicin constructs.

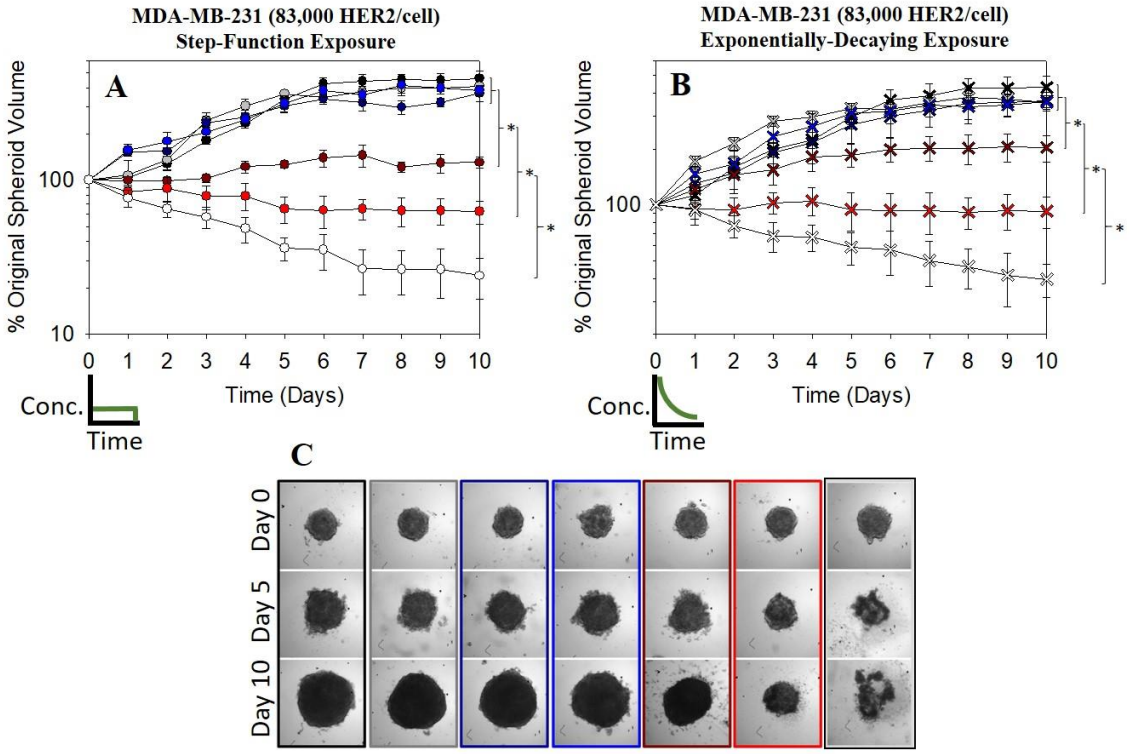

Figure 4.5: Efficacy of doxorubicin constructs against TNBC MDA-MB-231 spheroids (8.3×10^4 HER2 receptors per cell) under (A) step-wise therapy exposure and (B) exponentially decaying therapy exposure, in the form of sticky liposomes, non-functionalized releasing liposomes (burgundy symbols), trastuzumab-functionalized non-releasing liposomes (light blue symbols), non-functionalized non-releasing liposomes (dark blue symbols), and free doxorubicin (white symbols). Black symbols indicate untreated spheroids and light grey symbols indicate the effect of empty liposomes. (C) Representative images of MDA-MB-231 spheroids (83,000 HER2 receptors per cell) post-treatment with exponentially decaying concentrations of therapy in the perfusion chamber. * indicates *p*-values < 0.01.

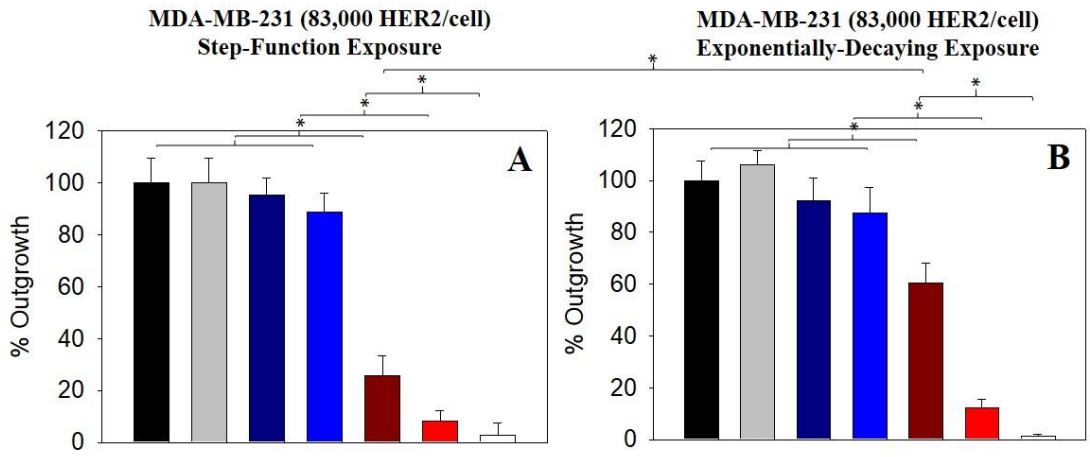

Figure 4.6: Outgrowth at the endpoint given in Figure 4.5 for MDA-MB-231 spheroids under (A) step-wise therapy exposure and (B) exponentially decaying therapy exposure, in the form of sticky liposomes, non-functionalized releasing liposomes (burgundy symbols), trastuzumab-functionalized non-releasing liposomes (light blue symbols), non-functionalized non-releasing liposomes (dark blue symbols), and free doxorubicin (white symbols). Black bars indicate untreated spheroids and light grey bars indicate the effect of empty liposomes. * indicates *p*-values < 0.01.

Similarly, on 231-LUNG3 (9.8 x 10^4 HER2 receptors per cell) and 231-PRI3 (7.2 x 10^4 HER2 receptors per cell) spheroids exposed to exponentially decaying concentrations of the therapy, sticky liposomal doxorubicin (red symbols) resulted in significantly smaller spheroid volumes at day 10 post-therapy when compared to all other liposomal constructs (*p*-values < 0.01) (Figure 4.7A,B). Outgrowth assays were complimentary to spheroid growth control experiments, where spheroids treated with sticky liposomal doxorubicin (red bars) resulted in significantly less outgrowth than treatment with all other forms of liposomal doxorubicin (Figure 4.8A,B). As with MDA-MB-231 spheroids, free doxorubicin (white symbols) resulted in the smallest spheroid volumes and lowest outgrowth percentages at Day 10. In contrast to the efficacy seen in MDA-MB-231, 231-LUNG3 and 231-PRI3 spheroids, and under identical incubation conditions, Figure 4.7C demonstrates that 231-ALN3 (3.1 x 10^4 HER2 receptors per cell)

spheroids exhibited similar growth patterns after treatment with either sticky (red symbols) or non-functionalized releasing (burgundy symbols) liposomes. This behavior translated into outgrowth activity that was comparable between sticky (red bars) and non-functionalized releasing (burgundy bars) liposomes (Figure 4.8C).

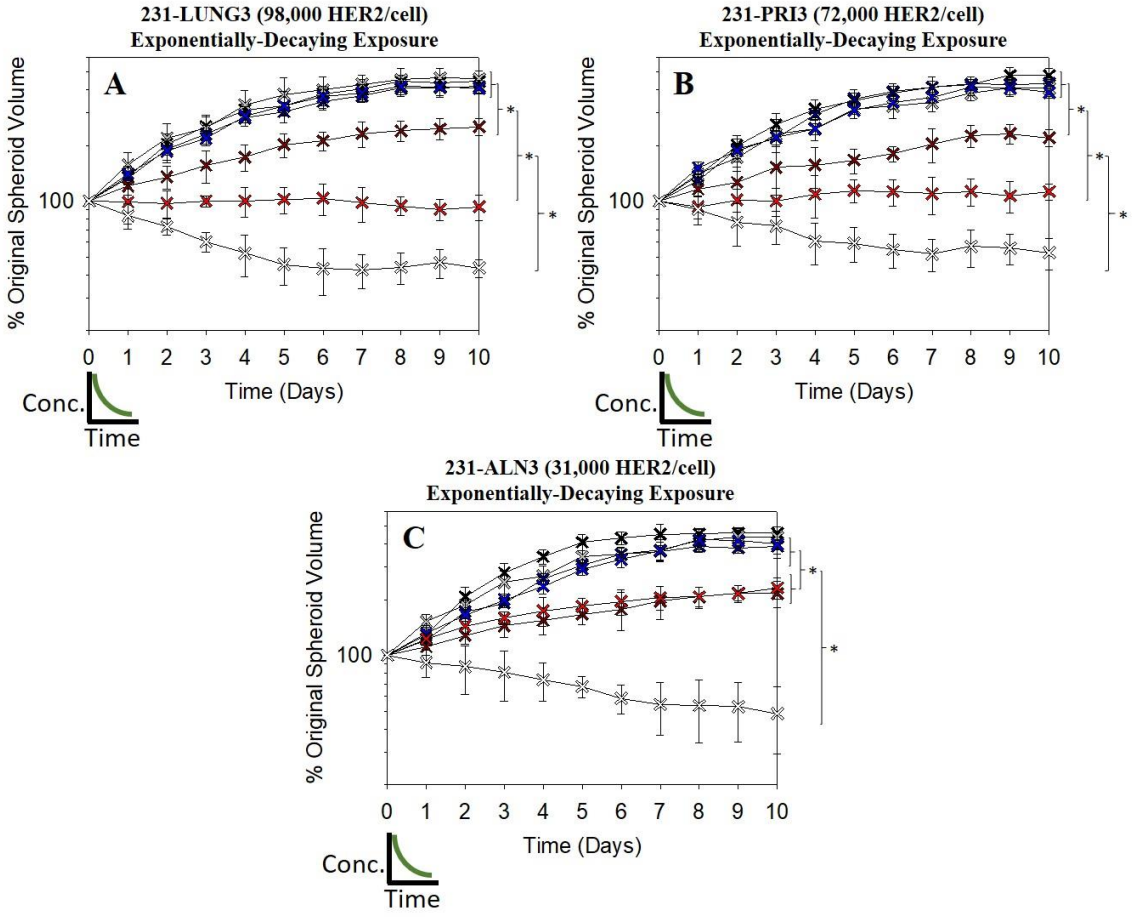

Figure 4.7: Efficacy of doxorubicin constructs against (A) 231-LUNG3, (B) 231-PRI3 and (C) 231-ALN3 spheroids under exponentially decaying therapy exposure, in the form of sticky liposomes, non-functionalized releasing liposomes (burgundy symbols), trastuzumab-functionalized non-releasing liposomes (light blue symbols), non-functionalized non-releasing liposomes (dark blue symbols), and free doxorubicin (white symbols). Black symbols indicate untreated spheroids and light grey symbols indicate the effect of empty liposomes. * indicates *p*-values < 0.01.

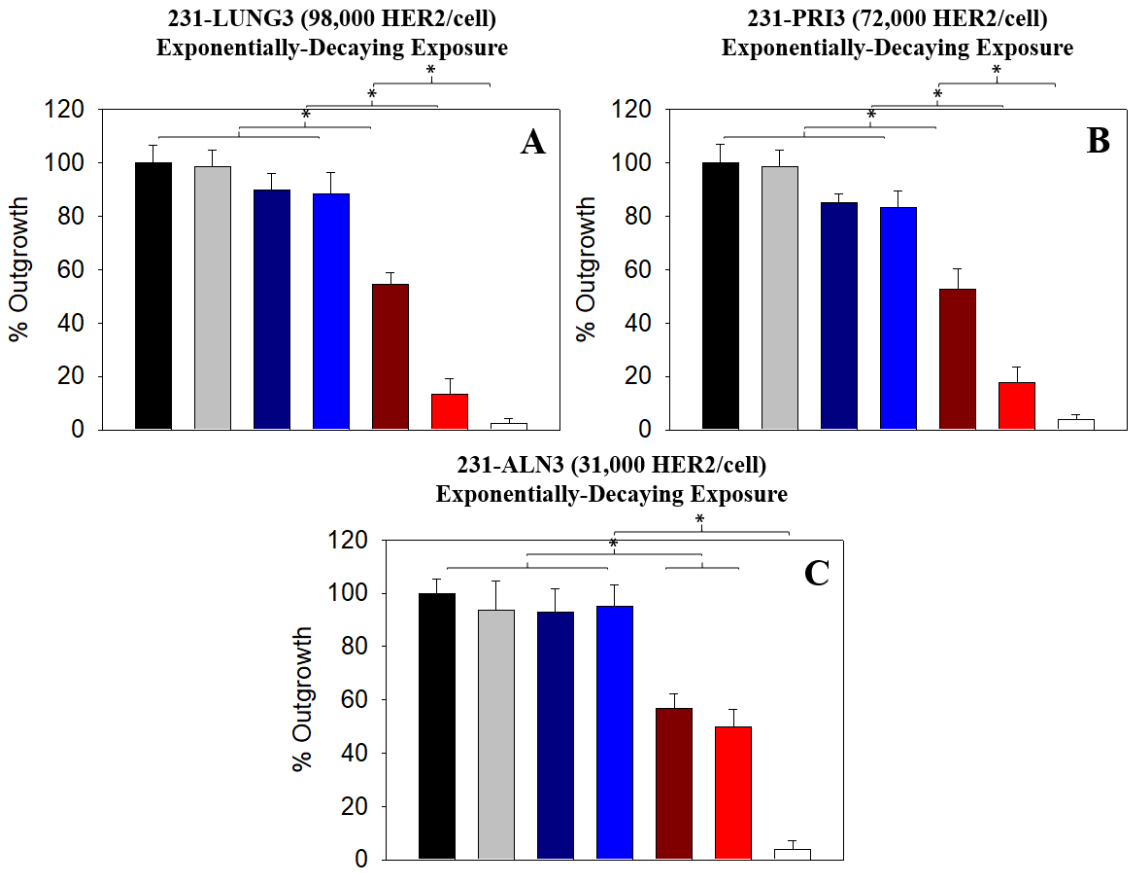

Figure 4.8: Outgrowth at the endpoint given in Figure 4.7 for (A) 231-LUNG3, (B) 231-PRI3 and (C) 231-ALN3 spheroids treated with exponentially decaying therapy exposure, in the form of sticky liposomes, non-functionalized releasing liposomes (burgundy symbols), trastuzumab-functionalized non-releasing liposomes (light blue symbols), non-functionalized non-releasing liposomes (dark blue symbols), and free doxorubicin (white symbols). Black bars indicate untreated spheroids and light grey bars indicate the effect of empty liposomes. * indicates *p*-values < 0.01.

4.4: Discussion

In this study, we exploited a previously established peptide-functionalized pH-responsive (sticky) liposome construct that has already demonstrated selective targeting and killing of otherwise "untargetable" breast cancer cells [64] in order to evaluate its pre-clinical feasibility as a targeted therapy for TNBC. To date, there exists no form of targeted therapy for patients with TNBC and the first line of treatment is typically systemic chemotherapy [63] . The use of a targeted therapy for these TNBC patients

could ultimately minimize the systemic toxicities associated with traditional chemotherapeutics while maximizing the therapeutic payload at the site of the tumor [9]. Although HER2-targeting nanoparticles, such as MM-302, have reached clinical trials and show promise for the treatment of HER2-positive breast cancer, they lose effectiveness against cancer cells expressing <200,000 HER2 copies/cell [23]. These limitations dictate the need for new approaches to target cancer cells with low (or variable) receptor expression in order to capitalize on the benefits of targeted therapies.

This work utilizes metastatic TNBC cell sublines derived from murine breast cancer models which reliably formed metastases in distant organs including right axillary lymph nodes and lungs. These cells lines not only provide a more clinically relevant and robust method for testing TNBC therapy in general because of their aggressiveness (as evidenced by their faster PDTs relative to the parent MDA-MB-231 cell line), but they also provide a wide range of HER2-expression levels from 3.1×10^4 to 9.8×10^4 HER2 receptors per cell for the explicit testing of HER2-targeted therapies.

Here we show that sticky liposomal doxorubicin, triggered to form a clustered display of HER2-targeting ligands on the liposome surface at acidic pH values matching that of the tumor interstitium ($pH\ 7.0 > pH \geq 6.0$) [28, 40], resulted in lower LD_{50} values and better control of spheroid growth using MDA-MB-231 breast cancer cell spheroids, as well as 231-LUNG3 and 231-PRI3 metastatic TNBC cell subline spheroids when compared to non-functionalized releasing liposomes and trastuzumab-functionalized or non-functionalized non-releasing liposomes. For these sticky liposomes, greater spheroid growth control strongly correlated with lesser spheroid outgrowth, most likely due to internalization of the nanoparticle and subsequent approximation of doxorubicin nearer to

its main molecular target (i.e. nucleus). On 231-ALN3 metastatic TNBC cell subline spheroids, sticky and non-targeting releasing liposomal doxorubicin resulted in similar spheroid growth control, most likely as a result of the minimal HER2 expressed by this subline (3.1×10^4 HER2 copies per cell) which was below the 40k receptor expression cutoff necessary to observe the 'sticky effect' *in vitro* (Table 4.3). This cell line ultimately defines the HER2 receptor limit at which sticky liposomes can no longer deliver enough doxorubicin to result in cytotoxicity.

For decades, the relevance of utilizing 3D multicellular spheroid systems over the traditional 2D cell cultures for the testing and development of therapies has become increasingly apparent, mainly due to differences in diffusion-related transport and varying drug sensitivities between the two platforms [69] [70]. Here we implement a perfusion chamber system that can not only accommodate multicellular spheroids, but also expose them to exponentially decaying concentrations of the therapy with half-life of clearance rates that are tunable using the embedded fluidics system. In this case, we use a flow rate of 20 µL per minute to mimic the $t_{1/2}$(clearance) observed for releasing and non-releasing liposomes (with or without functionalization), which was slightly shorter than 90 minutes. While untreated spheroid growth over time under conditions of flow was dampened compared to that observed under static conditions (Figure A8), the same overall trends existed for the efficacy of liposomal doxorubicin on controlling spheroid growth over all platforms. That is, sticky liposomal doxorubicin exhibited greater spheroid growth control when compared to all other liposomal constructs. However, differences were observed between the outcomes on each platform when spheroid growth after treatment with the therapy was normalized to that of the untreated condition

$\left(\frac{\%\ Original\ Spheroid\ Volume\ After\ Treatment}{\%\ Original\ Spheroid\ Volume\ After\ No\ Treatment}\right) * 100$. Figure 4.9 and Figure A.10 confirm that spheroid growth control was exaggerated for free doxorubicin and non-functionalized releasing liposomal doxorubicin under step-wise exposure of the therapy, when compared to exponentially decaying concentrations of the therapy. This demonstrates that platforms which utilize a step-wise function for the therapy exposure profile should only be used as qualitative (and not quantitative) assays for testing the efficacy of different therapies.

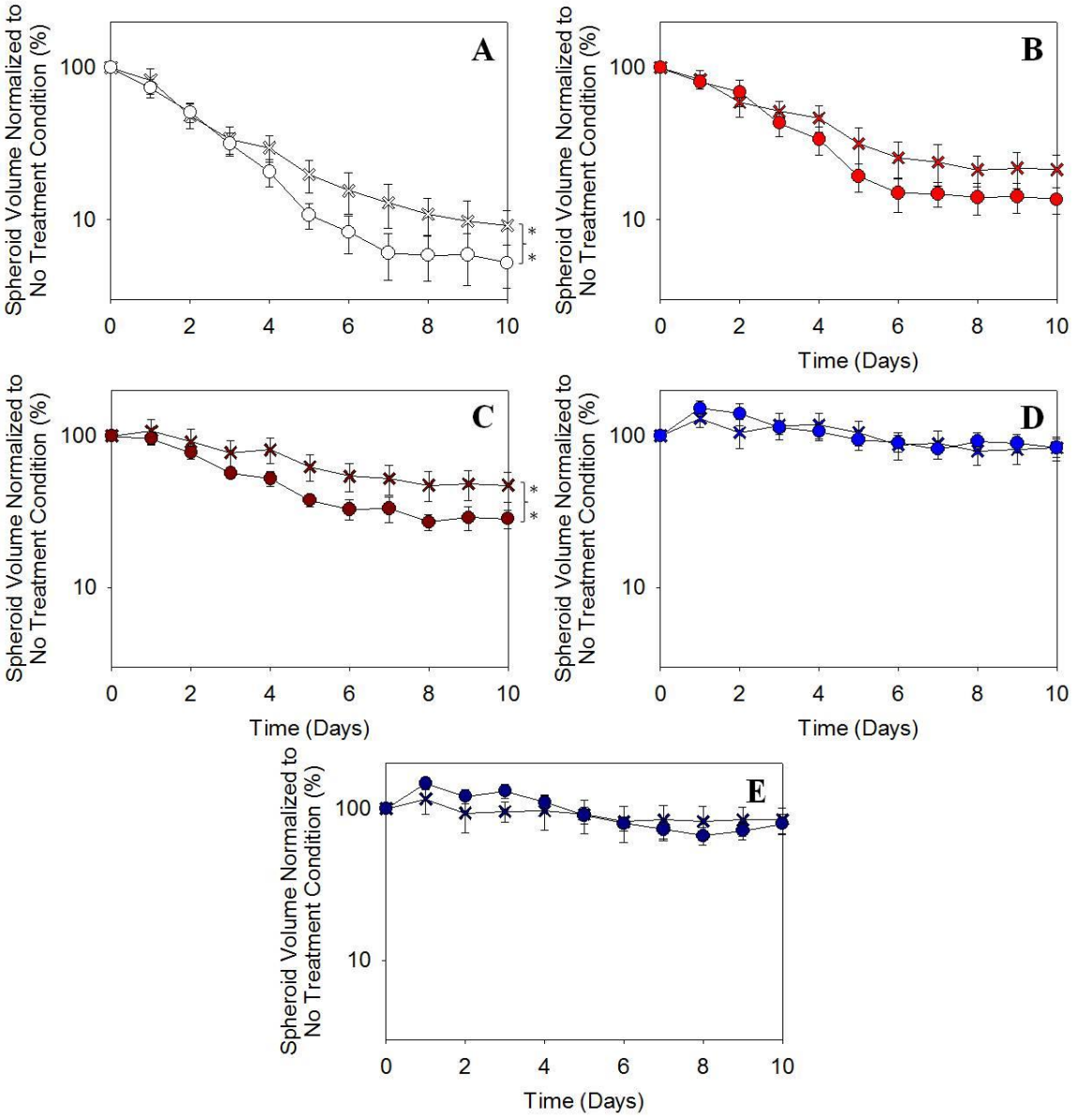

Figure 4.9: Effect of incubation platform on spheroid response to (A) free doxorubicin, (B) sticky liposomal doxorubicin, (C) non-functionalized releasing liposomal doxorubicin (D) trastuzumab-functionalized non-releasing liposomal, (E) non-functionalized non-releasing liposomal doxorubicin for step-wise therapy exposure (round symbols), and exponentially decaying therapy exposure (X symbols). ** indicates *p*-values <0.05.

In this work, we examined the potential for HER2-targeting peptide-

functionalized pH-responsive liposomes to serve as a targeted therapy for TNBC patients

with currently no targeted treatment options. On both TNBC cell monolayers and spheroids, HER2-targeting peptide-functionalized pH-responsive liposomal doxorubicin demonstrated selective and effective killing. While traditionally targeted therapies are developed by first identifying molecular markers that are overexpressed on the cell surface in order to formulate targeted therapies (such as nanoparticles or antibodies) against the overexpressed molecular marker, our approach utilizes the low receptor levels common to TNBC to harness the overall benefits of targeted therapy (i.e. increased drug delivery at the tumor with decreased systemic toxicity).

CHAPTER 5: DISSERTATION SUMMARY

5.1: Key findings

The key finding of this dissertation is that HER2-targeting sticky liposomal doxorubicin may be a viable option for the treatment of HER2-negative cancer (e.g. TNBC). More specifically, we have shown that (1) ligand presentation, local multivalency and cluster size on HER2-targeting sticky liposomes can tune functionality against both low and high HER2-expressing cells, (2) HER2-targeting sticky liposomal doxorubicin can selectively deliver lethal doses of chemotherapeutics and effectively kill breast cancer cells expressing low degrees of HER2 (<100,000 HER2 copies/cell and >40,000 HER2 copies/cell) and (3) in the presence of diffusion-limited transport and under physiologically relevant exposure conditions of the therapy, HER2-targeting sticky liposomal doxorubicin maintain their effectiveness in terms of controlling the growth of TNBC spheroids. These findings are significant for several reasons: (1) patients with tumors considered HER2-negative are typically treated with systemic chemotherapy which often results in unwanted off-target toxicities, (2) the spatial distribution of targeting ligands on the nanoparticle surface and its effects on cell interactions has generally been focused on 'molecular clusters' of ligands resulting in overall uniform functionalization and has only been reported in terms of increasing avidity on cell lines with overexpression of targets, but our findings suggest that it can play a significant role in nanoparticle reactivity, especially against traditionally "untargetable" low-receptor expressing cells, (3) targeted therapies are traditionally developed by first discovering molecular markers that are expressed to high degrees on

the cell surface then formulating the therapy against the overexpressed marker, but our findings suggest that an alternative strategy lies in the utilization of low receptor levels which can be specifically targeted by nanoparticles with ‘sticky patches’ of densely clustered targeting ligands.

5.2: Limitations and Future Studies

Chapters 2 and 3 of this dissertation focused on the design and development of HER2-targeting sticky liposomes, as well as determining the mechanism of action of sticky liposomes. It was demonstrated through dissociation rate constant experiments that sticky liposomes can be specifically bound on the cell surface by utilizing only one receptor underneath the projected area of the nanoparticle. However, it is clear that in the case where receptors are allowed to freely and laterally diffuse on the cell surface, they are recruited by the already bound liposome. Yet, it is not clear if the second (or more) recruited receptors are necessary for the observed internalization of liposomes. To fully elucidate these detailed interactions real-time single-particle tracking studies will need to be explored.

The entirety of this dissertation work (Chapters 2-4) was completed on *in vitro* testing platforms, from 2D cell monolayers to 3D multicellular spheroids. Although more physiologically relevant 3D cell culture systems such as multicellular spheroids can recapitulate the basic 3D architecture and environment of a tumor, including diffusion-limited transport and gradients for nutrients and waste, it is unknown whether these results will translate to efficacy *in vivo*. Future goals of this project include evaluating biodistributions, control of growth of metastasis and overall animal survival after surgical

removal of the primary tumor and treatment with HER2-targeting sticky liposomal doxorubicin.

Another potential area of improvement for this work lies in the overall therapeutic approach, mainly for further *in vivo* testing. As previously mentioned, HER2 expression on cells comprising a given tumor *in vivo* may range from HER2-negative to HER2-positive [24]. Because a common treatment option for HER2-positive cancer is trastuzumab, the greatest benefit in controlling tumor growth may lie in a dual therapy consisting of both trastuzumab and HER2-targeting sticky liposomal doxorubicin. This would allow us to harness the most effective targeting strategy for each cell type comprising the tumor.

Our group has shown that this new binding geometry is not limited to the particular receptor-ligand pair, but that it is generalizable to other receptors using small molecule ligands (PSMA - urea-based peptidomimetics). Another future direction, therefore, for this work lies in the use of different targeting ligands which target different receptors on different cancer types. A number of other well studied targets with well-known targeting ligands include the PSMA receptor [71], folate receptor [72] and the EGFR[73]. For each of these receptors, evidence of overexpression is always coupled with evidence of minimal expression, and it is the latter half where sticky liposomal doxorubicin has the advantage of specifically targeting and treating.

APPENDIX

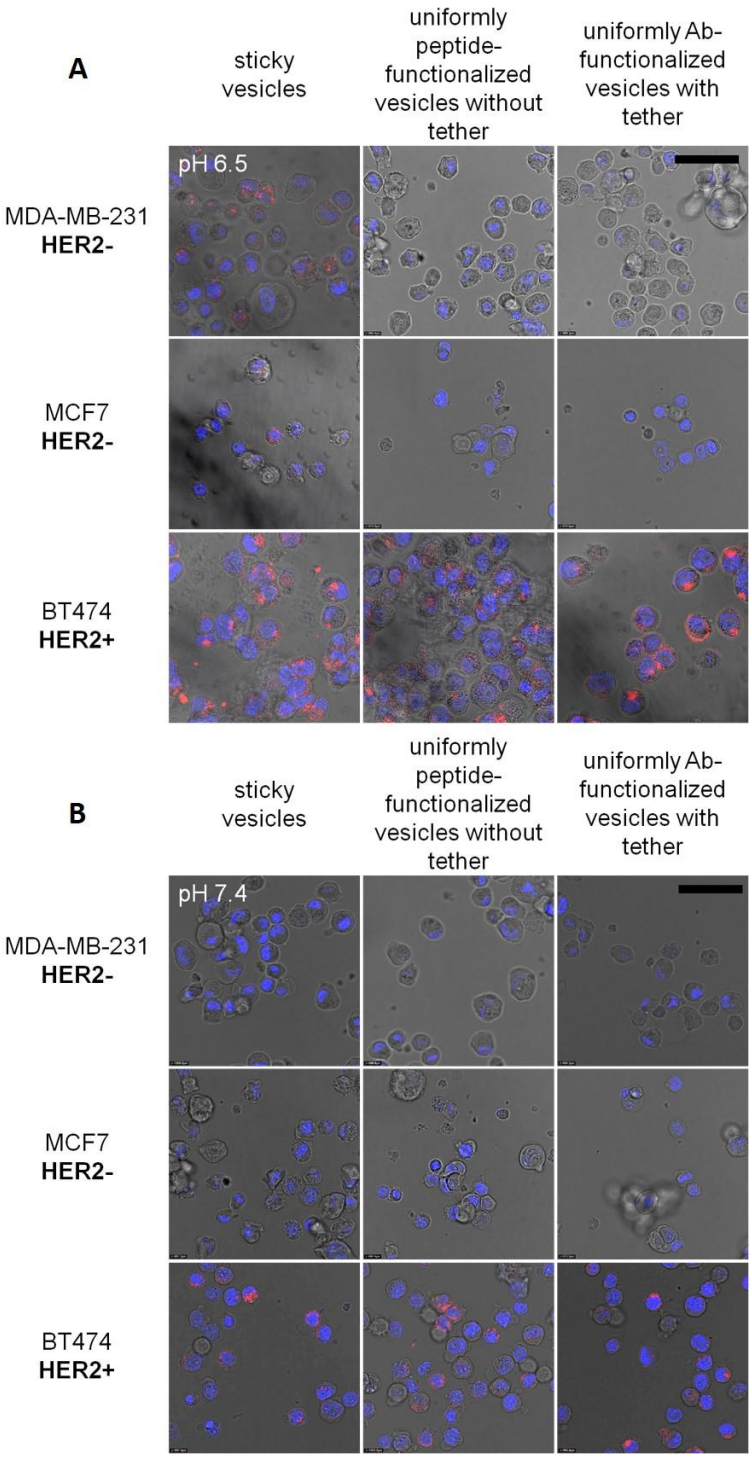

Figure A.1: Characteristic confocal fluorescence images of functionalized liposome uptake over time at extracellular pH 6.5 (A) and pH 7.4 (B) in HER2-negative MDA-MB-231, HER2-negative MCF7, and HER2-positive BT-474 breast cancer cells. Scale bar: 50 µm.

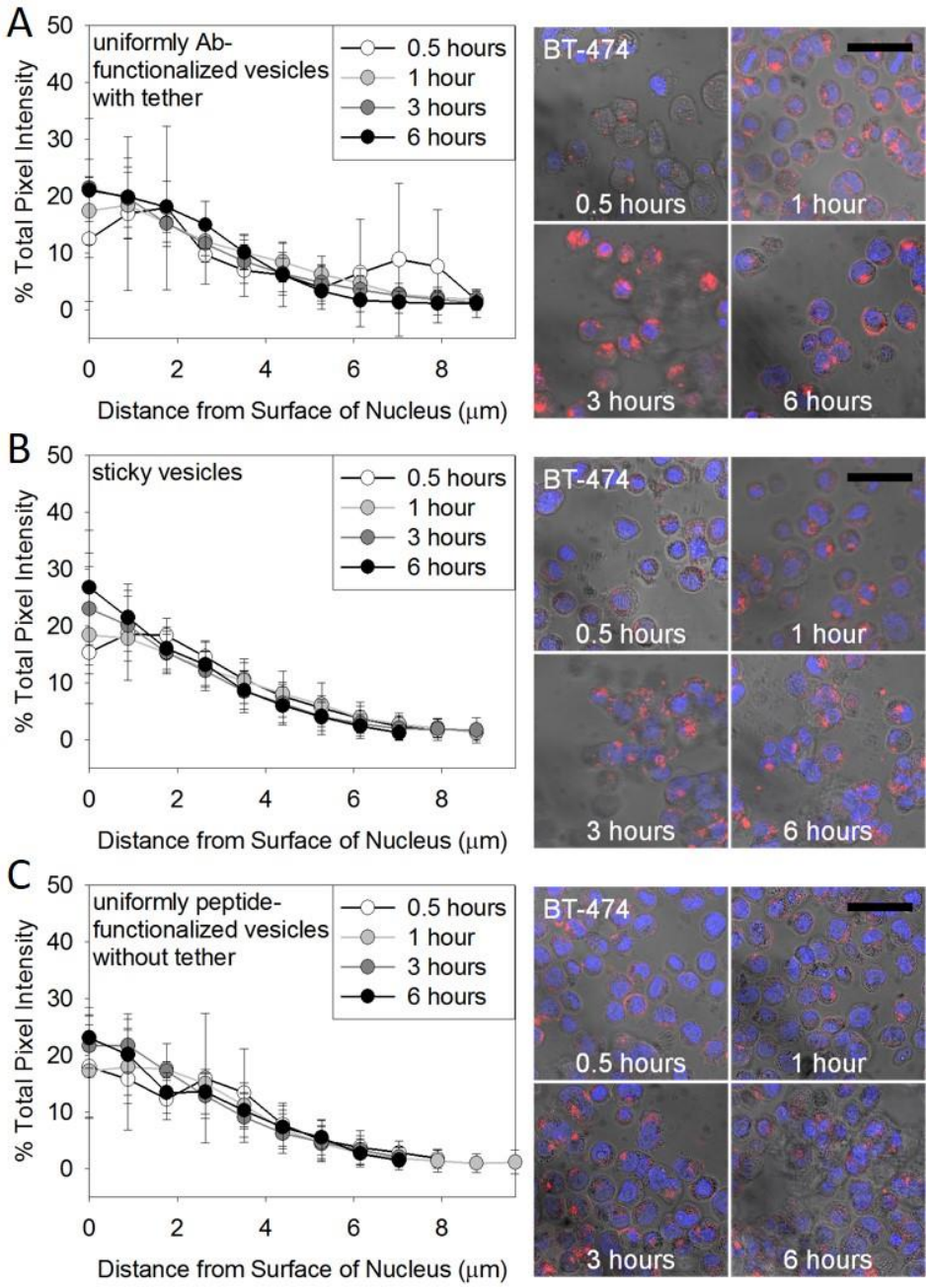

Figure A.2: Cytoplasmic distributions and characteristic confocal fluorescence images of uniformly Ab-functionalized liposomes (A), sticky liposomes (B), and uniformly peptide-functionalized liposomes (C) over time at extracellular pH 6.5 in HER2-positve BT-474 breast cancer cells. Per time point, n=10 cells were analyzed and averaged. Scale bar: 50 μm.

Table A.1: Flow cytometric analysis of endocytosis inhibition studies (from Figure 3.8) for sticky liposomes incubated with HER2-negative MCF7 and HER2-positive BT-474 breast cancer cells. Values correspond to geometric means of histograms collected for 50,000 events.

	Condition	**MCF-7**	**BT-474**
	Cells Only	17.4	28.0
Clathrin-Mediated Endocytosis Inhibitors	Cells+liposomes, 4°C	42.8	77.1
	Cells+liposomes, 37°C	99.3	216.8
	Chlorpromazine	54.9	188.3
	K+ Depletion	61.6	149.3
	Hypertonic Sucrose	74.2	118.8
Caveolae-Mediated Endocytosis Inhibitors	Cells+liposomes, 4°C	42.8	77.1
	Cells+liposomes, 37°C	99.3	651.3
	Filipin III	75.5	199.2
	Genistein	75.3	192.0
	MBCD	109.7	560.2

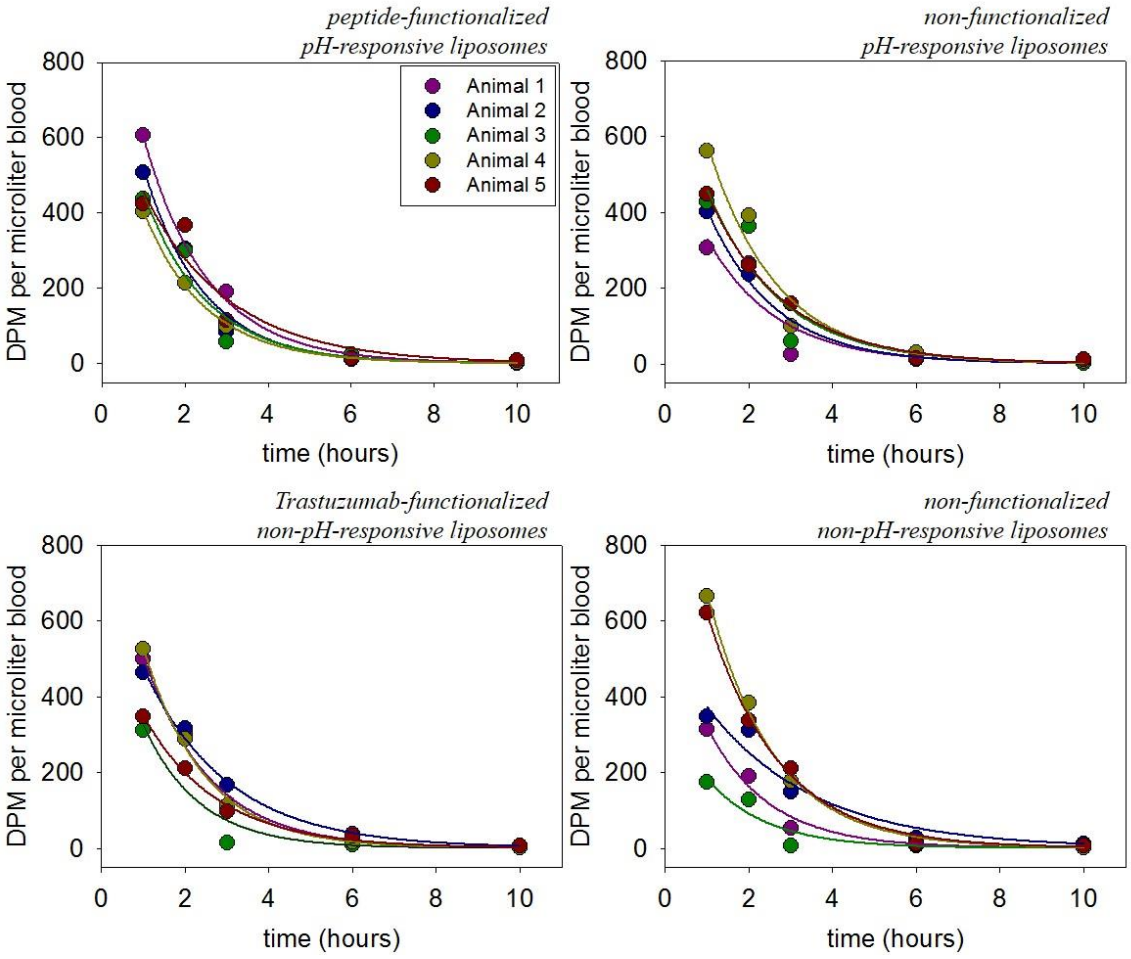

Figure A.3: Blood circulation of radiolabeled functionalized and non-functionalized, pH- and non-pH-responsive liposomes as a function of time.

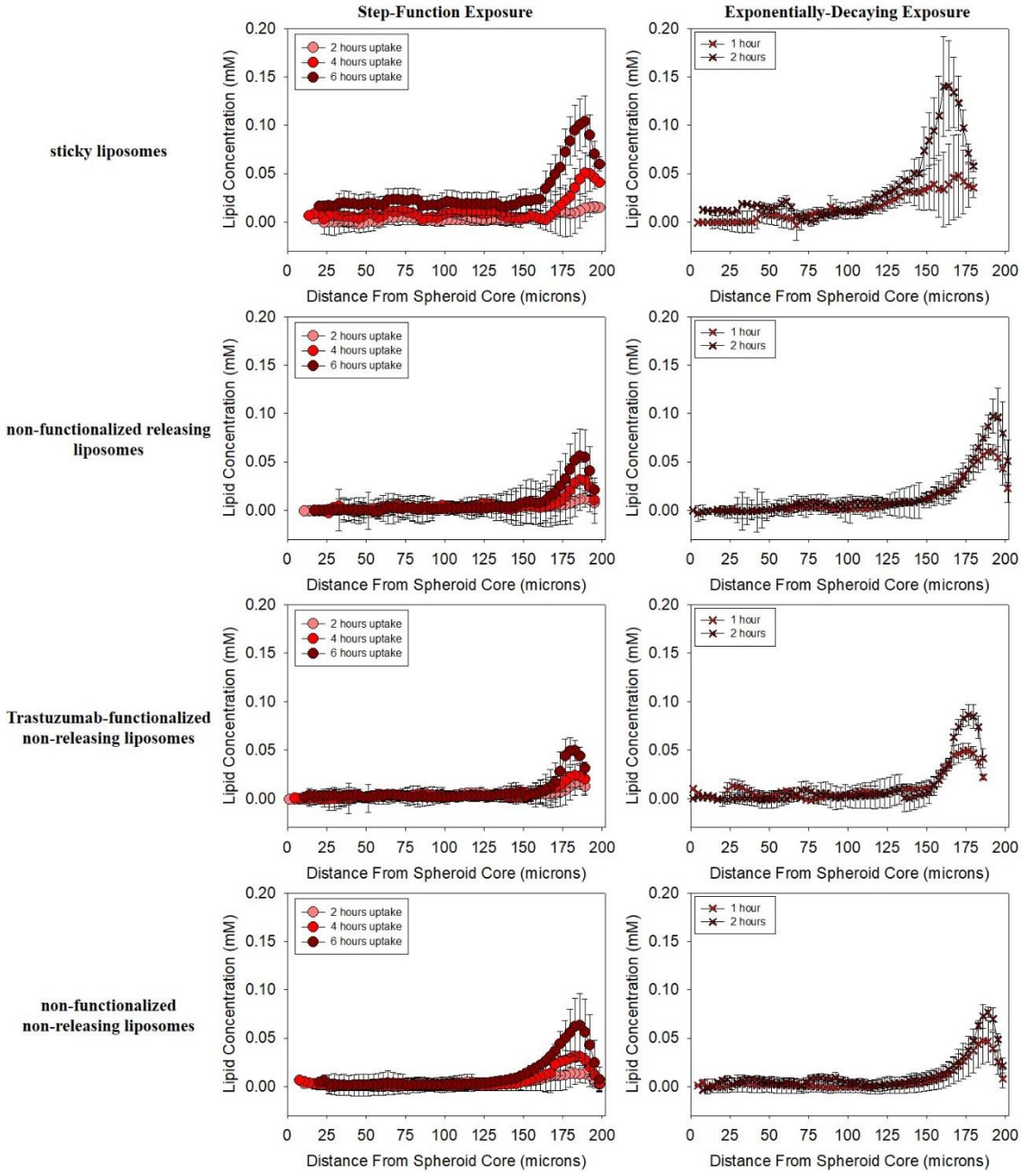

Figure A.4: Spatiotemporal profiles of fluorescent liposome uptake in MDA-MB-231 spheroids (83,000 HER2 receptors per cell).

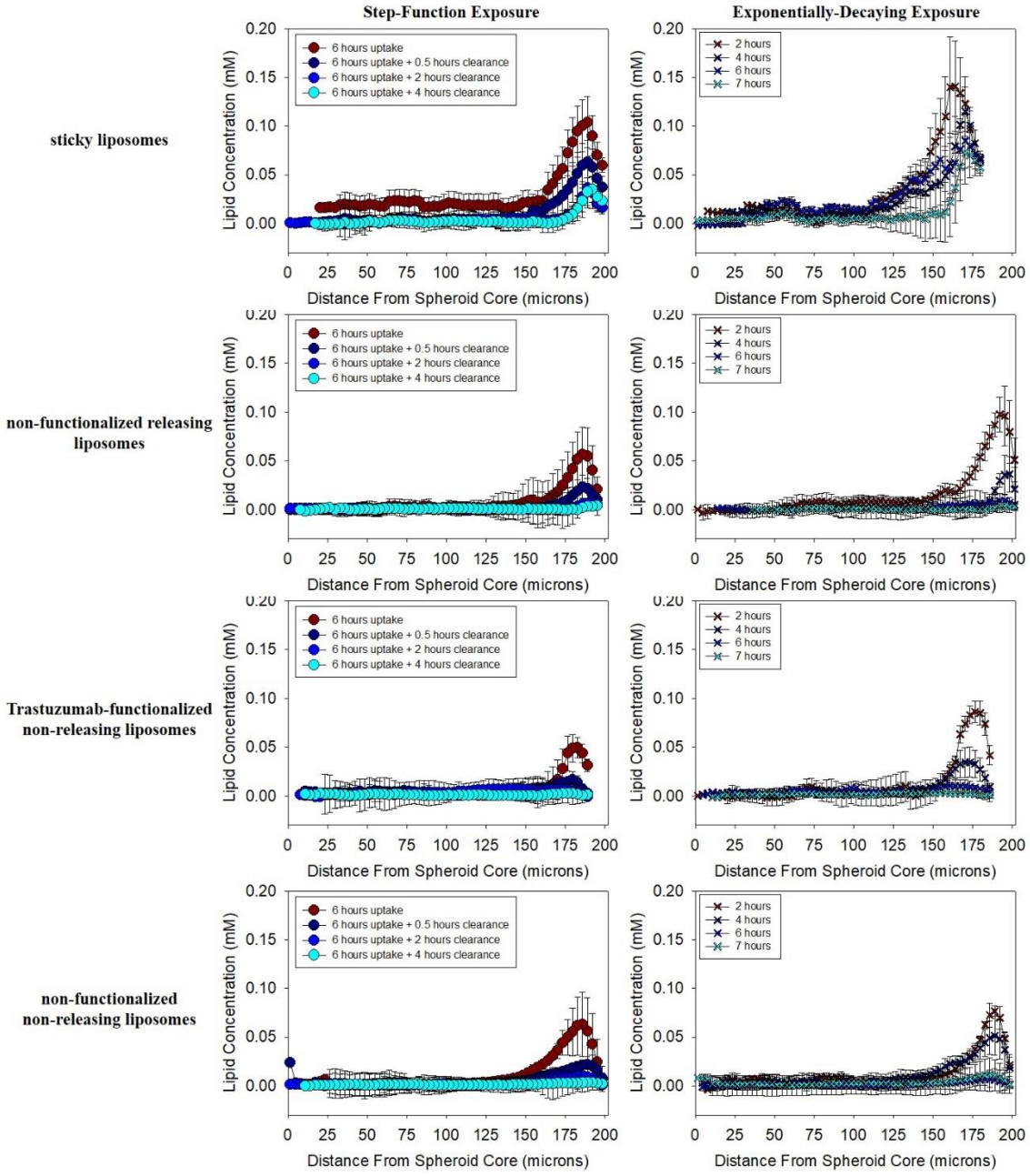

Figure A.5: Spatiotemporal profiles of fluorescent liposome clearance from MDA-MB-231 spheroids (83,000 HER2 receptors per cell).

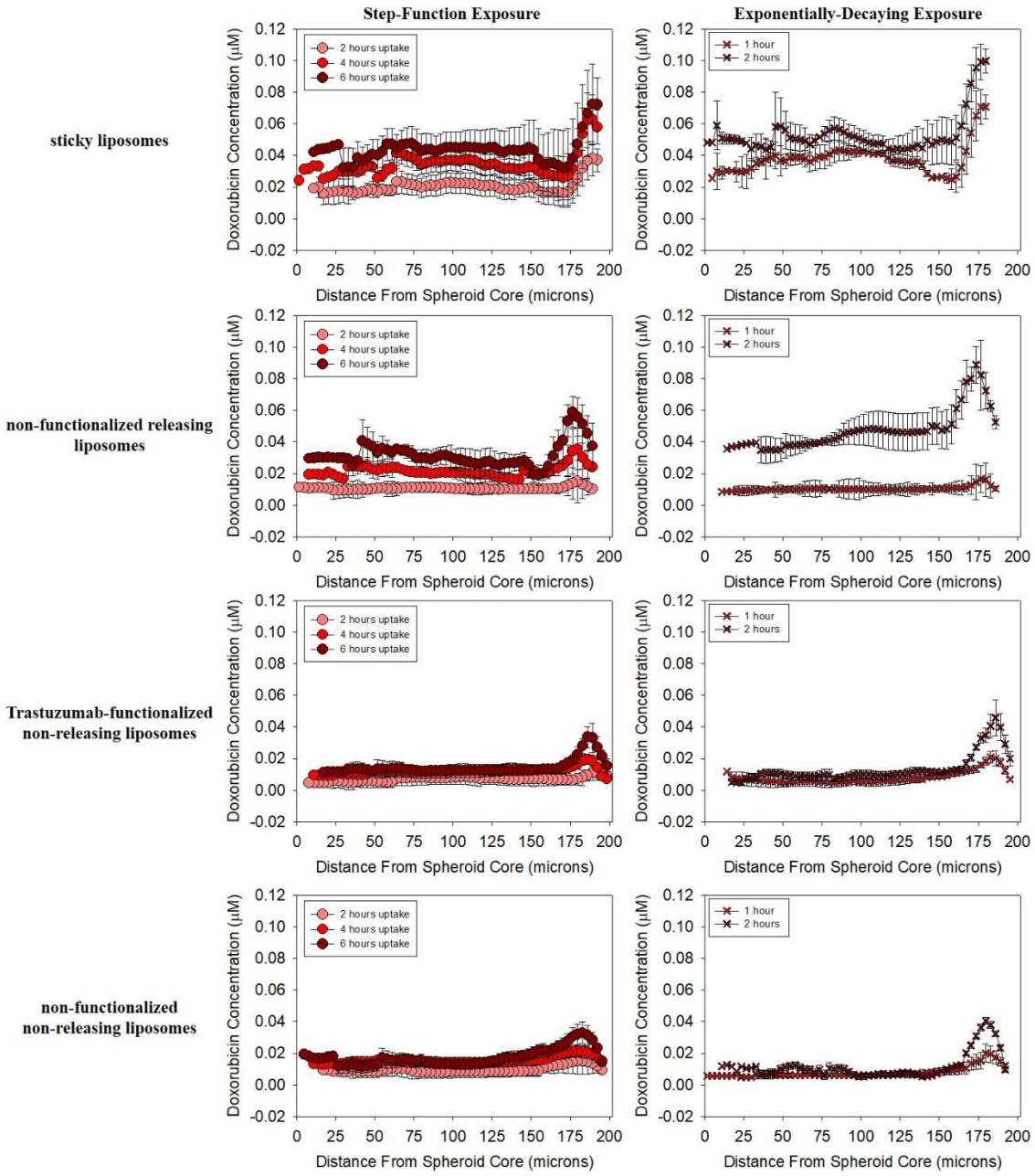

Figure A.6: Spatiotemporal profiles of doxorubicin uptake in MDA-MB-231 spheroids (83,000 HER2 receptors per cell).

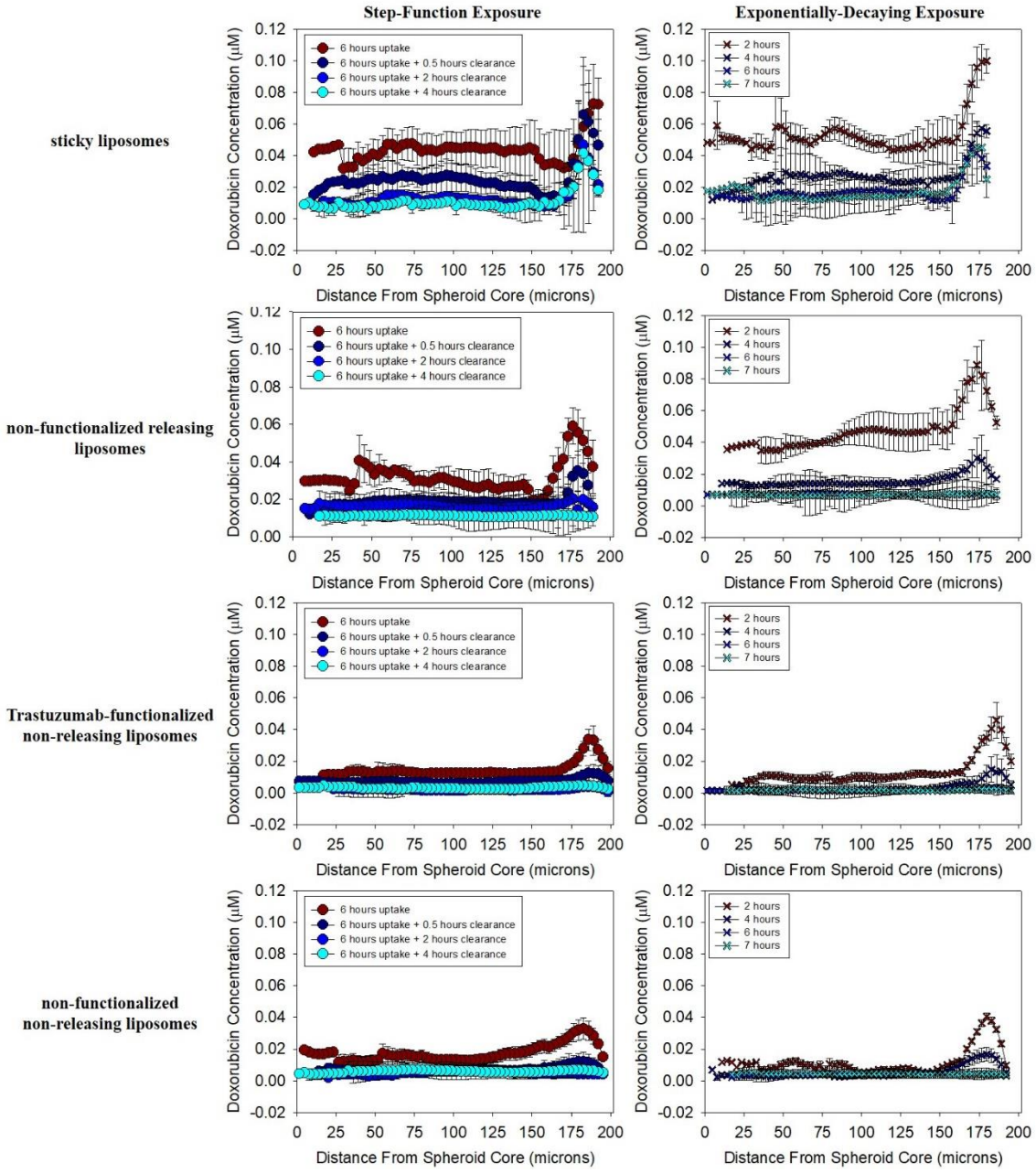

Figure A.7: Spatiotemporal profiles of doxorubicin clearance from MDA-MB-231 spheroids (83,000 HER2 receptors per cell).

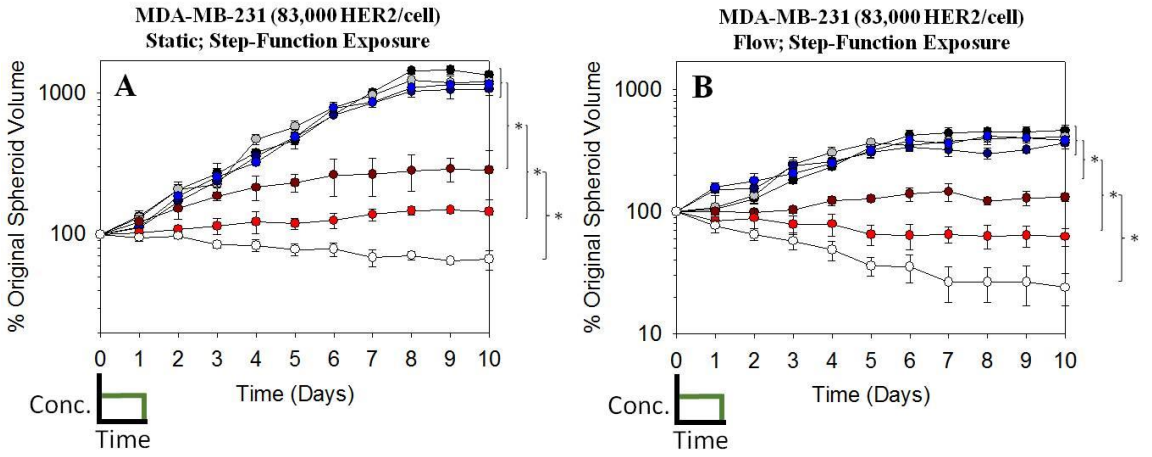

Figure A.8: Efficacy of doxorubicin constructs against TNBC MDA-MB-231 spheroids (8.3×10^4 HER2 receptors per cell) under (A) static conditions with step-wise therapy exposure and (B) flow conditions (20 µL/min) with step-wise therapy exposure in the form of peptide-functionalized pH-responsive (sticky) liposomes (red symbols), non-functionalized pH-responsive liposomes (burgundy symbols), trastuzumab-functionalized non-pH-responsive liposomes (light blue symbols), non-functionalized non-pH-responsive liposomes (dark blue symbols), and free doxorubicin (white symbols). Black symbols indicate untreated spheroids and light grey symbols indicate the effect of empty liposomes.

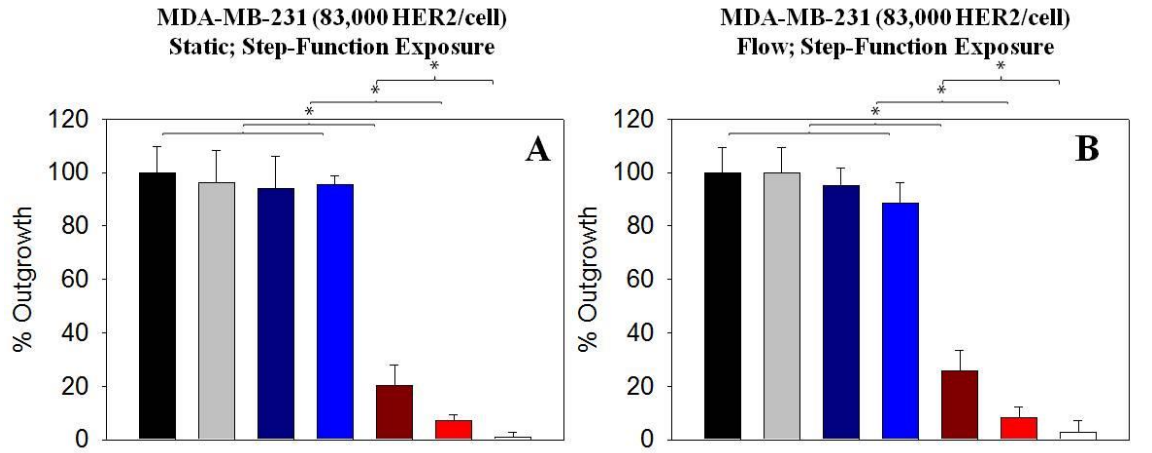

Figure A.9: Outgrowth at the endpoint given in Figure 4.5 for MDA-MB-231 spheroids under (A) static conditions with step-wise therapy exposure and (B) flow conditions (20 µL/min) with step-wise therapy exposure in the form of peptide-functionalized pH-responsive (sticky) liposomes (red bars), non-functionalized pH-responsive liposomes (burgundy bar), trastuzumab-functionalized non-pH-responsive liposomes (light blue bar), non-functionalized non-pH-responsive liposomes (dark blue bars), and free doxorubicin (white bars). Black bars indicate untreated spheroids and light grey bars indicate the effect of empty liposomes. * indicates p-values < 0.01.

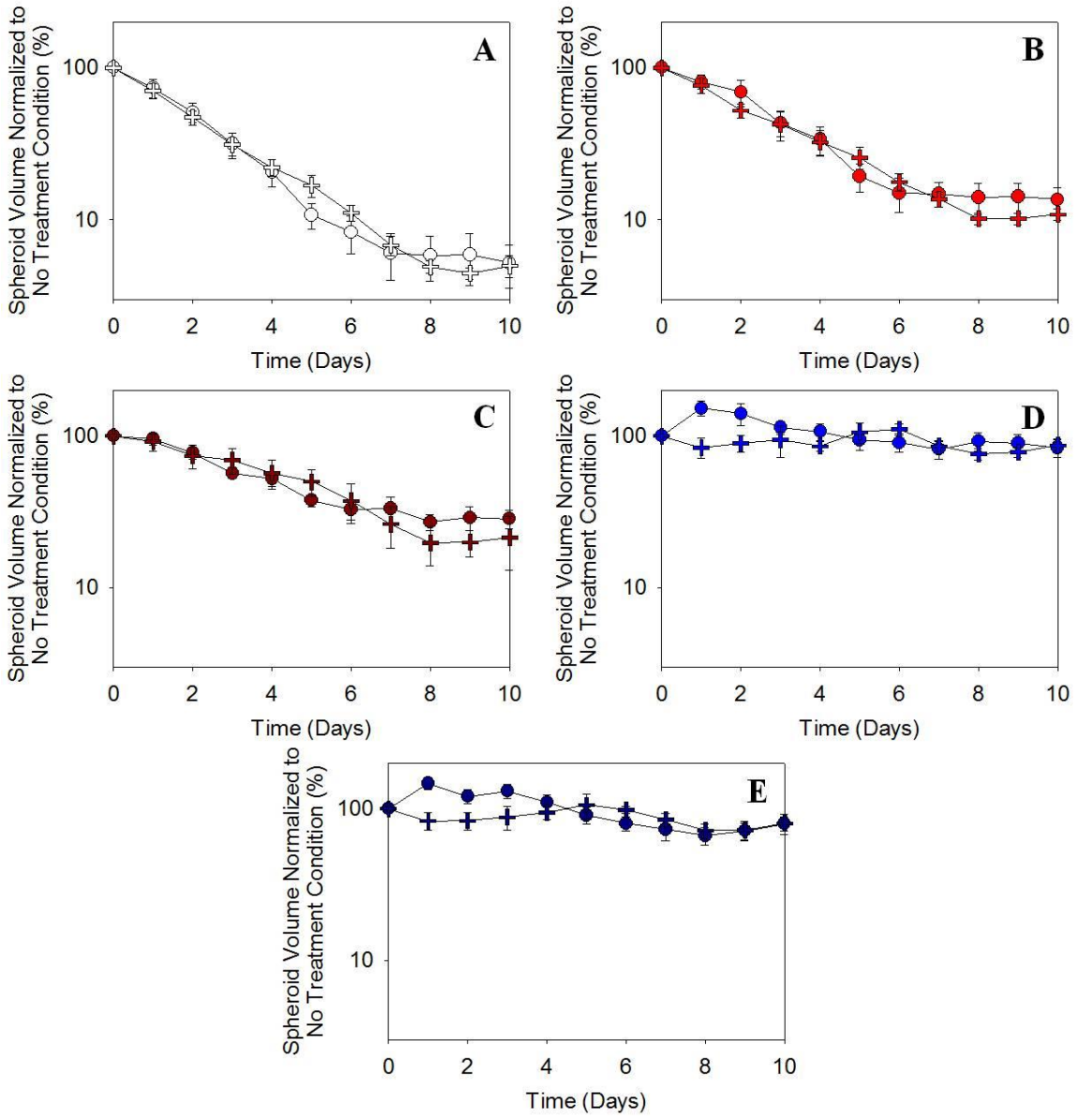

Figure A.10: Effect of incubation platform on spheroid response to (A) free doxorubicin, (B) sticky liposomal doxorubicin (cell internalization and interstitial release), (C) non-functionalized pH-responsive liposomal doxorubicin (no cell internalization, but interstitial release) (D) trastuzumab-functionalized non-pH-responsive liposomal doxorubicin (no cell internalization and no interstitial release), (E) non-functionalized non-pH-responsive liposomal doxorubicin (no cell internalization and no interstitial release) for static conditions with step-wise therapy exposure (+ symbols), flow conditions (20 µL/min) with step-wise therapy exposure (round symbols).

REFERENCES

[1] Howlader N NA, Krapcho M, Neyman N, Aminou R, Waldron W, Altekruse SF, Kosary CL, Ruhl J, Tatalovich Z, Cho H, Mariotto A, Eisner MP, Lewis DR, Chen HS, Feuer EJ, Cronin KA, Edwards BK. SEER Cancer Statistics Review, 1975-2008,. Bethesda, MD: National Cancer Institute; 2011.
[2] U.S. Breast Cancer Statistics. www.breastcancer.org2017.
[3] Rubin I, Yarden Y. The Basic Biology of HER2. Annals of Oncology. 2001;12:S3-S8.
[4] Moasser MM. The oncogene HER2; Its signaling and transforming functions and its role in human cancer pathogenesis. Oncogene. 2007;26:6469-87.
[5] Steelman LS, Chappell WH, Abrams SL, Kempf CR, Long J, Laidler P, et al. Roles of the Raf/MEK/ERK and PI3K/PTEN/Akt/mTOR pathways in controlling growth and sensitivity to therapy-implications for cancer and aging. Aging (Albany NY). 2011;3:192-222.
[6] Tai W, Mahato R, Cheng K. The role of HER2 in cancer therapy and targeted drug delivery. Journal of controlled release : official journal of the Controlled Release Society. 2010;146:264-75.
[7] Perez EA, Cortés J, Gonzalez-Angulo AM, Bartlett JMS. HER2 testing: Current status and future directions. Cancer Treatment Reviews. 2014;40:276-84.
[8] Ross JS, Fletcher JA, Linette GP, Stec J, Clark E, Ayers M, et al. The Her-2/neu gene and protein in breast cancer 2003: biomarker and target of therapy. The oncologist. 2003;8:307-25.
[9] Allen TM. Ligand-targeted therapeutics in anticancer therapy. Nat Rev Cancer. 2002;2:750-63.
[10] Nielsen DL, Andersson M, Kamby C. HER2-targeted therapy in breast cancer. Monoclonal antibodies and tyrosine kinase inhibitors. Cancer Treat Rev. 2009;35:121-36.
[11] Nahta R, Esteva FJ. Herceptin: mechanisms of action and resistance. Cancer letters. 2006;232:123-38.
[12] Cobleigh MA, Vogel CL, Tripathy D, Robert NJ, Scholl S, Fehrenbacher L, et al. Multinational Study of the Efficacy and Safety of Humanized Anti-HER2 Monoclonal Antibody in Women Who Have HER2-Overexpressing Metastatic Breast Cancer That Has Progressed After Chemotherapy for Metastatic Disease. Journal of Clinical Oncology. 1999;17:2639-.
[13] Viani GA, Afonso SL, Stefano EJ, De Fendi LI, Soares FV. Adjuvant trastuzumab in the treatment of her-2-positive early breast cancer: a meta-analysis of published randomized trials. BMC Cancer. 2007;7:153-.
[14] Muss HB, Thor AD, Berry DA, Kute T, Liu ET, Koerner F, et al. c-erbB-2 expression and response to adjuvant therapy in women with node-positive early breast cancer. The New England journal of medicine. 1994;330:1260-6.
[15] Thor AD, Berry DA, Budman DR, Muss HB, Kute T, Henderson IC, et al. erbB-2, p53, and efficacy of adjuvant therapy in lymph node-positive breast cancer. Journal of the National Cancer Institute. 1998;90:1346-60.
[16] Paik S, Bryant J, Park C, Fisher B, Tan-Chiu E, Hyams D, et al. erbB-2 and response to doxorubicin in patients with axillary lymph node-positive, hormone receptor-negative breast cancer. Journal of the National Cancer Institute. 1998;90:1361-70.

[17] Onitilo AA, Engel JM, Stankowski RV. Cardiovascular toxicity associated with adjuvant trastuzumab therapy: prevalence, patient characteristics, and risk factors. Therapeutic Advances in Drug Safety. 2014;5:154-66.
[18] Slamon DJ, Leyland-Jones B, Shak S, Fuchs H, Paton V, Bajamonde A, et al. Use of Chemotherapy plus a Monoclonal Antibody against HER2 for Metastatic Breast Cancer That Overexpresses HER2. New England Journal of Medicine. 2001;344:783-92.
[19] Park JW, Hong K, Kirpotin DB, Colbern G, Shalaby R, Baselga J, et al. Anti-HER2 immunoliposomes: enhanced efficacy attributable to targeted delivery. Clinical cancer research : an official journal of the American Association for Cancer Research. 2002;8:1172-81.
[20] Merrimack Announces Encouraging Clinical Data From Expanded Phase 1 Study of MM-302 for the Treatment of Advanced HER2-Positive Breast Cancer. 2013.
[21] MM-302 Plus Trastuzumab vs. Chemotherapy of Physician's Choice Plus Trastuzumab in HER2-Positive Locally Advanced/Metastatic Breast Cancer Patients (HERMIONE). ClinicalTrials.gov2017.
[22] Lee H, Shields AF, Siegel BA, Miller KD, Krop I, Ma CX, et al. 64Cu-MM-302 Positron Emission Tomography Quantifies Variability of Enhanced Permeability and Retention of Nanoparticles in Relation to Treatment Response in Patients with Metastatic Breast Cancer. Clinical cancer research : an official journal of the American Association for Cancer Research. 2017.
[23] Hendriks BS, Klinz SG, Reynolds JG, Espelin CW, Gaddy DF, Wickham TJ. Impact of tumor HER2/ERBB2 expression level on HER2-targeted liposomal doxorubicin-mediated drug delivery: multiple low-affinity interactions lead to a threshold effect. Molecular cancer therapeutics. 2013;12:1816-28.
[24] Koltz B, Hicks D, Whitney-Miller C. HER2 testing in gastric and esophageal adenocarcinoma: new diagnostic challenges arising from new therapeutic options. Biotechnic & Histochemistry. 2012;87:40-5.
[25] Joy AA, Ghosh M, Fernandes R, Clemons MJ. Systemic treatment approaches in her2-negative advanced breast cancer—guidance on the guidelines. Current Oncology. 2015;22:S29-S42.
[26] Bajagur Kempegowda G, Karve S, Bandekar A, Adhikari A, Khaimchayev T, Sofou S. pH-dependent formation of lipid heterogeneities controls surface topography and binding reactivity in functionalized bilayers. Langmuir. 2009;25:8144-51.
[27] Bandekar A, Sofou S. Floret-shaped solid domains on giant fluid lipid vesicles induced by pH. Langmuir. 2012;28:4113-22.
[28] Helmlinger G, Yuan F, Dellian M, Jain RK. Interstitial pH and pO2 gradients in solid tumors in vivo: high-resolution measurements reveal a lack of correlation. Nature medicine. 1997;3:177-82.
[29] Press MF, Cordon-Cardo C, Slamon DJ. Expression of the HER-2/neu proto-oncogene in normal human adult and fetal tissues. Oncogene. 1990;5:953-62.
[30] Kirpotin DB, Drummond DC, Shao Y, Shalaby MR, Hong K, Nielsen UB, et al. Antibody Targeting of Long-Circulating Lipidic Nanoparticles Does Not Increase Tumor Localization but Does Increase Internalization in Animal Models. Cancer research. 2006;66:6732-40.

[31] Elias DR, Poloukhtine A, Popik V, Tsourkas A. Effect of ligand density, receptor density, and nanoparticle size on cell targeting. Nanomedicine: nanotechnology, biology and medicine. 2013;9:194-201.
[32] Avvakumova S, Fezzardi P, Pandolfi L, Colombo M, Sansone F, Casnati A, et al. Gold nanoparticles decorated by clustered multivalent cone-glycocalixarenes actively improve the targeting efficiency toward cancer cells. Chemical communications (Cambridge, England). 2014;50:11029-32.
[33] Gray BP, Li S, Brown KC. From phage display to nanoparticle delivery: functionalizing liposomes with multivalent peptides improves targeting to a cancer biomarker. Bioconjugate chemistry. 2013;24:85-96.
[34] Martin AL, Li B, Gillies ER. Surface functionalization of nanomaterials with dendritic groups: toward enhanced binding to biological targets. Journal of the American Chemical Society. 2009;131:734-41.
[35] van Dongen MA, Dougherty CA, Banaszak Holl MM. Multivalent polymers for drug delivery and imaging: the challenges of conjugation. Biomacromolecules. 2014;15:3215-34.
[36] Poon Z, Chen S, Engler AC, Lee H-i, Atas E, von Maltzahn G, et al. Ligand-Clustered "Patchy" Nanoparticles for Modulated Cellular Uptake and In Vivo Tumor Targeting. Angewandte Chemie International Edition. 2010;49:7266-70.
[37] Karasseva NG, Glinsky VV, Chen NX, Komatireddy R, Quinn TP. Identification and characterization of peptides that bind human ErbB-2 selected from a bacteriophage display library. Journal of protein chemistry. 2002;21:287-96.
[38] Bandekar A, Sofou S. Floret-Shaped Solid Domains on Giant Fluid Lipid Vesicles Induced by pH. Langmuir : the ACS journal of surfaces and colloids. 2012;28:4113-22.
[39] Kempegowda GB, Karve S, Bandekar A, Adhikari A, Khaimchayev T, Sofou S. pH-Dependent Formation of Lipid Heterogeneities Controls Surface Topography and Binding Reactivity in Functionalized Bilayers. Langmuir : the ACS journal of surfaces and colloids. 2009;25:8144-51.
[40] Vaupel P, Kallinowski F, Okunieff P. Blood flow, oxygen and nutrient supply, and metabolic microenvironment of human tumors: a review. Cancer research. 1989;49:6449-65.
[41] Allen TM, Brandeis E, Hansen CB, Kao GY, Zalipsky S. A new strategy for attachment of antibodies to sterically stabilized liposomes resulting in efficient targeting to cancer cells. Biochimica et Biophysica Acta (BBA) - Biomembranes. 1995;1237:99-108.
[42] Tokutomi S, Ohki K, Ohnishi SI. Proton-induced phase separation in phosphatidylserine/phosphatidylcholine membranes. Biochimica et biophysica acta. 1980;596:192-200.
[43] Feigenson GW, Buboltz JT. Ternary phase diagram of dipalmitoyl-PC/dilauroyl-PC/cholesterol: nanoscopic domain formation driven by cholesterol. Biophys J. 2001;80:2775-88.
[44] Bell GI. Models for the specific adhesion of cells to cells. Science. 1978;200:618-27.
[45] van der Meel R, Vehmeijer LJ, Kok RJ, Storm G, van Gaal EV. Ligand-targeted particulate nanomedicines undergoing clinical evaluation: current status. Advanced drug delivery reviews. 2013;65:1284-98.

[46] Ghaghada KB, Saul J, Natarajan JV, Bellamkonda RV, Annapragada AV. Folate targeting of drug carriers: a mathematical model. Journal of controlled release : official journal of the Controlled Release Society. 2005;104:113-28.
[47] de Gennes PG. Conformations of Polymers Attached to an Interface. Macromolecules. 1980;13:1069-75.
[48] Carey LA, Perou CM, Livasy CA, Dressler LG, Cowan D, Conway K, et al. Race, breast cancer subtypes, and survival in the Carolina Breast Cancer Study. Jama. 2006;295:2492-502.
[49] Gradishar WJ. Emerging approaches for treating HER2-positive metastatic breast cancer beyond trastuzumab. Annals of Oncology. 2013;24:2492-500.
[50] Ballangrud AM, Yang WH, Palm S, Enmon R, Borchardt PE, Pellegrini VA, et al. Alpha-particle emitting atomic generator (Actinium-225)-labeled trastuzumab (herceptin) targeting of breast cancer spheroids: efficacy versus HER2/neu expression. Clinical cancer research : an official journal of the American Association for Cancer Research. 2004;10:4489-97.
[51] Seol H, Lee HJ, Choi Y, Lee HE, Kim YJ, Kim JH, et al. Intratumoral heterogeneity of HER2 gene amplification in breast cancer: its clinicopathological significance. Modern pathology : an official journal of the United States and Canadian Academy of Pathology, Inc. 2012;25:938-48.
[52] Martelotto LG, Ng CK, Piscuoglio S, Weigelt B, Reis-Filho JS. Breast cancer intra-tumor heterogeneity. Breast Cancer Research. 2014;16:210.
[53] Ringhieri P, Mannucci S, Conti G, Nicolato E, Fracasso G, Marzola P, et al. Liposomes derivatized with multimeric copies of KCCYSL peptide as targeting agents for HER-2-overexpressing tumor cells. International Journal of Nanomedicine. 2017;12:501-14.
[54] Haran G, Cohen R, Bar LK, Barenholz Y. Transmembrane ammonium sulfate gradients in liposomes produce efficient and stable entrapment of amphipathic weak bases. Biochimica et biophysica acta. 1993;1151:201-15.
[55] McDevitt MR, Barendswaard E, Ma D, Lai L, Curcio MJ, Sgouros G, et al. An alpha-particle emitting antibody ([213Bi]J591) for radioimmunotherapy of prostate cancer. Cancer research. 2000;60:6095-100.
[56] Ovcaricek T, Frkovic SG, Matos E, Mozina B, Borstnar S. Triple negative breast cancer – prognostic factors and survival. Radiology and Oncology. 2011;45:46-52.
[57] Guo P, Huang J, Wang L, Jia D, Yang J, Dillon DA, et al. ICAM-1 as a molecular target for triple negative breast cancer. Proc Natl Acad Sci U S A. 2014;111:14710-5.
[58] Nakai K, Hung M-C, Yamaguchi H. A perspective on anti-EGFR therapies targeting triple-negative breast cancer. American Journal of Cancer Research. 2016;6:1609-23.
[59] San Paulo A, García R. High-resolution imaging of antibodies by tapping-mode atomic force microscopy: attractive and repulsive tip-sample interaction regimes. Biophysical Journal. 2000;78:1599-605.
[60] Lim RYH, Huang N-P, Köser J, Deng J, Lau KHA, Schwarz-Herion K, et al. Flexible phenylalanine-glycine nucleoporins as entropic barriers to nucleocytoplasmic transport. Proceedings of the National Academy of Sciences. 2006;103:9512-7.
[61] Foulkes WD, Smith IE, Reis-Filho JS. Triple-Negative Breast Cancer. New England Journal of Medicine. 2010;363:1938-48.

[62] Dent R, Trudeau M, Pritchard KI, Hanna WM, Kahn HK, Sawka CA, et al. Triple-negative breast cancer: clinical features and patterns of recurrence. Clinical cancer research : an official journal of the American Association for Cancer Research. 2007;13:4429-34.
[63] Oakman C, Viale G, Di Leo A. Management of triple negative breast cancer. Breast (Edinburgh, Scotland). 2010;19:312-21.
[64] Sempkowski M, Zhu C, Menzenski MZ, Kevrekidis IG, Bruchertseifer F, Morgenstern A, et al. Sticky Patches on Lipid Nanoparticles Enable the Selective Targeting and Killing of Untargetable Cancer Cells. Langmuir : the ACS journal of surfaces and colloids. 2016;32:8329-38.
[65] Durand RE, Olive PL. Resistance of tumor cells to chemo- and radiotherapy modulated by the three-dimensional architecture of solid tumors and spheroids. Methods in cell biology. 2001;64:211-33.
[66] O'Brien MER, Wigler N, Inbar M, Rosso R, Grischke E, Santoro A, et al. Reduced cardiotoxicity and comparable efficacy in a phase III trial of pegylated liposomal doxorubicin HCl (CAELYX™/Doxil®) versus conventional doxorubicin for first-line treatment of metastatic breast cancer. Annals of Oncology. 2004;15:440-9.
[67] Iorns E, Drews-Elger K, Ward TM, Dean S, Clarke J, Berry D, et al. A New Mouse Model for the Study of Human Breast Cancer Metastasis. PLOS ONE. 2012;7:e47995.
[68] Chang MY, Seideman J, Sofou S. Enhanced loading efficiency and retention of 225Ac in rigid liposomes for potential targeted therapy of micrometastases. Bioconjugate chemistry. 2008;19:1274-82.
[69] Sutherland RM, Eddy HA, Bareham B, Reich K, Vanantwerp D. Resistance to adriamycin in multicellular spheroids. International Journal of Radiation Oncology*Biology*Physics. 1979;5:1225-30.
[70] Goodman TT, Chen J, Matveev K, Pun SH. Spatio-Temporal Modeling of Nanoparticle Delivery to Multicellular Tumor Spheroids. Biotechnology and bioengineering. 2008;101:388-99.
[71] Silver DA, Pellicer I, Fair WR, Heston W, Cordon-Cardo C. Prostate-specific membrane antigen expression in normal and malignant human tissues. Clinical Cancer Research. 1997;3:81-5.
[72] Parker N, Turk MJ, Westrick E, Lewis JD, Low PS, Leamon CP. Folate receptor expression in carcinomas and normal tissues determined by a quantitative radioligand binding assay. Analytical biochemistry. 2005;338:284-93.
[73] Nicholson R, Gee J, Harper M. EGFR and cancer prognosis. European journal of cancer. 2001;37:9-15.